2010

Studies of nanoparticles from a group of uniform materials based on organic salts (GUMBOS)

Aaron Tesfai
Louisiana State University and Agricultural and Mechanical College, atesfa1@lsu.edu

STUDIES OF NANOPARTICLES FROM A GROUP OF UNIFORM MATERIALS BASED ON ORGANIC SALTS (GUMBOS)

A Dissertation
Submitted to the Graduate Faculty of the
Louisiana State University and
Agricultural and Mechanical College
In partial fulfillment of the
Requirements for the degree of
Doctor of Philosophy

In
The Department of Chemistry

By
Aaron Tesfai
B.S., University of Missouri, Columbia, 2003
May, 2010

To my parents, Tesfai Tsehaie and Turu Negash, and my brother Benyam Tesfai for your gracious support over the years.

ACKNOWLEDGEMENTS

The completion of this work would not have been possible without the generosity and support of many people:

Dr. Isiah M. Warner: You have been instrumental in ensuring my academic, professional and financial well being during my tenure. I am eternally inspired by your passion in science. It has been a tough and tedious journey but I am fortunate enough to have had you on my side, challenging and stimulating my scientific curiosity. I am grateful and indebted to you for your wise and invaluable guidance, continued interest, and unwavering support throughout the tenure of my graduate studies. Your scientific intuition has inspired and enriched my growth as a student, a researcher, and a scientist.

Doctoral Research Committee Members: **Dr. Daniel Hayes, Dr. Jayne Garno, Dr. Kermit Murray, and Dr. Kip Matthews II**, for your time and helpful discussions over the years.

Post Doctoral Researchers: **Dr. Bilal El Zahab**, **Dr. Sayo Fakayode, Dr, Min Li, Dr. Susmita Das, and Dr. Santhosh Challa** for taking the time to provide guidance and support.

Funding Agencies: National Institutes of Health, National Science Foundation, Philip W. West Endowment

The Warner Research Group, for helpful research discussions and being my family away from home. I value your support and friendship.

TABLE OF CONTENTS

DEDICATION……... ii

ACKNOWLEDGEMENTS……..……..……...…..…….... iii

LIST OF TABLES……...……..……..……... vii

LIST OF FIGURES……..…….…… … viii

LIST OF ABBREVIATIONS……...…… xiii

ABSTRACT…….....…… xvi

CHAPTER 1. INTRODUCTION…….....…… 1
1.1 Ionic Liquids.…….…..... 1
1.1.1 Room Temperature Ionic Liquids…….. 4
1.1.2 Frozen Ionic Liquids……..... 6
1.2 Group of Uniform Materials Based on Organic Salts……. 6
1.3 Nanoparticles……... 8
1.3.1 Applications and Importance of Size Control of Nanoparticles……. 10
1.3.1.1 Drug Delivery……...……..... 10
1.3.1.2 Bioimaging ……..……...……...…….. 10
1.3.1.3 Microbial Detection……...….. 10
1.3.1.4 Environmental Applications……... 11
1.4 Synthetic Methods for Size Controlled Nanoparticles……..…. 11
1.4.1.1 Template Synthesis……..... 11
1.4.1.2 Chemical Vapor Condensation (CVC)……..... 12
1.4.1.3 Metal Reduction (Colloids)……..... 12
1.4.1.4 Sonochemical…….. 13
1.5 Nanoparticles Derived from GUMBOS: NanoGUMBOS……. 13
1.5.1 Methods for Size Control for NanoGUMBOS..... 15
1.5.1.2 Melt-Emulsion-Quench Technique…….…… 15
1.5.1.3 Reprecipitation……... 16
1.5.1.4 Reverse Micelle Synthesis…….. 18
1.5.1.5 Aerosol Synthesis…… 21
1.5.1.6 Hydrogel Synthesis……. 21
1.6 Analytical Techniques Used in this Study…….. 24
1.6.1 Scanning Electron Microscopy……... 24
1.6.2 Transmission Electron Microscopy……. 25
1.6.3 Differential Interference Contrast…… 26
1.6.4 Fluorescence Microscopy……. 27
1.6.5 Atomic Force Microscopy…… 27
1.6.6 UV-visible Spectroscopy (UV-vis)…….. 28
1.6.7 Fluorescence Spectroscopy……. 32

1.6.8 Superconducting Quantum Interference Device (SQUID)…… 33
1.7 Scope of Dissertation…….. 36
1.8 References……... 37

CHAPTER 2. CONTROLLABLE FORMATION OF IONIC LIQUID MICRO- AND NANOPARTICLES VIA MELT-EMULSION-QUENCH APPROACH…….. 42
2.1 Introduction.....…. 42
2.2 Materials and Methods……... 44
2.2.1 Electron Microscopy Characterization…… 45
2.2.2 Method 1: (Surfactantless Mode) Preparation of Nano- and MicroGUMBOS…….. 45
2.2.3 Method 2: (Surfactant-Assisted Mode) Preparation of NanoGUMBOS……... 46
2.3 Results and Discussion…… 47
2.3.1 Method 1: Characterization of NanoGUMBOS……..…. 47
2.3.2 Modified Method 1: Characterization of MicroGUMBOS.…… 48
2.3.3 Fluorescent Labeling of MicroGUMBOS…….. 48
2.3.4 Method 2: Characterization of NanoGUMBOS.…… 48
2.4 Conclusions……..…….. 52
2.5 References……..... 53

CHAPTER 3. MAGNETIC AND NON-MAGNETIC NANOPARTICLES FROM A GROUP OF UNIFORM MATERIALS BASED ON ORGANIC SALTS…….. 55
3.1 Introduction…… 55
3.2 Materials and Methods……... 58
3.2.1 Materials…… 58
3.2.2 Preparation of NanoGUMBOS and Magnetic NanoGUMBOS….…… 58
3.2.3 UV-vis Characterization…… 59
3.2.4 Electron Microscopy Characterization……... 59
3.2.5 Atomic Force Microscopy Characterization……..…… 60
3.2.6 Superconducting Quantum Interference Device Characterization…….. 61
3.3 Results and Discussion……..... 61
3.3.1 Particle Size Control……..……. 61
3.3.2 Nonmagnetic NanoGUMBOS of $[Bm_2Im][BF_4]$…….…….. 63
3.3.3 Magnetic $[Bm_2Im][FeCl_4]$ GUMBOS Particles……. 66
3.4 Conclusions……..…….. 74
3.5 References…….. 74

CHAPTER 4. FLUORESCENT NANOPARTICLES FROM A GROUP OF UNIFORM MATERIALS BASED ON ORGANIC SALTS……... 77
4.1 Introduction…….. 77
4.2 Materials and Methods…… 78

4.2.1 Materials……..…….... 78
4.2.2 Synthesis and Characterization of Fluorescent GUMBOS..... 79
4.2.3 Synthesis of Fluorescent NanoGUMBOS……..... 80
4.2.3.1 Reprecipitation…….... 80
4.2.3.2 In-situ Ion Exchange…… 80
4.2.3.3 Hydrogel Preparation…….. 82
4.3 Characterization of Fluorescent NanoGUMBOS……..... 82
4.4 Absorption and Fluorescent Studies of GUMBOS and NanoGUMBOS…….. 83
4.5 Results and Discussion……. 84
4.5.1 Synthesis, Characterization and Optical Properties of Fluorescent GUMBOS…… 84
4.5.2 Synthesis, Characterization, and Optical Properties of Fluorescent NanoGUMBOS……... 85
4.5.2.1 Reprecipitation…….. 85
4.5.2.2 In-Situ Ion Exchange…… 86
4.5.2.3 Hydrogel Preparation……. 91
4.5.3 Comparison of Three Synthetic Methods……... 94
4.6 Conclusions……..……... 95
4.7 References……... 95

CHAPTER 5. CONCLUSIONS AND FUTURE STUDIES……... 97
5.1 Concluding Remarks……..……. 97
5.2 Future Studies…….. 98

APPENDIX: LETTERS OF PERMISSION……..……... 101

VITA…….. 105

LIST OF TABLES

Table **Page**

1 Effect of reagent concentration on particle size……. 67

2 Effect of reagent concentration on particle size……..... 72

LIST OF FIGURES

Figure **Page**

1.1 Common cations and anions used in combination for the synthesis of ILs……2

1.2 Number of publications on ILs per year from 1986 to 2009…….……3

1.3 Number of patents on ILs per year from 1986 to 2009.....3

1.4 Applications of ILs in the various fields of physical chemistry, electrochemistry, biology, analytical chemistry, solvents and catalysts, and engineering, modified from reference 36.....5

1.5 Examples of various applications of GUMBOS…….……....7

1.6 Number of publications that reflect the growing interest in nanotechnology since 1990…….....8

1.7 Number of patents that reflect the growing interest in nanotechnology since 1990……...9

1.8 Steps of the melt–emulsion–quench method for synthesizing nano- and microparticles using no surfactant (Method 1) and employing surfactant (Method 2). In Method 1, the first step (a) melting of hydrophobic IL in a hot water bath, whereas addition of melted IL to a surfactant solution is performed in Method 2. Homogenization and probe sonication are performed in (b), quenching of o/w emulsion to solidify nanoparticles (c) modified from reference 38……..17

1.9 Schematic of micelle formation at surfactant concentration exceeding the CMC…...17

1.10 Preparation of fluorescent nanoGUMBOS using the reprecipitation method. (A) GUMBOS solution in solvent (1 mM ethanol), (B) dispersant (5 mL water), and (C) nanoparticle suspension in dispersant.……18

1.11 Molecular structure of sodium bis(2-ethylhexyl) sulfosuccinate (AOT).……...…….19

1.12 Four principal microenvironments in the reverse micellar system……..20

1.13 Basic processes for nanoparticle formation within AOT reverse micelles. Individual reverse micelles are shown without surfactant for brevity.…….……22

1.14 Representation of the aerosol process for formation of nanoGUMBOS……..23

1.15 Basic processes for nanoparticle formation within hydrogels modified from reference 71……..23

1.16 Diagram of scanning electron microscope modified from reference 40.....……25

1.17 Diagram of transmission electron microscope modified from reference 40..…….29

1.18 Diagram of differential interference contrast modified from reference 72.……30

1.19 Diagram of fluorescence microscopy modified from reference 73……..……..30

1.20 Diagram of atomic force microscopy modified from reference 74...……..31

1.21 Representation of a UV-visible spectrometer modified from reference 75…….32

1.22 The Jablonski Diagram. Radiative transitions are indicated with solid arrows, and radiationless transitions are indicated with dashed arrows…….....34

1.23 Diagram of a Spectrofluorometer …….……..35

1.24 Diagram of a Superconducting Quantum Interference Device..……..35

2.1 Schematic showing the steps involved in the melt–emulsion–quench method for synthesizing nano- and microGUMBOS using surfactantless (Method 1) and surfactant-assisted (Method 2) procedures. In Method 1, the first step (a) entails the melting of [bm_2Im][PF_6] in a hot water bath, whereas dropwise addition of molten [bm_2Im][PF_6] to a surfactant solution is performed at this stage in Method 2. The residual steps are homogenization and probe sonication (b), followed by rapid quenching in an ice bath to achieve particle solidification (c)…..……...49

2.2 Photographs showing the various stages of nanoGUMBOS formation following Method 1, as summarized in 2.1: (A) solid [bm_2Im][PF_6] in water at room temperature; (B) molten-state [bm_2Im][PF_6] phase separated from water at 70 °C; (C) o/w emulsion containing [bm_2Im][PF_6] as the inner phase; (D) [bm_2Im][PF_6] nanoGUMBOS crop suspended in water at room temperature. In these images, [bm_2Im][PF_6] was stained with a water-insoluble dye (Nile Red) for visualization purposes…….....50

2.3 Electron micrographs of [bm_2Im][PF_6] nanoGUMBOS synthesized using Method 1: (a) SEM image (15 kV) showing an average nanoparticle diameter of 90 ± 32 nm. (b) TEM image (80 kV) with an average nanoGUMBOS diameter measured as 88 ± 34 nm. It was observed that an electronic beam focused on a spot for an extended time would melt the particles. Therefore, high magnification exposure time was minimized for TEM. (c) Electronic beam focused on a spot showing the particles melting……..50

2.4 Solid [bm_2Im][PF_6] microGUMBOS prepared using Method 1 with average diameter of ~ 3-μm imaged with (a) SEM, (b) Optical microscopy (DIC), (c) Optical microscopy (fluorescence), (d) Overlay of DIC and fluorescence.…….……51

2.5 Representative TEM image of 45 ± 7 nm [bm_2Im][PF_6] nanoGUMBOS synthesized based upon Method 2, employing Brij® 35 as emulsifying agent.…….....51

3.1 Basic processes for nanoparticle formation within AOT reverse micelles. Individual reverse micelles are shown without free surfactants. (a) [Bm_2Im][BF_4] nanoGUMBOS. (b) [Bm_2Im][$FeCl_4$] magnetic nanoGUMBOS……....62

3.2 Exchange reaction at (A) the micellar core and (B) magnetic GUMBOS synthesis at the micellar core. ……..63

3.3 TEM micrographs of [Bm_2Im][BF_4] nanoGUMBOS synthesized according to the approach shown in Figure 3.1a and imaged by TEM at the indicated magnifications with average particle diameters of: (A) 14.7 ± 2.2 nm, (B) 20.8 ± 1.8 nm, (C) 34.3 ± 4.8 nm, and (D) 68.0 ± 17.0 nm. Images were taken using an LVEM5 electron microscope with an accelerating voltage of 5 kV without staining…….……...66

3.4 Size distributions of nanoGUMBOS synthesized via Figure 3.1a in water-containing AOT reverse micelles at various reagent concentrations: [AOT] = 0.1 M; molar reagent concentrations: 0.3, 0.4, 0.5, and 0.6 M…….....67

3.5 Images of [Bm_2Im][BF_4] nanoGUMBOS synthesized in Figure 3.1a acquired with tapping mode AFM at a frequency of 150 kHz. (A) 60 × 60 μm^2 topographical image and (B) simultaneously acquired phase image. (C) Zoom-in view 12 × 12 μm^2 view and (D) corresponding phase channel.…….…….68

3.6 Size distributions of nanoGUMBOS synthesized via Figure 3.1a in water-containing AOT reverse micelles at reagent concentration: [AOT] = 0.1 M; molar reagent concentration: 0.4M…….68

3.7 Melting point of bulk [Bm_2Im][$FeCl_4$]. The melting point of [Bm_2Im][$FeCl_4$] is -2.66 °C.....69

3.8 UV-vis of [Bm_2Im][$FeCl_4$] in acetonitrile GUMBOS show three absorption peaks at (528, 617, and 684 nm) characteristic of [$FeCl_4^-$]……...69

3.9 Micrographs of magnetic [Bm_2Im][$FeCl_4$] GUMBOS particles synthesized in Figure 3.1b obtained from TEM revealing mean particle sizes of (A) 98.0 ± 17 nm and (B) 199.0 ± 26 nm. Images were taken using an LVEM5 electron microscope with an accelerating voltage of 5 kV without staining….……72

3.10 Size distributions of magnetic GUMBOS particles (shown in Figure 4) at various reagent concentrations: [AOT] = 0.1 M; molar reagent concentrations: 0.3 and 0.4 M……..73

3.11 Differently sized samples of magnetic [Bm_2Im][$FeCl_4$] nanoGUMBOS synthesized in Figure 3.1b imaged by tapping mode AFM for 20 × 20 μm2 scan areas at an 180 kHz driving frequency. (A) Topographical image of magnetic nanoGUMBOS with a diameter near 100 nm and (B) the matching phase image. (C) Topography of 200-nm GUMBOS particles and (D) the corresponding phase frame……..……..73

3.12 Magnetic susceptibility of bulk [Bm_2Im][$FeCl_4$] alongside [Bm_2Im][$FeCl_4$] nanoGUMBOS synthesized in Figure 3.1b…….……....74

4.1 Synthesis of [Rhod][TPB] by anion exchange reaction……..79

4.2 Preparation of fluorescent nanoGUMBOS using the reprecipitation method. (A) GUMBOS solution in solvent (1 mM acetone), (B) dispersant (5 mL water), and (C) nanoparticle suspension in dispersant…….……..…….....80

4.3 Basic processes for nanoparticle formation within AOT reverse micelles. Individual reverse micelles are shown without free surfactants. [Rhod][TPB] nanoGUMBOS……..81

4.4 Basic processes for nanoparticle formation within hydrogels modified from reference 17……...……..83

4.5 Absorbance profile for 1.76 μM [Rhod][TPB] in acetone; λ_{ex} = 525 nm.……84

4.6 Fluorescence excitation and emission spectra for 1.76 μM [Rhod][TPB] in acetone; λ_{ex} = 525 nm, λ_{em} = 550 nm..……...84

4.7 Reprecipitation: TEM micrograph of [Rhod][TPB] fluorescent nanoGUMBOS with an average diameter near 89 ± 17 nm…….. 85

4.8 Reprecipitation: Absorbance spectrum of the [Rhod][TPB] nanoGUMBOS (blue) 1.76 μM. Absorbance spectrum of [Rhod][Cl] dissolved in water (red) 1.76 μM……..…… 86

4.9 Reprecipitation: Normalized fluorescence spectrum of the [Rhod][TPB] nanoGUMBOS (blue) 1.76 μM. Fluorescence spectrum of [Rhod][Cl] dissolved in water (red) 1.76 μM at the excitation wavelength (λ_{ex} = 525 nm)……...87

4.10 Reprecipitation: Comparison between the fluorescence emission spectrum of the freely dissolved [Rhod][Cl] GUMBOS (1.76 μM in water; red profile) and [Rhod][TPB] nanoGUMBOS (blue profile) for matched concentration at the excitation wavelength (λ_{ex} = 525 nm).…….87

4.11 In-situ ion exchange: TEM micrograph of [Rhod][TPB] fluorescent nanoGUMBOS with an average diameter near 89 ± 11 nm.…….88

4.12 In-situ ion exchange: Absorbance spectrum of the [Rhod][TPB] nanoparticles (blue) 1.76 μM. Absorbance spectrum of [Rhod][Cl] dissolved in water (red) 1.76 μM.…….88

4.13 In-situ ion exchange: Comparison between the normalized fluorescence emission spectrum of the freely dissolved [Rhod][Cl] (in water; red profile), freely dissolved [Rhod][Cl] (in reverse micelle; green profile) and [Rhod][TPB] nanoGUMBOS (blue profile) for matched concentration..…….....90

4.14 In-situ ion exchange: Comparison between the fluorescence emission spectrum of freely dissolved [Rhod][Cl] (in reverse micelle; green profile) and [Rhod][TPB] nanoGUMBOS (blue profile) for matched concentration…….90

4.15 Hydrogel Synthesis: TEM micrograph of [Rhod][TPB] fluorescent nanoGUMBOS with an average diameter near 124 ± 35nm.…….……..…….91

4.16 Hydrogel synthesis: Absorbance spectrum of the [Rhod][TPB] particles (blue) 1.76 μM. Absorbance spectrum of [Rhod][Cl] dissolved in water (red) 1.76 μM.....…… 92

4.17 Hydrogel preparation: Comparison between the fluorescence emission spectrum of the freely dissolved [Rhod][Cl] (in water; red profile) and [Rhod][TPB] GUMBOS particles (blue profile) for matched concentration…….93

4.18 Fluorecence emission of [Rhod][Cl] in water(red) and [Rhod][Cl] in gel(green) excited at their respective absorption maxima.……....93

4.19 Comparison between the fluorescence emission spectrum of the [Rhod][TPB] particles using reprecipitation, in-situ ion exchange, and hydrogel methods. [Rhod][TPB] nanoGUMBOS synthesized using (In-situ ion exchange; blue profile), [Rhod][TPB] GUMBOS particles (Hydrogel; green profile), and [Rhod][TPB] nanoGUMBOS (Reprecipitation; red profile). [Rhod][TPB] nanoGUMBOS were synthesized at the same concentration……94

LIST OF ABBREVIATIONS

Abbreviation	Name
AFM	Atomic Force Microscopy
AOT	Sodium bis(2-ethylhexyl) sulfosuccinate
BETI	bis(perfluoroethylsulfonyl)imide
BF_4	Tetrafluoroborate
$[Bm_2Im][Cl]$	1-Butyl-2,3-dimethylimidazolium chloride
$[Bm_2Im][PF_6]$	1-Butyl-2,3-dimethylimidazolium hexafluorophosphate
Brij-35	Polyoxyethylene (23) lauryl ether
$[C_4mpyrr][NTF_2]$	1-butyl-1-methyl-pyrrolidinium bis(trifluoromethylsulfonyl)imide
CdSe	Cadmium Selenide
Cl	Chloride
CMC	Critical Micelle Concentration
$CoFe_2O_3$	Cobalt Iron(III) Oxide
CVC	Chemical Vapor Condensation
DIC	Differential Interference Contrast
DLS	Dynamic Light Scattering
$[EtNH_3][NO_3]$	Ethyl Ammonium Nitrate
Fe_2O_3	Iron (III) Oxide
$FeCl_3.6H_2O$	Iron (III) Chloride Hexahydrate
$FeCl_4$	Iron (III) Chloride Tetrachloroferrate
FILMPs	Frozen Ionic Liquid Microparticle
FILNPs	Frozen Ionic Liquid Nanoparticle
FWHM	Full Width at Half Maximum

GUMBOS	Group of Uniform Materials Based On Organic Salts
HeLa	Henrietta Lacks
IL	Ionic Liquid
In-situ	In Place
$NaBF_4$	Sodium Tetrafluoroborate
$NaBH_4$	Sodium Borohydride
NH_3	Ammonium
NiO	Nickel Oxide
NO_3	Nitrate
NTF_2	bis (trifluoromethane)sulfonamide
OLEDs	Organic Light Emitting Diodes
PAMAM	Polyamidoamine
PCP	Pentachlorophenol
PDI	Polydispersity Index
PEC	Photoelectriccatalytic
PF_6	Hexafluorophosphate
Pyr	Pyridinium
[Rhod]	Rhodamine 6G Chloride
RTIL	Room Temperature Ionic Liquid
SEM	Scanning Electron Microscopy
SQUID	Superconducting Quantum Interference Device
TEM	Transmission Electron Microscopy
Ti	Titanium
TiO_2	Titanium Dioxide

TPB	Tetraphenyl Borate
UV-vis	Ultraviolet-visible Spectroscopy
VOCs	Volatile Organic Compounds

ABSTRACT

Ionic liquids (ILs) are defined as organic salts with melting points below 100 °C. ILs typically consist of bulky organic cations with anions of varying sizes. Inefficient packing between the cation and anion lead to lower melting points in ILs as compared to traditional salts such as sodium chloride. ILs have garnered significant interest due to their interesting properties such as low volatility, high thermal stability, and tunability. This dissertation presents a study of nanoparticles from an emergent class of compounds derived from a group of uniform materials based on organic salts (GUMBOS). Many GUMBOS are ILs, but some have melting points above 100 °C which is higher than the melting temperature defined for conventional ILs.

The first part of this dissertation explores the synthesis and characterization of nanoparticles derived from GUMBOS. NanoGUMBOS have significant advantages as compared to traditional nanoparticles since they encompass the unique properties of ILs. The tunability of nanoGUMBOS eliminates the need for chemically attaching or functionalizing the surface of these novel nanoparticles for applications such as drug delivery or biomedical imaging. In this study, nanoparticles derived from GUMBOS were synthesized and their size, dispersity, and morphology were characterized using electron microscopy.

The second part of this dissertation focuses on the development of magnetic and fluorescent nanoparticles derived from GUMBOS. The magnetic nanoGUMBOS were synthesized using an *in situ* ion exchange emulsion preparation method. These nanoparticles are advantageous because the magnetic functionality is in the anionic component of the nanoGUMBOS themselves. Controllable formation of these magnetic nanoGUMBOS was achieved in this study and is important for potential applications in hyperthermia treatment as well as drug delivery. The fluorescent nanoGUMBOS were synthesized using three different methods: reprecipitation, *in situ* ion exchange, and a hydrogel preparation technique. This study

investigates the size, dispersity, and the spectral properties of the nanoGUMBOS. These nanoparticles are uniformly fluorescent because the cationic component of the GUMBOS is the fluorophore. These novel fluorescent nanoGUMBOS rival traditional nanoparticles in that they do not involve intricate and tedious dye encapsulation procedures. Size-controlled synthesis of fluorescent nanoGUMBOS is important for potential applications in biomedical imaging.

CHAPTER 1

INTRODUCTION

1.1 Ionic Liquids

Ionic liquids (ILs) are defined as organic salts with melting points less than 100°C.[1-3] Unlike conventional salts with high melting points such as sodium chloride, ILs are typically composed of bulky organic cations with a wide range of sizes for the anions. The lower melting points of ILs have been attributed to inefficient packing of the cation and anion combinations.[4] It has been established that ILs are extremely tunable materials in that a simple manipulation of either the anion or the cation may result in significant changes in their physical properties, thus rendering them useful for a number of applications.[1, 5-9] Due to their unique nature, ILs can dissolve a wide variety of materials such as organic, inorganic, and organometallic compounds. For example, the solubility of an IL can be significantly influenced by exchanging its anion. Common anions such as hexafluorophosphate [PF_6^-], bis (trifluoromethane)sulfonamide [NTF_2^-], and bis(perfluoroethylsulfonyl)imide [$BETI^-$] are hydrophobic and result in ILs which are typically water-insoluble. However, anion-exchange to nitrate [NO_3^-], or chloride [Cl^-] produces ILs which are often water-soluble. In addition, common cations such as phosphonium [PH_4^+], ammonium [NH_3^+], pyridinium [Pyr^+], and imidazolium [Im^+] in the presence of weakly coordinating anions can influence the physical properties of ionic liquids. Increasing the alkyl chain length of the cation, for example, can result in an IL that is hydrophobic while decreasing the hydrocarbon chain length can render the IL hydrophilic. Figure 1.1 illustrates the various cations and anions that are commonly used to synthesize ILs. Based on the anion, the resulting IL can be hydrophobic or hydrophilic.

Due to their unique characteristics, ILs are regarded as "green" solvents since their use decreases the environmental levels of volatile organic compounds which are traditionally used as solvents.[10] It should also be noted that ILs display other useful properties including low volatility, wide electrochemical window, high ionic conductivity, high thermal, chemical, and air stability, and recyclability.[1, 3, 10-14] Because of their desirable properties, ILs have recently gained considerable interest as evidenced by the increase in the number of publications and patents over the last 10 years. Data for 2009 represents only part of the year for ionic liquid publications and patents, respectively, shown in Figure 1.2 and 1.3.

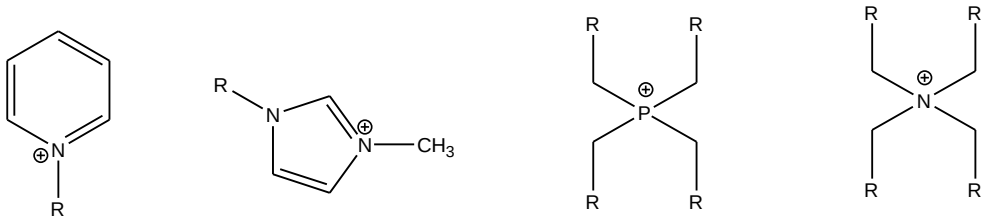

1-alkyl-pyridinium 1-alkyl-3-methyl-imidazolium Tetraalkyl-phosphonium Tetraalkyl-ammonium

Common anions:

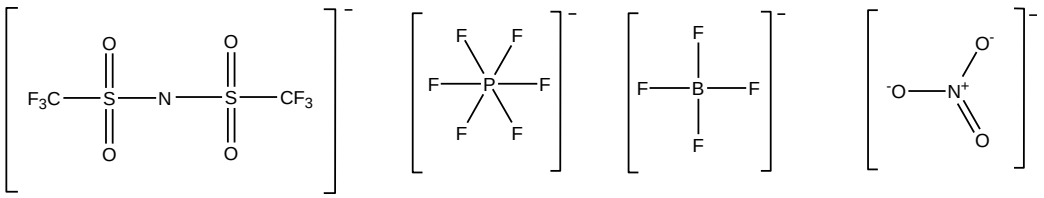

bis(trifluoromethylsulfonyl)imide hexafluorophosphate tetrafluoroborate nitrate

Increasing Hydrophobicity

Figure 1.1 Common cations and anions used in combination for the synthesis of ILs.

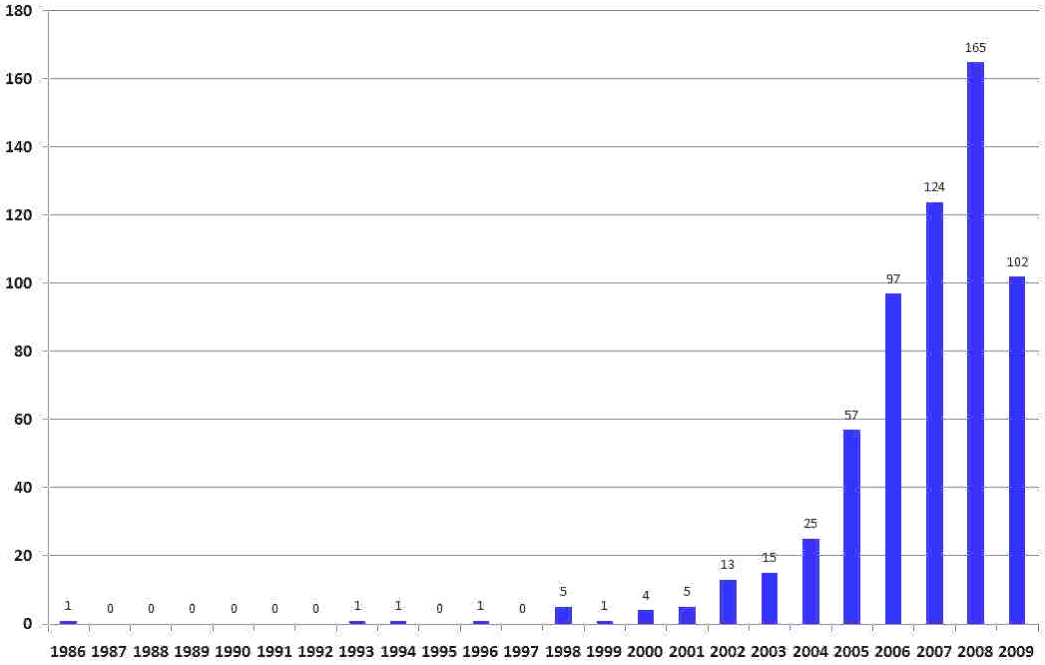

Figure 1.2 Number of publications on ILs per year from 1986 to 2009.

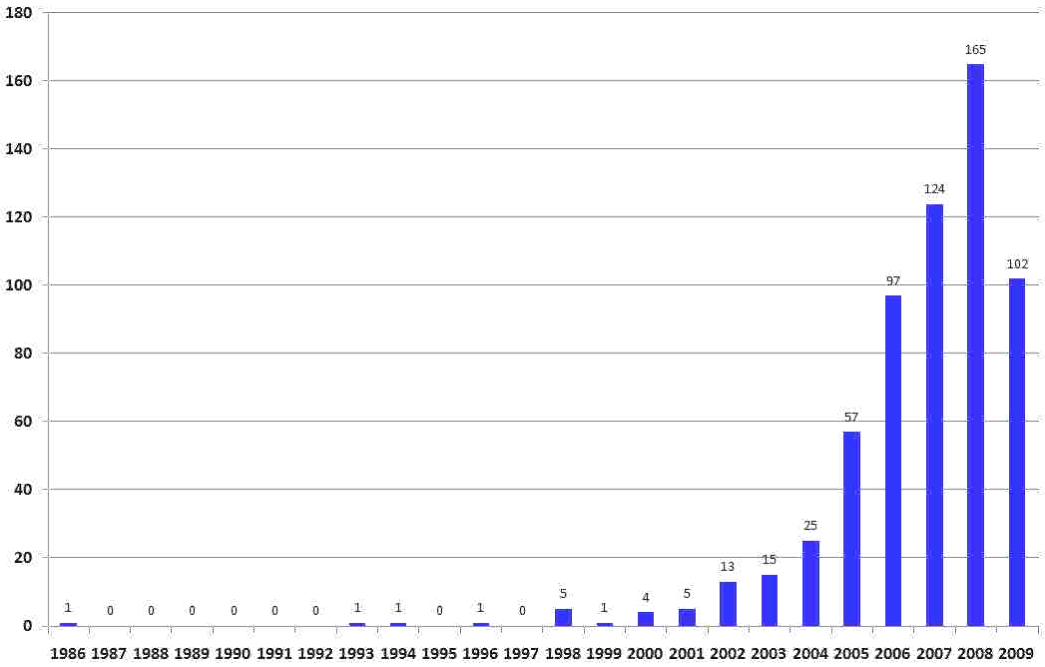

Figure 1.3 Number of patents on ILs per year from 1986 to 2009.

1.1.1 Room Temperature Ionic Liquids

The term room temperature ILs (RTILs) has been used for salts that are liquids near room temperature. The discovery in 1914 of the first RTIL $[EtNH_3][NO_3]$ with a melting point of 12 °C is attributed to Walden.[15] Initially, RTILs were synthesized and employed as electrolytes in batteries. In 2008, Plechkovaa, et al. reported a broad range of applications for ILs in areas such as physical chemistry, electrochemistry, biological areas, analytics, solvents and catalysts, and engineering (Figure 1.4). Specifically, RTILs have been employed for many analytical applications including chromatography,[16-19] extractions,[7-9, 20] catalysis,[21, 22] and nanosynthesis.[23-25] RTILs have been used as stationary phases in gas chromatography,[5, 16-18] as stationary phases[26, 27] and mobile phase modifiers[6, 19] in liquid chromatography, and in capillary electrophoresis as permanent coatings[28, 29] and background electrolyes.[30]

In addition to their use in chromatography, applications of RTILs have gained interest for use in extractions and catalysis. More specifically, they have been used in biphasic extractions of metals,[7, 31, 32] organic acids,[8] chlorophenols,[9] antibiotics,[33] and proteins.[34] In addition, RTILs have been used in biocatalysis[22] and as solvents for organic reactions.[21, 35]

Recently, RTILs have sparked interest in their use as organized media for the templating of nanomaterials. Gao *et al.* reported the use of thiol-functionalized ILs as stabilizers for the synthesis of palladium nanowires.[23] In addition, Ryu *et al.* investigated the use of 1-ethyl-3-methylimidazolium ethylsulfate as a solvent in the synthesis of gold nanorods to achieve control over their shape.[24] Recently, Shigeyasu and coworkers reported 1-butyl-1-methyl-pyrrolidinium bis(trifluoromethylsulfonyl)imide

[C_4mpyrr][NTF_2] RTIL nanoparticles. These nanoparticles were synthesized under low pressure and were obtained from vaporized RTIL [C_4mpyrr][NTf_2]. Particles of 10 nm in diameter were further selected with a differential mobility analyzer.[25]

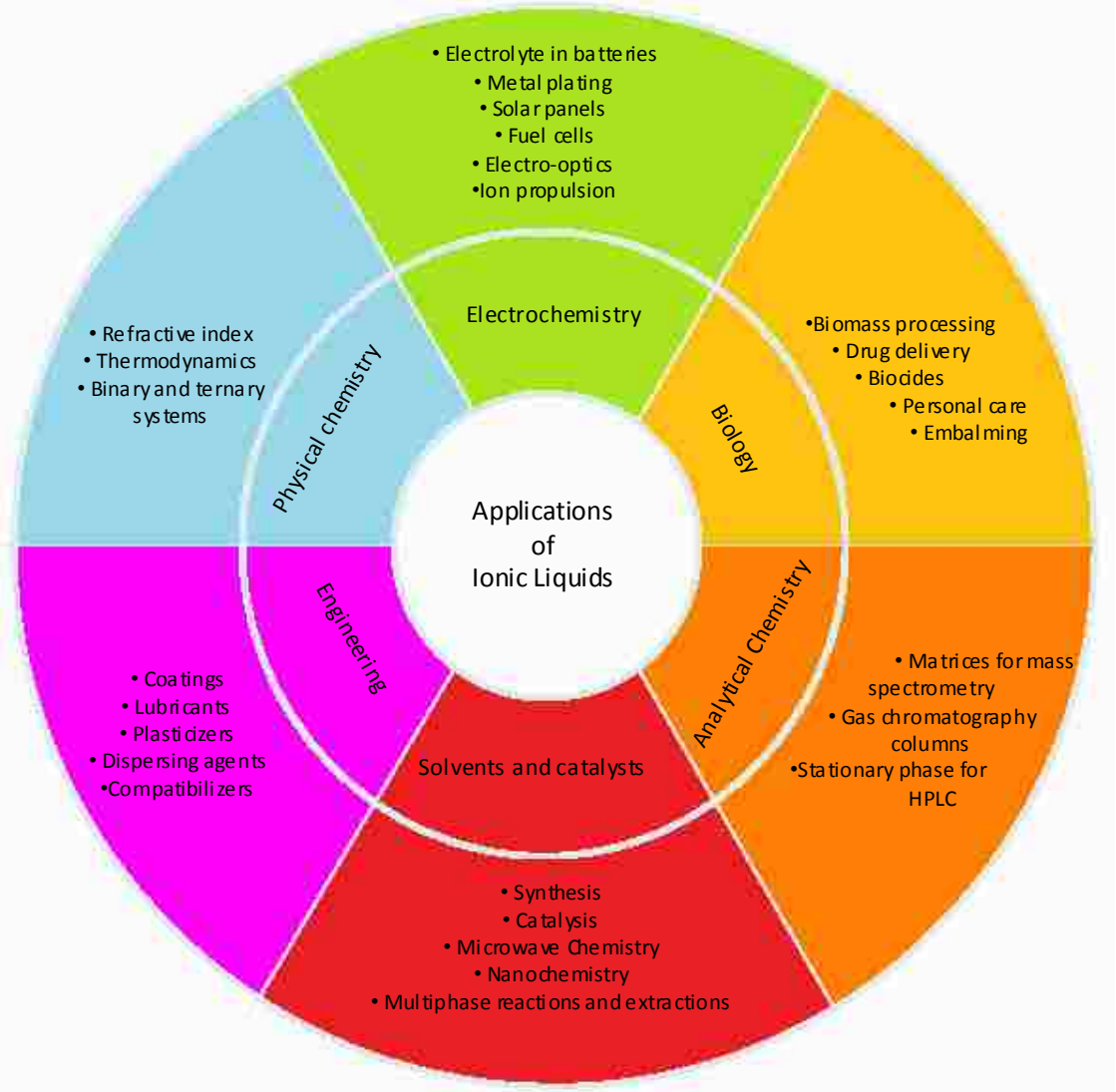

Figure 1.4 Applications of ILs in the various fields of physical chemistry, electrochemistry, biology, analytical chemistry, solvents and catalysts, and engineering, modified from reference.[36]

1.1.2 Frozen Ionic Liquids

Apart from their use in the liquid state, ILs have also gained interest for their use in the frozen state. Frozen ILs are defined as ILs with melting points between 25 and 100°C. In 2007, Rutten *et al.* employed frozen ILs as templates for rewriteable imaging.[37] In addition, the Warner research group recently reported the first nano- and microparticles derived from frozen ILs. A **G**roup of **U**niform **M**aterials **B**ased on **O**rganic **S**alts (GUMBOS) are largely ILs but some have melting points above 100 °C. Nano- and microparticles derived from GUMBOS (which will be discussed in detail in Section 1.5) with average diameters of 88 nm and 3 μm respectively, were synthesized using a facile melt-emulsion-quench approach. In a second method, an emulsifying agent was employed to further control the size of the nanoparticles.[38] Nanoparticles synthesized from GUMBOS are likely to have significant advantages over conventional nanoparticles in that the properties of the GUMBOS are tunable. For example, nanoGUMBOS can be made of functional materials. Due to their ease of functionalization, they do not require lengthy activation procedures to cover the surface with task-specific active groups. Instead the functional groups can be built into the cations and anions. This provided simplicity makes it possible for nanoparticles derived from GUMBOS to be used in applications such as biomedical imaging and drug delivery.[38]

1.2 Group of Uniform Materials Based on Organic Salts (GUMBOS)

Many GUMBOS are ILs, but some have melting points above 100 °C. GUMBOS are interesting materials in that a simple variation of either the anion or the cation can lead to an effective combination of properties, thus rendering them useful for a multitude of applications. For example, GUMBOS can be designed to be biocompatible by

synthesizing GUMBOS from vitamins, amino acid pre-cursors, or drugs. In addition to biocompatible GUMBOS, fluorescent GUMBOS can be similarly synthesized by employing a fluorescent dye as the cation. To produce magnetic GUMBOS, $FeCl_4$ could be used as the paramagnetic anion. A dual functional fluorescent magnetic GUMBOS can be potentially synthesized by employing a fluorescent cationic dye combined with a paramagnetic anion for biomedical applications. Furthermore, gold shell coated GUMBOS can be synthesized for biomedical applications as well. GUMBOS can also be designed to be antibacterial by employing an antibacterial cation (Figure 1.5).

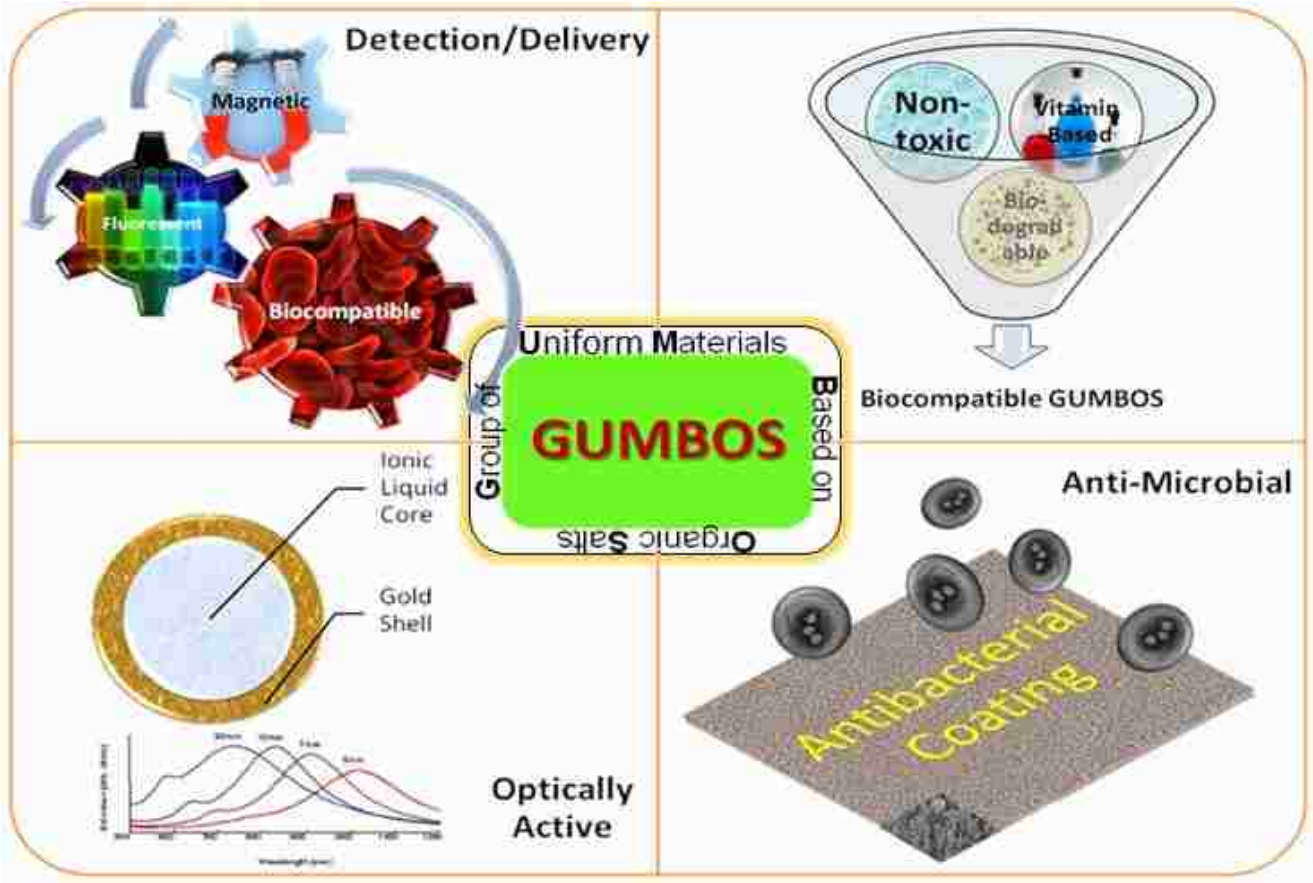

Figure 1.5 Examples of various applications of GUMBOS.

1.3 Nanoparticles

Nanotechnology has garnered considerable attention as evidenced by the increasing number of nanotechnology research publications and patents since the early 90's. Data for 2009 represents only part of the year for nano publications and patents as shown in Figures 1.6 and 1.7, respectively.

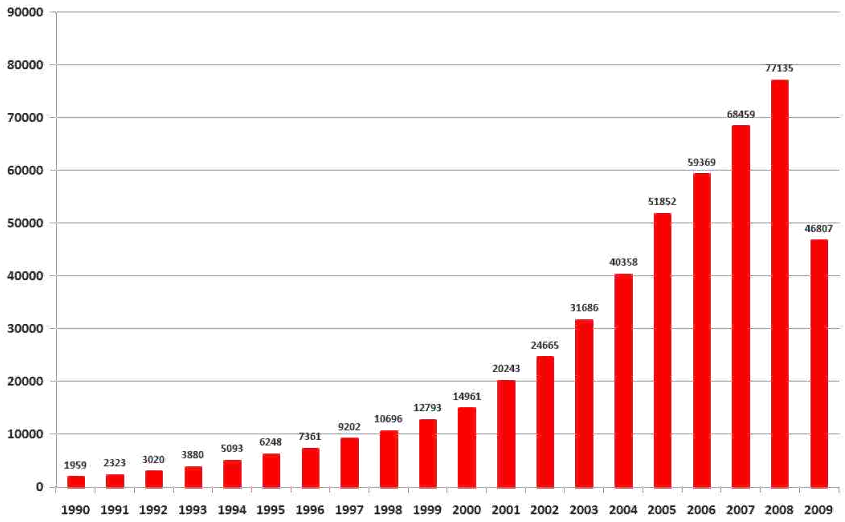

Figure 1.6 Number of publications that reflect the growing interest in nanotechnology since 1990.

Nanoparticles are defined as particles with sizes of 100 nm or less.[39] Nanoparticles are an interesting group of materials that typically exhibit properties which differ from that of the parent bulk material.[40] These materials have a higher surface area to volume ratio compared to their parent bulk materials. Due to this feature, distinct properties are observed. For example, at the macroscale, properties such as surface adsorption have no effect on catalytic activity.[40] However, at the nanoscale, catalytic activity can be significantly improved.[40] Likewise, larger scale particles have limited solubility; however, at the nanoscale, nanoparticles exhibit an enhancement in solubility which is

important in applications such as drug delivery.[40] In medical applications, specific cells in the body are able to uptake particles more efficiently at the nanoscale compared to micrometer particles.[41] In addition to the aforementioned properties that nanoparticles exhibit, spectral changes of fluorescent nanoparticles can also be observed at the nanoscale.[42] As the bulk material approaches nanoscale dimensions, an increase in bandgap energy state relative to the bulk material is usually observed for semiconductor nanoparticles.[40] The bandgap is usually size dependent, typically resulting in a shift to shorter wavelengths with decreasing sizes often observed with semiconductor nanoparticles.[42] Thus, semiconductor nanoparticles often have unique physical and chemical properties which are significantly influenced by the particle size and morphology.[43-46] For example, the spectral properties of semiconductor nanoparticles are often directly correlated to their size.[47] The absorption band for bulk CdSe extends to 690 nm while the λ_{max} of nanoparticles derived from CdSe shifts to 530 nm. The size of the particles also influences their physical and chemical properties such as melting point and phase transition temperature.[48]

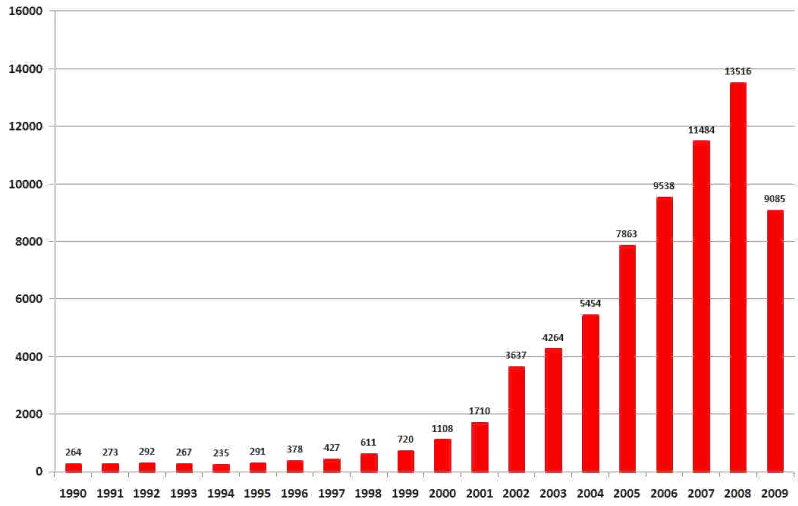

Figure 1.7 Number of patents that reflect the growing interest in nanotechnology since 1990.

1.3.1 Applications and Importance of Size Control of Nanoparticles

1.3.1.1 Drug Delivery

Nanoparticles have gained considerable interest for proposed applications in drug delivery,[41, 49] bio-imaging,[49, 50] microbial detection,[51-53] and environmental applications.[54, 55] Nanoparticles are important in drug delivery because they provide a significantly higher intracellular uptake than micron size and larger scale particles. Because of their size, nanoparticles can diffuse through small capillaries and enter deeply within tissues.[41, 49] For example, Chithrani *et al.* reported that the uptake of nanoparticles by mammalian HeLa cells is dependent on the size of the nanoparticle. Furthermore, a 50 nm nanoparticle was taken up by the cells more efficiently than larger size nanopartlces.[56, 57]

1.3.1.2 Bioimaging

Nanoparticles have also found applications in bio-imaging. For example, the identification of pathogenic bacteria has been obtained in conventional fluorophore-based labeling systems. Labeling oligonucleotide targets with 13 nm gold nanoparticles as compared to fluorescent reporters such as organic dyes improved the selectivity 3-fold relative to conventional fluorescent reporter targets.[50]

1.3.1.3 Microbial Detection

Another area of interest where nanoparticles have been employed is in microbial detection. Quantum dots with sizes of 3-10 nm have been used as fluorescent labels in microbial detection. It has been demonstrated that when quantum dots were used as fluorescent labels, the microbial detection system demonstrated as high as a 9-fold higher signal as well as a significant increase in photostability and multiplexing capability as compared to conventional organic dyes.[51-53]

1.3.1.4 Environmental Applications

Particle size also plays a significant role in environmental applications. Quan *et al.* used TiO_2 nanotubes for the degradation of pentachlorophenol (PCP) using photoelectriccatalytic (PEC) processes. It was observed that the kinetic constant of the PEC degradation of PCP was 86.5% higher in TiO_2 nanotubes with diameters ranging from 30 to 90 nm as compared to a Ti film. In addition, 70% of the total organic compounds were removed when using the TiO_2 nanotubes, while only 50% was removed using the Ti films.[55]

1.4 Synthetic Methods for Size Controlled Nanoparticles

1.4.1.1 Template Synthesis

Templates can be divided into two categories: "soft" and "hard" templates. Soft templates encompass micelles, naturally occurring gels, and reverse micelles.[40] Micelles are organized assemblies of polar head groups and nonpolar tails. The nonopolar tails form the core of the micelle while the polar head groups orient themselves towards the aqueous microenvironment. Hydrophobic nanoparticles can therefore be synthesized in the core of the micelle. Reverse micelles also consist of hydrophobic and hydrophilic domains. They are formed in the presence of an organic solvent and relatively small amounts of water. The polar head groups spontaneously form the core of the micelle and the nonpolar tails orient themselves towards the bulk organic solvent. The core of the micelle contains pockets of water and acts as nanoreactors for the synthesis of nanoparticles. Size control for the above micellar methods can be achieved by varying parameters such as concentration of reagent, temperature, solvent composition, and molar ratio of water to surfactant. Hydrogels can also be used to synthesize nanoparticles of a

well controlled size. Hydrogels are polymeric networks with a three dimensional configuration. Hydrogels can be formed from naturally occurring bile salts. Increasing the concentration of bile salts dissolved in an acidic buffer ~pH 6.0 above its critical micelle concentration (cmc) (concentration at which micellization occurs) causes the gelation of water and results in a hydrogel with both hydrophilic and hydrophobic domains. Nanoparticles of a well controlled size can be synthesized within these rigid domains. Size control can be achieved by varying the reagent concentration. On the other hand, hard templates include porous materials such as anodic alumina membranes and.[58] During the process of anodizing, an insulating oxide layer on a conductive metal oxide anode in an electrolytic solution of dilute polyprotic acid is created. The metal oxide is typically composed of aluminium. Hexagonally packed pore channels are created and are easy to fabricate. Size control for the hard-templating method is dependent on the pore geometry of the template such as the pore diameter.

1.4.1.2 Chemical Vapor Condensation (CVC)

CVC consists of a reaction chamber and a precursor delivery system. Individual molecules located in the heating tube begin to decompose and form nanoparticles. The nanoparticles then condense onto a surface cooled with liquid nitrogen thus allowing for the particles to be collected.[59] Although nanoparticles can be produced, controlling their size is often difficult.

1.4.1.3 Metal Reduction

This process involves the reduction of metal ions by chemical reductants.[40] For the synthesis of traditional nanoparticles such as gold nanoparticles, $NaBH_4$ reduces Au^{3+} ions to neutral gold atoms. Supersaturation occurs and gold precipitates as nanoparticles.

Particle size can be controlled by parameters such as pH and concentration of reducing agent.

1.4.1.4 Sonochemical

Sonochemistry involves chemical reactions between molecules in the presence of ultrasound radiation (20 kHz to 100 MHz). The processes that occur in sonochemistry involve the following: formation, growth, and collapse of a bubble formed in a liquid. Chemical bonds are broken during the final stage which occurs in less than a nanosecond. Due to the collapse occurring on such a fast time scale, extremely high cooling rates are produced. Crystallization of the products is prevented due to the extremely high cooling rates, thus resulting in amorphous nanoparticles. This method is simple and particle size can be controlled by varying the concentration of the initial metal compounds.[59]

1.5 Nanoparticles Derived from GUMBOS: NanoGUMBOS

NanoGUMBOS have distinctly different properties from traditional nanoparticles in that GUMBOS are tunable by varying the structure of the cation/anion. In fact, GUMBOS can potentially mimic the properties of several nanoparticles commonly cited in the literature due to their inherent tunability.[60-62] Nanoparticles such as quantum dots are known to be cytotoxic, therefore it is of importance to develop biocompatible nanoparticles for applications in nanomedicine. NanoGUMBOS can be synthesized from biologically-friendly materials such as amino acids, thereby leading to non-toxic nanoparticles for use in biomedical applications.

Fluorescent nanoparticles such as quantum dots are known to be highly luminescent, however they are known to be toxic to human tissue. Fluorescent nanoGUMBOS can be synthesized and used in biomedical applications as well. For

example, a fluorescent nanoparticle can be synthesized from GUMBOS using a fluorescent dye as the cation and a biocompatible anion such as an amino acid ester.

Magnetic nanoparticles such as iron oxide nanoparticles require laborious synthesis procedures. However, magnetic nanoGUMBOS can be rapidly prepared and easily functionalized. NanoGUMBOS synthesized with a paramagnetic anion such as $FeCl_4$ can be employed and paired with an organic cation for possible applications in drug delivery and magnetic hyperthermia treatment of cancer.[63]

To enjoy both fluorescent and magnetic properties, the cation can be composed of a fluorescent dye, while the anion can be comprised of a paramagnetic species. Therefore, a nanoparticle synthesized from these dual-functional GUMBOS could be uniformly fluorescent and magnetic. These dual functional nanoGUMBOS could potentially be used for simultaneous detection and treatment of tumors. The fluorescent portion of the nanoparticle could be used to detect for the presence of the tumor by means of antibodies. Then the environment of the tumor could be subjected to a high frequency magnetic field and the particles would absorb the energy from the high frequency magnetic field and convert it to heat. Thus, the nanoparticles would become powerful sources of heat and destroy the tumor cells which are sensitive to temperatures above 41 °C. The synthesis of conventional magnetic fluorescent nanoparticles is often laborious and tedious as compared with the synthesis of nanoGUMBOS. For example, a magnetic nanoparticle is typically synthesized initially. Next, a layer of silica is coated around the magnetic nanoparticle followed by functionalization of silica with amine groups. Finally, a fluorescent molecule is conjugated on the surface of the silica.[64] In contrast, dual functional nanoGUMBOS could potentially be advantageous compared to conventional

magnetic fluorescent nanoparticles because both functional properties could possibly be built into the cation and the anion. Also, the synthesis of dual functional nanoGUMBOS is facile and rapid compared to the intricate synthesis of conventional magnetic fluorescent nanoparticles.[64, 65]

NanoGUMBOS can also be coated with gold nanoshells. The use of gold nanoshells as photothermal labels allows one to work in a broad spectral region, from 600 to 1500 nm. Therefore, nanoGUMBOS coated with gold could be employed for applications in drug delivery.

NanoGUMBOS can also be synthesized to be antibacterial by using an antibacterial cation for applications as hydrophobic coatings for medical tools and treatment materials. The effective activity of antimicrobial nanoGUMBOS is hypothesized to increase as the particle size decreases due to an increased surface area to volume ratio.

1.5.1 Methods for Size Control for NanoGUMBOS

1.5.1.2 Melt-Emulsion-Quench Technique

The melt-emulsion quench technique involves the melting of a hydrophobic GUMBOS dispersed in water raised above the melting point of the GUMBOS. Homogenization and probe sonication were subsequently employed to form the oil-in-water (o/w) emulsion and reduce the size of the emulsion. The o/w emulsion was then rapidly cooled in an ice-water bath to form discrete solid nanoGUMBOS outlined in Figure 1.8. MicroGUMBOS can be achieved by employing homogenization for 30 seconds and then rapidly cooling on ice. Another method to synthesize nanoparticles of a well controlled size follows the aforementioned steps; however, in this case nanoparticles

are formed with the aid of a non-ionic surfactant, Brij 35. The hydrophobic GUMBOS was melted in one vial. In another vial, a solution of a 1% aqueous solution of Brij-35 was added. The melted GUMBOS was added to the aqueous solution of Brij-35 while undergoing homogenization and probe sonication to form the oil-in-water (o/w) emulsion and reduce the size of the emulsion. The o/w emulsion was then quenched on ice to produce solid nanoGUMBOS. Surfactant monomers are always in dynamic equilibrium with the micelle. Above a certain concentration of the surfactant monomers called the critical micelle concentration (CMC), micelle formation occurs and the organized assemblies of surfactant monomers are formed. The hydrophobic tails form the core of the assembly and the polar head groups orient themselves towards the aqueous medium as shown in Figure 1.9. The surfactant typically orients itself between the oil and water phase of the nanoparticle to prevent coalescence or aggregation. A surfactant typically is used to control the size and to reduce the polydispersity of the nanoparticle.

1.5.1.3 Reprecipitation

In the reprecipitation method, the fluorescent GUMBOS is dissolved in a solvent such as acetone or in short chain alcohols at a millimolar concentration. Next, an aliquot of the solution is added to a specific volume of a poor solvent (which is a solvent that is miscible with the solvent that was used to dissolve the fluorescent GUMBOS) while undergoing sonication. It is important to note that the fluorescent GUMBOS must not be soluble in the nonsolvent. The fluorescent GUMBOS now precipitates into the nonsolvent as outlined in Figure 1.10. Particle size can be controlled by the concentration of fluorescent GUMBOS, choice of solvent, sonication, and addition of surfactants.

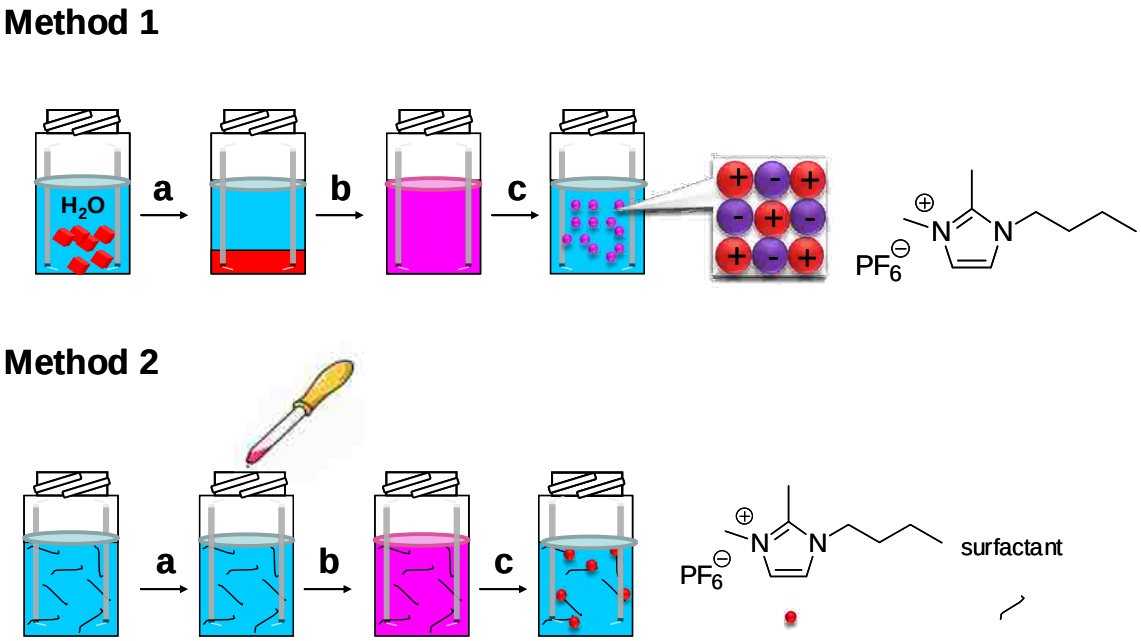

Figure 1.8 Steps of the melt–emulsion–quench method for synthesizing nano- and microparticles using no surfactant (Method 1) and employing surfactant (Method 2). In Method 1, the first step (a) melting of hydrophobic IL in a hot water bath, whereas addition of melted IL to a surfactant solution is performed in Method 2. Homogenization and probe sonication are performed in (b), quenching of o/w emulsion to solidify nanoparticles (c) modified from reference.[38]

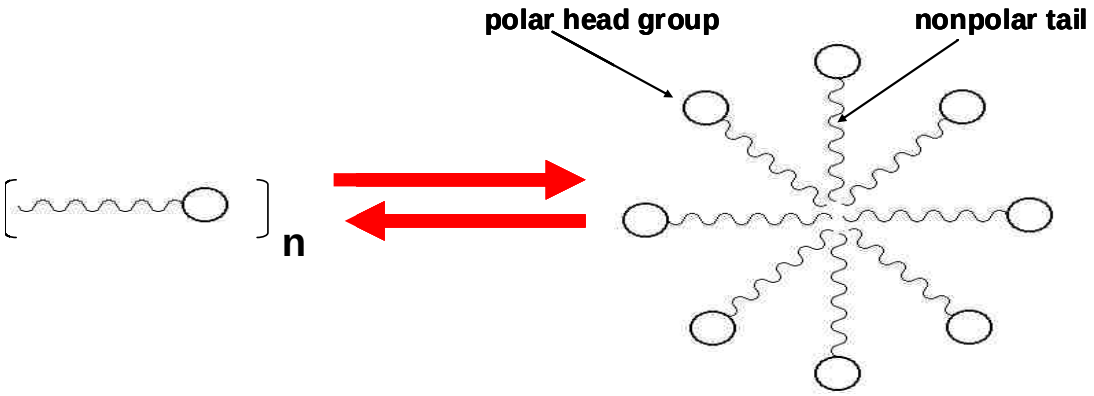

Figure 1.9 Schematic of micelle formation at surfactant concentration exceeding the CMC.

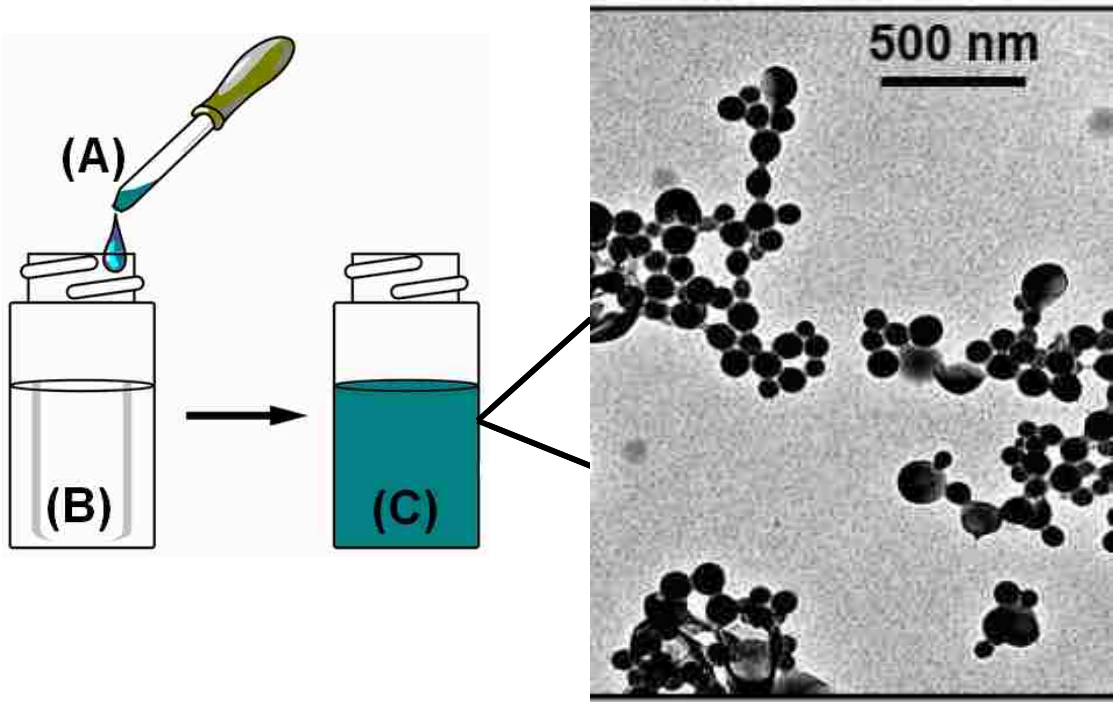

Figure 1.10 Preparation of fluorescent nanoGUMBOS using the reprecipitation method. (A) GUMBOS solution in solvent (1 mM ethanol), (B) dispersant (5 mL water), and (C) nanoparticle suspension in dispersant.[66]

1.5.1.4 Reverse Micelle Synthesis

Difficulties in the synthesis of monodispersed nanoparticles have lead researchers to attempt to control their sizes using surfactants and organic ligands.[67] In recent years, amphiphilic molecules or surfactants containing both hydrophilic and hydrophobic groups have attracted much attention for their ability to form reverse micelles.[68] AOT reverse micelles have proven to be significant in syntheses of nanoparticles due to their ability to solubilize relatively large amounts of water of well controlled size (water pools).[69] These nanometer-sized water pools can be adjusted by varying the molar ratio of water to surfactant. The pockets of water not only act as nanoreactors for the synthesis of nanoparticles, but also reduce nanoparticle aggregation. Therefore, AOT reverse micelles are a suitable organized medium for synthesizing nanoparticles with a narrow size

distribution. As mentioned above, amphiphilic molecules are an attractive class of organized media for investigation due to their ability to form reverse micelles in nonpolar media. Instead of the polar head groups of the micelle extending outward, as shown in conventional micelles (Figure 1.11), the hydrophilic head groups in reverse micelles form the core of the assembly and the hydrophobic domains protrude outward. The polar head groups aggregate toward the interior of the micelle, and therefore small amounts of water can be encapsulated.

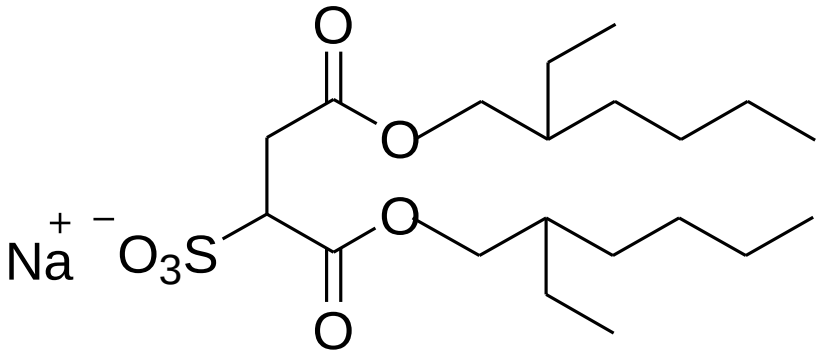

Figure 1.11 Molecular structure of sodium bis(2-ethylhexyl) sulfosuccinate (AOT).

Both cationic and anionic surfactants have been used to form reverse micelles.[70] However, the anionic surfactant AOT is well known for the formation of reverse micelles when solubilized in nonpolar solvents followed by the addition of small amounts of water. AOT is composed of two hydrophobic tails with a polar sulfonate head group as shown in Figure 1.11. As previously stated, when the reverse micelle forms, water is encapsulated. In this reverse micellar system, four microenvironments are observed and are represented in Figure 1.12. The four microenvironments are the AOT interface, the hydrocarbon region, an inner free water pool, and a bound water region.[68] When water is solubilized in

reverse micelles, it can be bound at the sulfonate head groups and can also be bound to the sodium counter ions. These two processes are termed the "bound water layer." Water that is less tightly bound to the polar head groups exhibits characteristics of bulk water and this aqueous microenvironment is termed "the inner free water pool."[68] The water pools that are formed in the interior of the reverse micelle can vary with a relationship that correlates the concentration of water to the concentration of the surfactant, or R = $[H_2O]$/[surfactant].

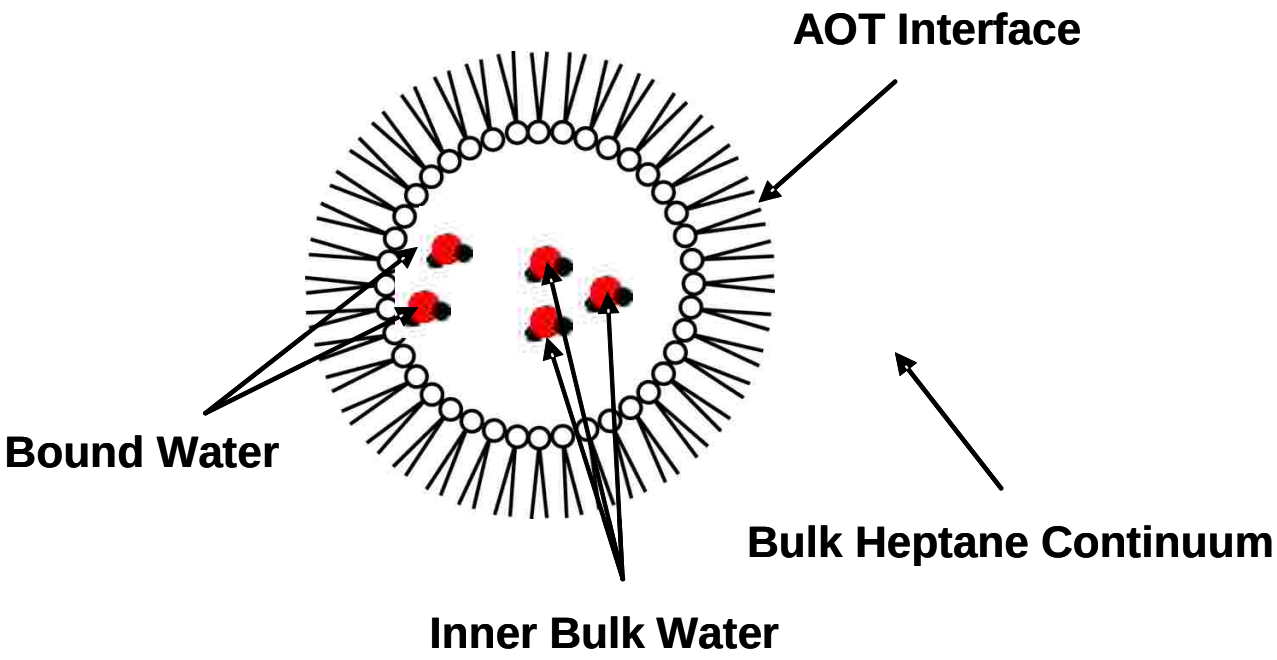

Figure 1.12 Four principal microenvironments in the reverse micellar system.

In the reverse micellar method (Figure 1.13), two identical w/o emulsions are mixed together, each containing the desired reagents (A) and (B). After combining the two microemulsion solutions, particles are produced by the following steps: (1) Diffusion of reverse micelles; (2) surfactant layer opening and coalescence (temporary fusion); (3) diffusion of solubilized molecules; (4) reaction between the solubilized molecules and particle formation (C) as well as water soluble salt (D), and (5) decoalescence (fission) to return as reverse micelles.[70] Particle size can be controlled by varying the surfactant

concentration, reagent concentration, choice of nonpolar solvent, temperature, mixing duration, and the molar ratio of water to surfactant.

1.5.1.5 Aerosol Synthesis

The aerosol approach requires a micromolar solution of GUMBOS dissolved in anhydrous methanol. The solution is then aerosolized using a constant output atomizer, and removal of water is achieved by subsequent passage of the aerosol through a silica gel drier. Then the aerosol passes through the electrostatic classifier which separates the particles by size. Next the solvent is evaporated with a tube furnace with an operating temperature of 25-400 °C. The flow direction valve can be adjusted to allow particles to be collected onto the filter paper or characterized using the particle size counter. The dried particles are then collected on a 2 μm PTFE filter paper. Particle size and distribution are obtained using a particle size counter as shown in Figure 1.14.

1.5.1.6 Hydrogel Synthesis

In the hydrogel method, the compound of interest is dissolved in an ethanolic solution. Sodium deoxycholate is dissolved in an acidic buffer and an aliquot of the ethanolic solution is rapidly injected into the acidic sodium deoxycholate solution while undergoing sonication. Sodium deoxycholate (NaDC) consists of both hydrophobic (steroid backbone) and hydrophilic (OH) groups. NaDC forms hydrophobic interactions between the hydrophobic domains above its cmc which causes primary micelles. As the concentration increases, secondary micelles form due to hydrophilic interactions between the OH groups. Decreasing the pH causes the protonation of COO^- groups present within NaDC. This protonation results in more hydrogen bonding and ultimately leads to the

gelation of water which results in a hydrogel. Particles can then precipitate within either the hydrophobic or hydrophilic domains of the hydrogel (Figure 1.15).

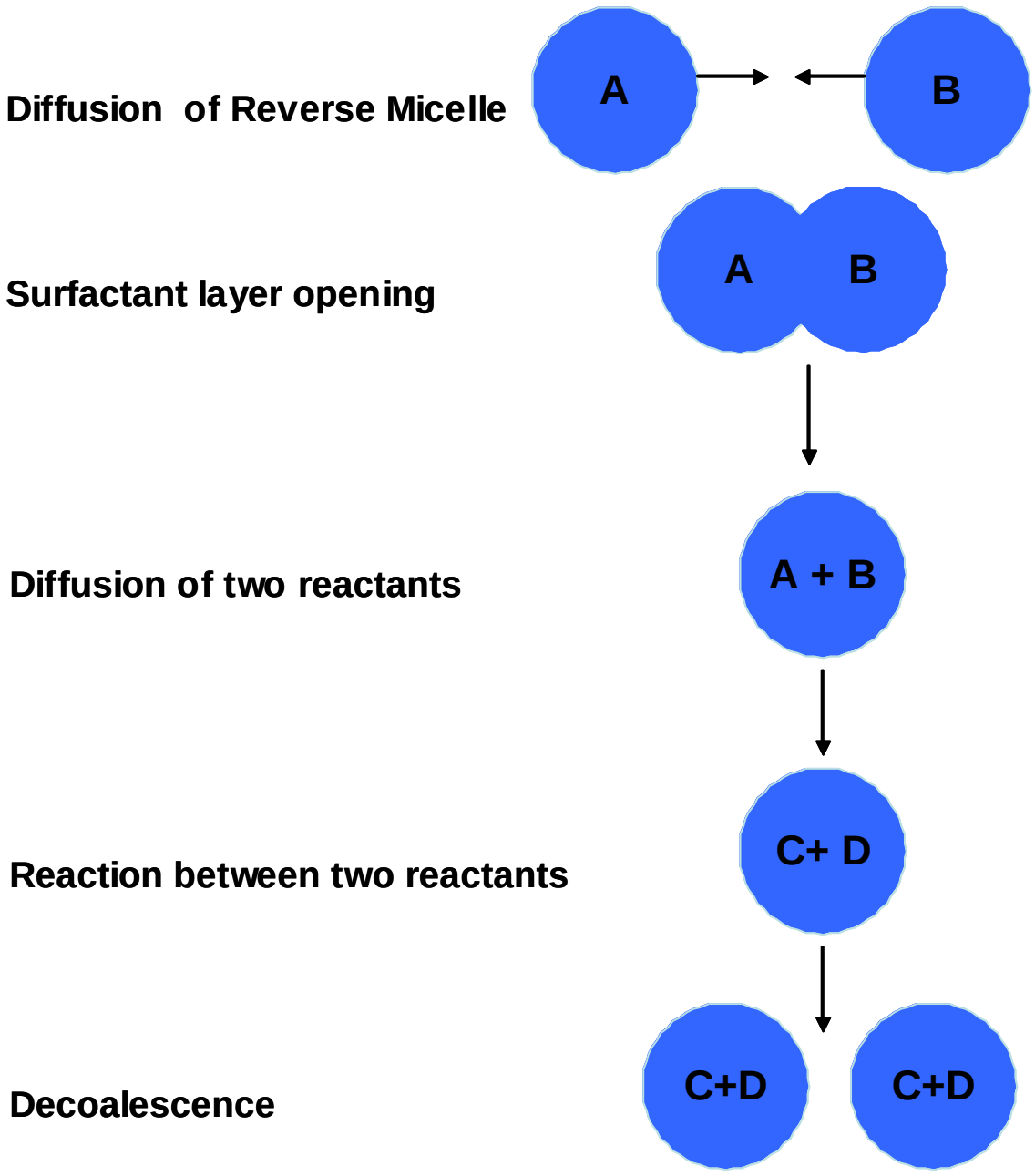

Figure 1.13 Basic processes for nanoparticle formation within AOT reverse micelles. Individual reverse micelles are shown without surfactant for brevity.[63]

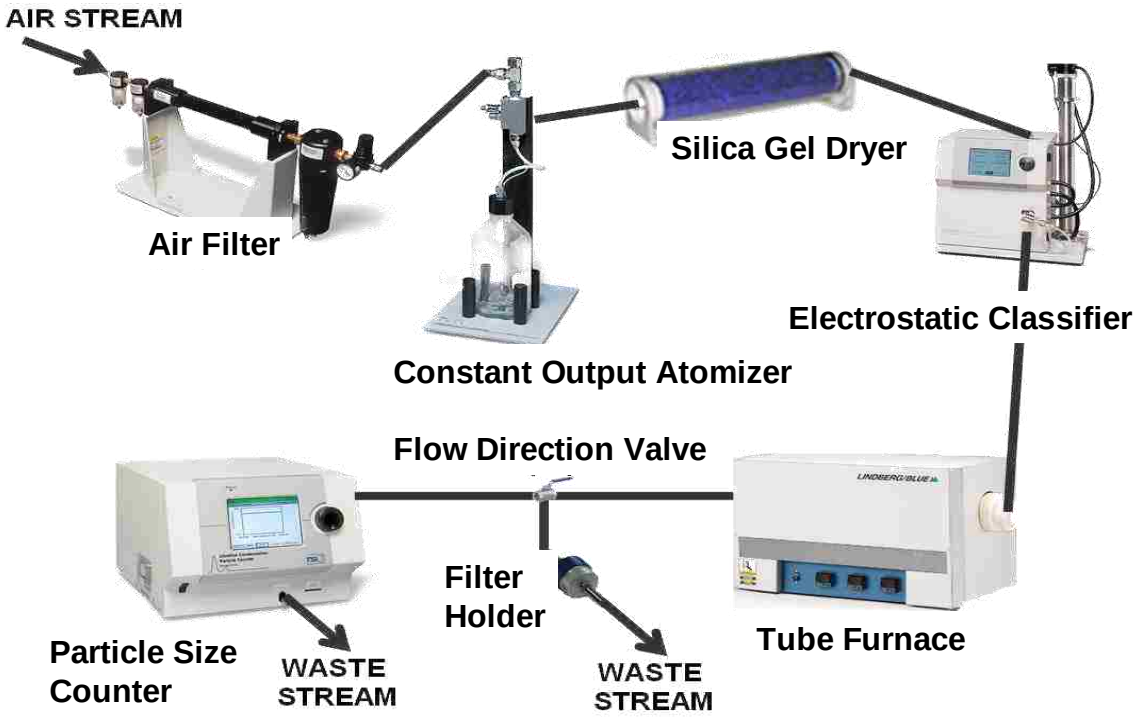

Figure 1.14 Representation of the aerosol process for formation of nanoGUMBOS.

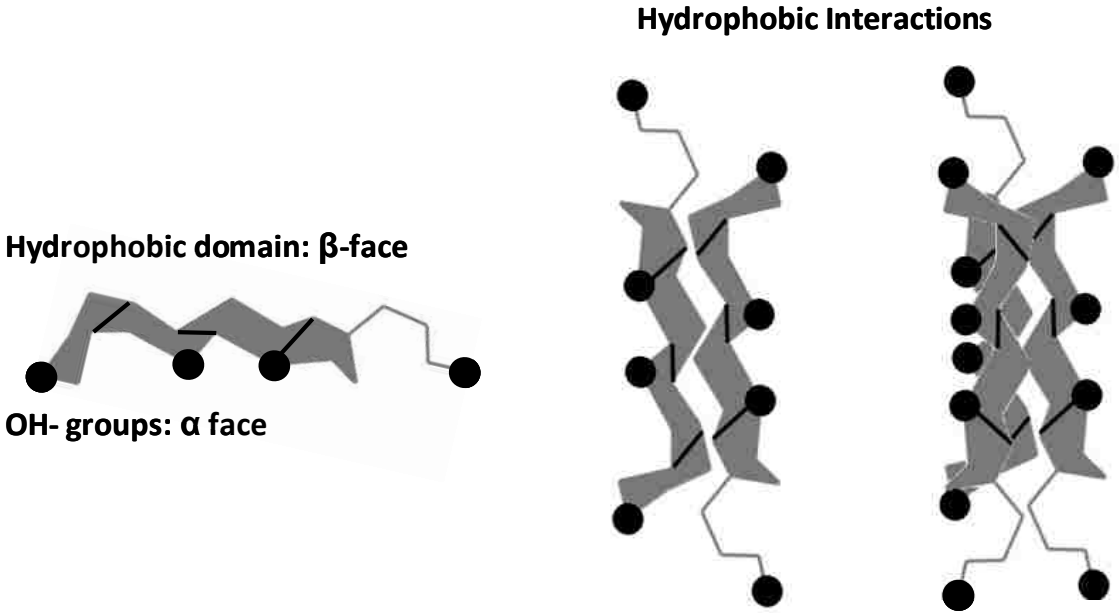

Figure 1.15 Basic processes for nanoparticle formation within hydrogels modified from reference.[71]

1.6 Analytical Techniques Used in this Study

1.6.1 Scanning Electron Microscopy

Scanning Electron Microscopy (SEM) (Figure 1.16) is a technique used for characterization of particle size and morphology. An electron gun is used to generate electrons. Because the electron beam which exits the electron gun is divergent, a condenser lens is employed to focus the electrons. The lenses in the scanning electron microscope are controlled by a magnetic field. Therefore, a series of condensing lenses are used to focus the electrons down the column. Astigmation of the image can also occur due to imperfections in the magnetic lenses and contaminants present within in the column. Therefore to correct for the imperfections in the magnetic lenses and contaminants present within the column, stigmator lenses housed in the objective lens are used. Scanning coils scan the focused electron beam across the sample, and the objective lens focuses the beam to a small spot on the sample. Backscattered and secondary electrons leave the sample once the electron beam comes in contact with the sample. The secondary electrons are collected by a photomultiplier tube that amplifies the electron signal. The surface features that face the detector will result in more backscattered and secondary electrons and therefore an enhancement in the signal. Backscattered electrons are collected by a semiconductor array. The SEM samples are prepared onto a metal stub with conductive tape. In addition, the samples in SEM have to be electrically conductive. Therefore a sputter coater is used to coat the sample placed on the metal stub with gold. The spatial resolution of a conventional SEM is ~ 1-5 nm.

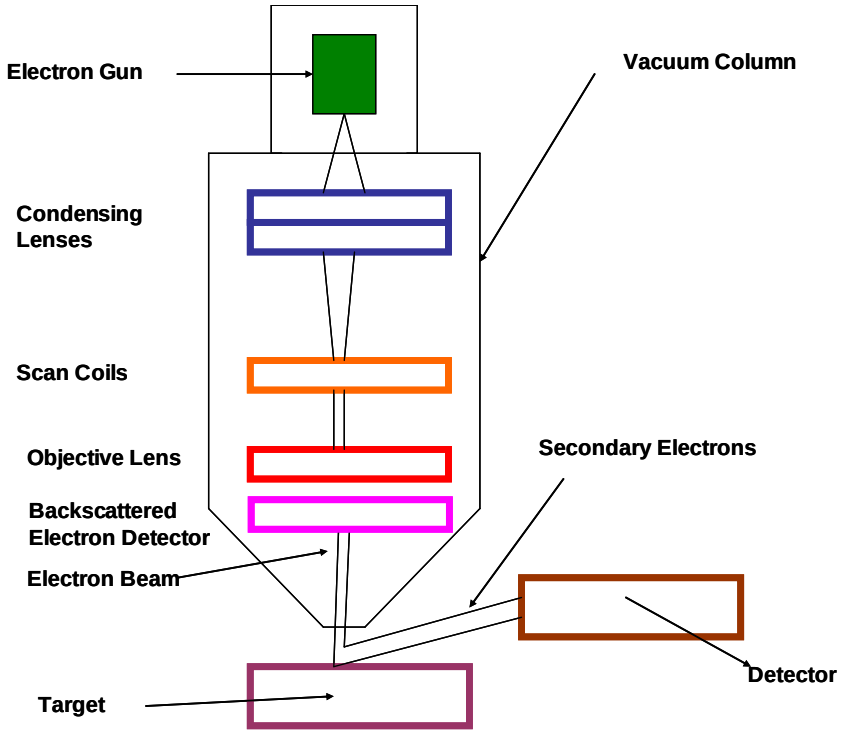

Figure 1.16 Diagram of scanning electron microscope modified from reference.[40]

1.6.2 Transmission Electron Microscopy

Transmission Electron Microscopy (TEM) (Figure 1.17) is a technique used to characterize particle size. The electron gun accelerates the electrons between 100 and 400 kV. The electrons are focused into a thin beam by the condenser lenses. The electron beam hits the sample and parts of it are transmitted. The transmitted electrons are then focused by the objective lens. The projector lens projects the electrons onto a phosphor screen where the image is finally captured by a photographic camera or a charge-coupled device (CCD) camera. The darker regions of the sample indicate fewer electrons were transmitted through the sample, and the lighter regions indicate more electrons were transmitted through the sample. The CCD camera functions by converting photons into an image. Photons are produced from electrons directed onto the phosphor screen. To take an image, the phosphor screen is raised to allow access to the CCD camera. After

the image is captured, the phosphor screen returns to its original position. Samples are typically placed on a carbon coated copper grid ~ 100 μm thick and 3 mm in diameter. During imaging, the morphology of the sample can change due to heat being produced from the high-voltage electronic beam. Also, using a TEM can often be costly and difficult to maintain. However, many types of samples can be imaged with TEM such as electrically insulating, semiconducting, or conducting for example. In addition, the spatial resolution of a conventional TEM is < 1 nm.

1.6.3 Differential Interference Contrast

Differential interference contrast (DIC) (Figure 1.18) is an optical microscopy technique used to view transparent samples. The light source is a tungsten lamp. The unpolarized light passes through a polarizing filter which polarizes the light into one plane. The light passes through the 1st prism which splits the beam of light into two beams traveling in different directions. The distance between the two beams is referred to as "shear distance." The condenser focuses the two beams which pass through the sample. The paths of the beams are altered due to many factors such as the thickness, slope, and refractive index of the sample. The light passes through the sample and is then focused by the objective. The 2nd prism recombines the two beams into the same plane. Thus, the second prism functions to remove the shear and the original path difference that was originally present between the two beams. The light is then collected by a detector. The spatial resolution for a conventional DIC is ~ 200 nm. When performing DIC, it is often observed that one side of an object will appear bright while the other side will appear to be lighter. This difference in intensity will result in a shadow which yields a

pseudo three-dimensional appearance. Therefore, this pseudo three-dimensional appearance is not a correct assessment of the geometry of the sample.

1.6.4 Fluorescence Microscopy

Fluorescence microscopy (Figure 1.19) is an optical microscopy technique used to view fluorescent compounds. In fluorescence microscopy, the excitation light source is passed by the excitation filter and reflected by a dichroic mirror onto the sample via objective lens. The molecules within the specimen will absorb a photon of light, which will result in the promotion of an electron to a higher energy state. Relaxation of the electron back down to the ground state will result in the emission of a photon, leading to fluorescence. Fluorescence occurs in all directions and the fluorescence emission is collected by the objective and is passed through the dichroic mirror. The emission filter blocks any undesired excitation wavelengths. The fluorescence emission is then collected by a detector which converts the photons to an electrical signal. The image is then generated by a computer which processes the electrical signal. The spatial resolution for a conventional fluorescence microscope is ~ 200 nm. Fluorescence microscopy is an interesting and important technique that has garnered interest in the biomedical field. The identification of cells and cellular components can be investigated with this technique. For example, cells and diseased tissues can be visualized with the fluorescence microscopy.

1.6.5 Atomic Force Microscopy

Atomic force microscopy (AFM) (Figure 1.20) is an imaging technique used for surface characterization. The AFM consists of a cantilever with a sharp tip at its end that is used to scan the surface of the material. Typically the tip is scanned over the surface of a

sample and deflection of the cantilever is caused by forces between the tip and the sample. The deflection is measured using a laser beam reflected from the top surface of the cantilever into a set of photodiodes. The surface is scanned by the tip to yield a three-dimensional image of the surface of the sample. A constant force between the tip and the sample is maintained by the use of a feedback mechanism which controls the distance between the tip and the sample. The piezoelectric tube scans the sample by moving it in three dimensions; the x, y, and z dimensions. The spatial resolution of a conventional AFM is ~ 1 nm. AFM is advantageous in that it can be performed at ambient conditions, no vacuum is required, and no expensive high energy beam is needed.

Tapping mode imaging was employed throughout this dissertation and thus will be discussed here. Tapping mode AFM is often performed when the surfaces of samples are easily damaged or weakly bound to their substrate. Tapping mode is often the mode of choice because the tip does not drag across the surface of the sample. This mode avoids problems such as electrostatic forces and adhesion to substrates that often occur when other modes of AFM are employed. In tapping mode imaging, the cantilever is oscillated near its resonant frequency. The tip then lightly touches or taps the surface of the sample.

1.6.6 UV-visible Spectroscopy (UV-vis)

UV-vis absorption spectroscopy is used for analysis of molecules that absorb ultraviolet and visible light (photons). When a molecule absorbs a photon of light, electrons in the molecule are promoted to a higher energy level. In a spectrophotometer, illustrated in Figure 1.21, light passes through a monochromator which selects a wavelength. This monochromatic light passes through the sample and the transmitted

light is often detected by use of a photomultiplier tube or photodiode-array. By plotting absorbance units versus the wavelength, an absorption spectrum is obtained. The Beer-Lambert law is used to describe absorbance; $A = \varepsilon bc$, where ε is the molar absorptivity ($L \cdot mol^{-1} \cdot cm^{-1}$), b is the path length in centimeters, and c is the concentration of the sample. λ_{max} is the wavelength of maximum absorption.

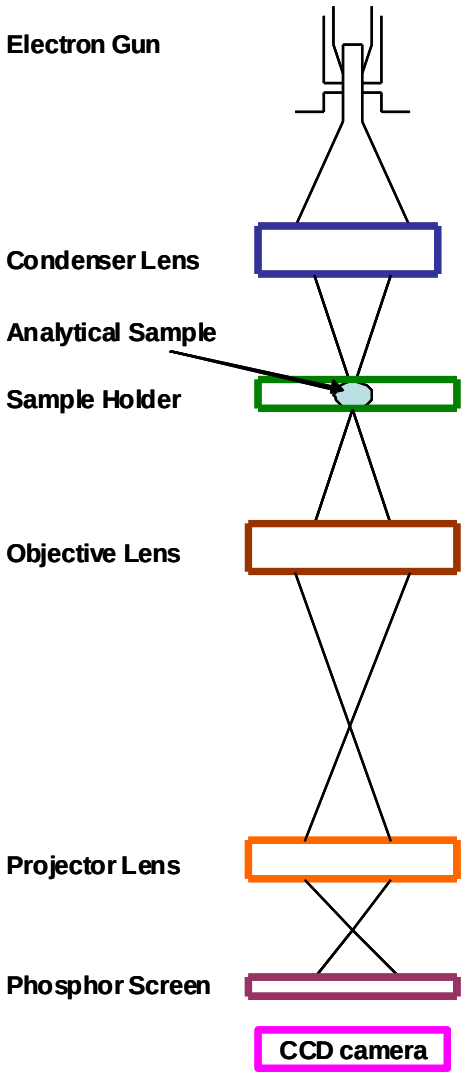

Figure 1.17 Diagram of transmission electron microscope modified from reference.[40]

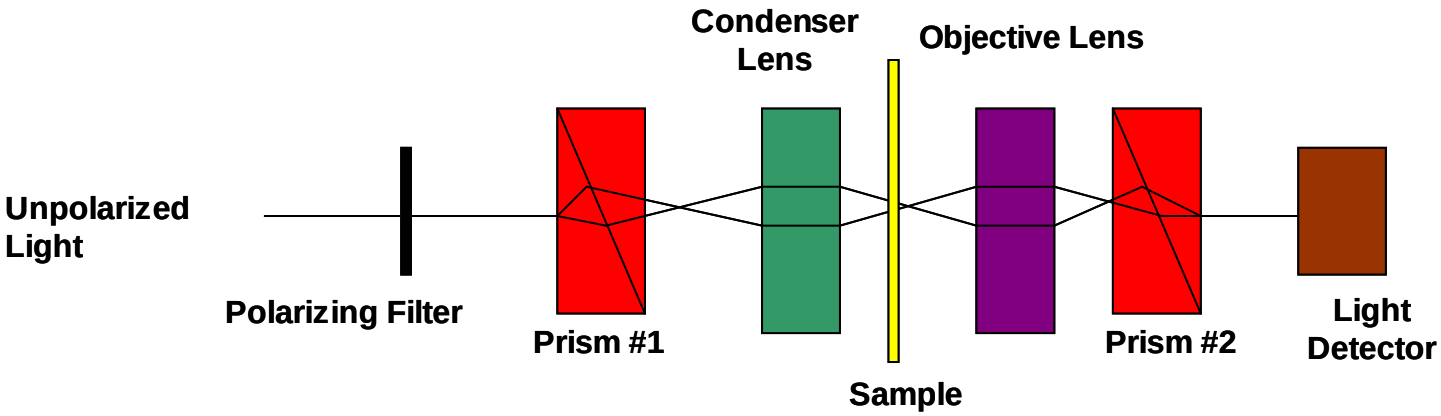

Figure 1.18 Diagram of differential interference contrast modified from reference.[72]

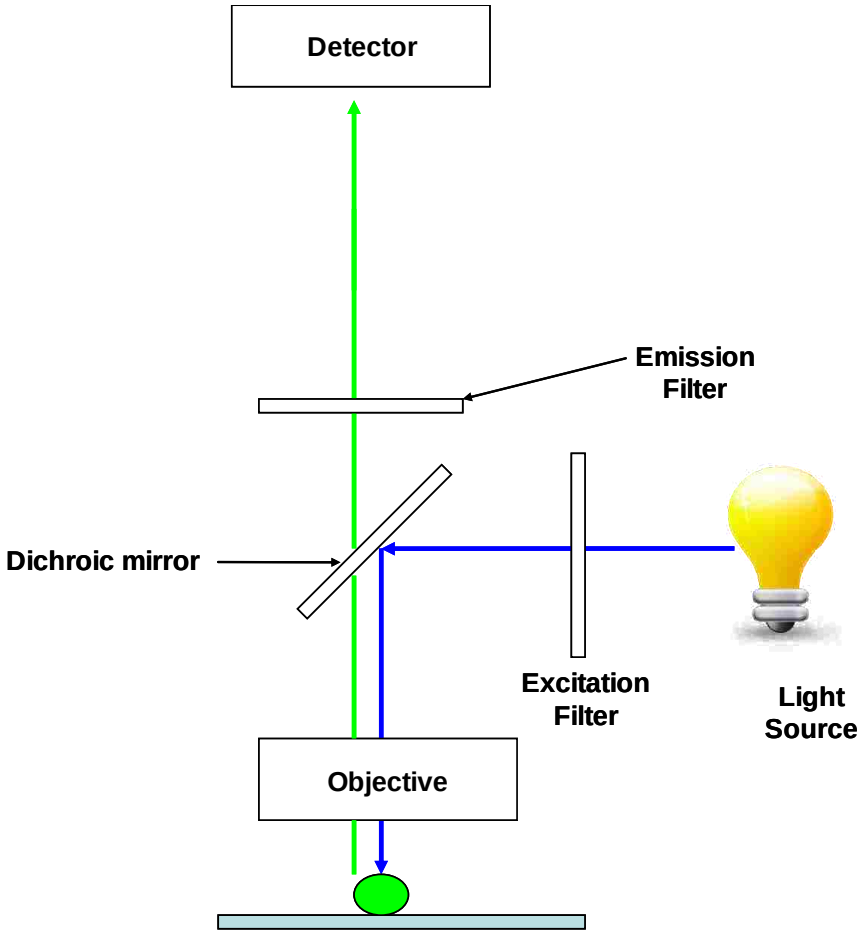

Figure 1.19 Diagram of fluorescence microscopy modified from reference.[73]

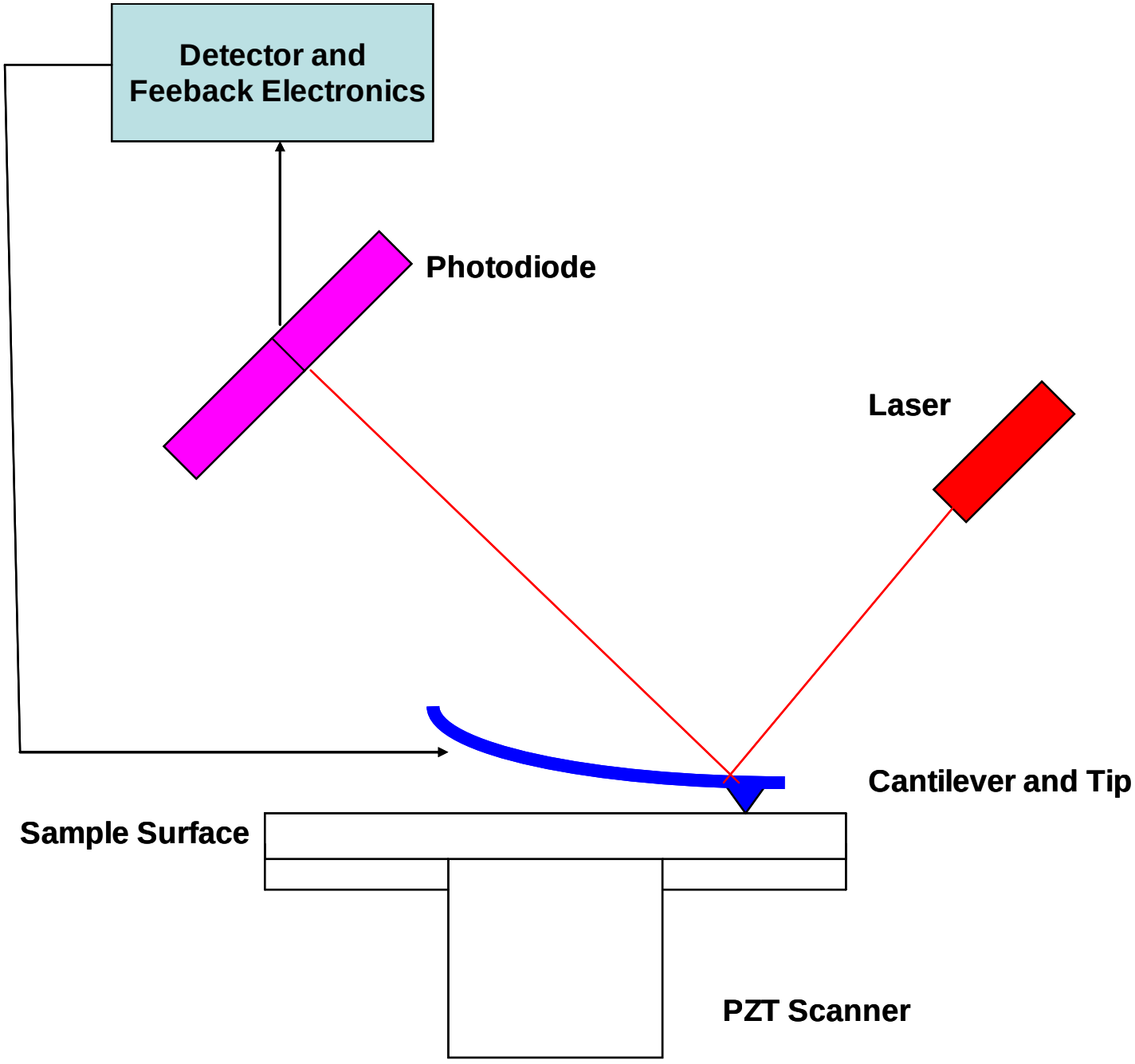

Figure 1.20 Diagram of atomic force microscopy modified from reference.[74]

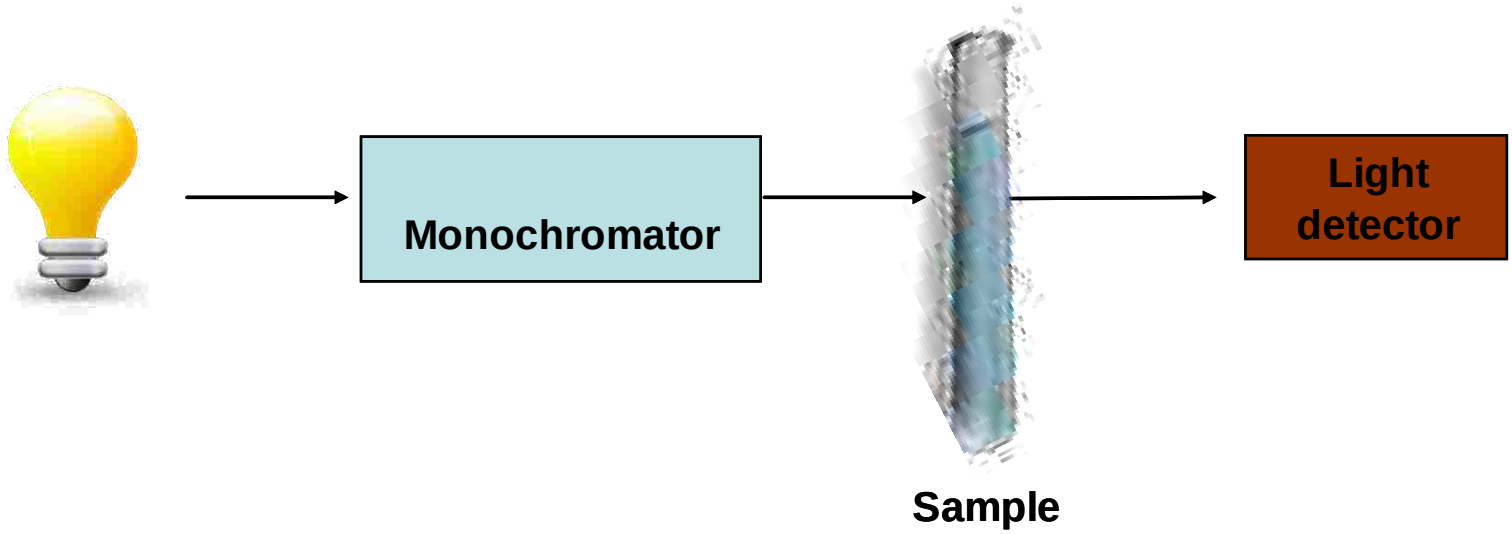

Figure 1.21 Representation of a UV-visible spectrometer modified from reference.[75]

1.6.7 Fluorescence Spectroscopy

In fluorescence spectroscopy, a molecule absorbs a photon which promotes an electron from the ground energy state to a higher energy state. Non-radiative processes can occur before emission takes place. Internal conversion is the result of the transition between a higher and lower energy state. The spin state remains the same whereas in intersystem crossing, the spin state is different. Intersystem crossing is the transition of states of different multiplicities from the singlet (S_1) to the triplet (T_1) state. Multiplicity is defined as; M= 2S + 1, where S is the spin on the molecule (sum of all electronic spins). Organic molecules typically have an even number of electrons, thus resulting in a singlet state. S = ½ - ½ = 0; M = 2(0) + 1 = 1. When two electrons have unpaired spins, a triplet state is formed. S = ½ $^{+}$ ½ = 1; M = 2(1) + 1 = 3. Phosphorescence occurs via

emission of a photon from the T_1 state, while fluorescence is the radiative transition of states of the same multiplicities which occurs from the lowest vibrational level of the S_1 state, as shown in Figure 1.22. The equation to describe fluorescence intensity and instrumental parameters is: $I(f) = 2.3\ I_o\ \varepsilon bc\ \Phi_f\ f(\theta)\ g(\gamma)$, where, I_o is incident photon flux, ε is molar absorptivity, b is path length, c is concentration of sample, Φ_f is fluorescence quantum efficiency, $f(\theta)$ is instrumental collection efficiency, and $g(\gamma)$ is response factor for PMT and/or gratings. To measure an excitation spectrum, a single emission wavelength is chosen to monitor the excitation. To measure an emission spectrum, a single excitation wavelength is chosen to monitor the emission. The emission wavelength is always shifted to longer wavelengths than the excitation wavelength and this is known as the Stokes shift.

A spectrofluorometer consists of a light source, excitation and emission monochromators, a sample chamber, and a detector or photomultiplier tube (Figure 1.23). The excitation source produces light ranging from 200 to 900 nm. The excitation light passes through the monochromators to decrease the light outside of the chosen excitation wavelength. The transmitted light then passes through the sample, and the fluorescence emission is passed through the emission monochromator. The emission monochromator is placed at 90° angle from the excitation monochromator to minimize scattering. The fluorescence emission is then collected by a detector, typically a photomultiplier tube.

1.6.8 Superconducting Quantum Interference Device (SQUID)

A SQUID is capable of measuring the magnetic susceptibility of a material. Magnetic susceptibility is defined as the magnetization of a material in the presence of a magnetic field. Magnetization M, is given by $M = \chi_m H$, where χ_m is the magnetic response and H

is the magnetic field strength. Paramagnetic materials or materials that possess at least one unpaired electron have a linear relationship between magnetization and applied magnetic field. From the slope of the line, one can determine the magnetic susceptibility of a material, χ_m.

To perform a measurement in the SQUID, a sample is passed through superconducting wires. The superconducting wires are located outside a sample chamber at the center of the magnet. The sample passes through the coils and the magnetic moment of the sample induces a current in the detection coils. Variations in the output voltage signal of the SQUID are produced due to variations in the current in the detection coils. The variations in the output voltages are in turn directly related to the magnetic moment of the sample.

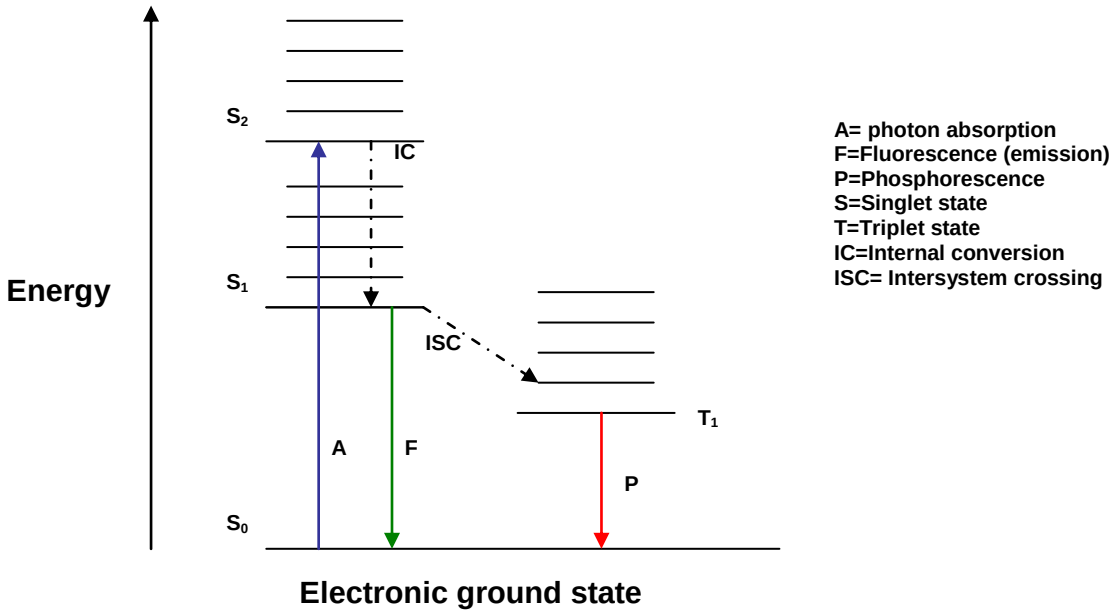

Figure 1.22 The Jablonski Diagram. Radiative transitions are indicated with solid arrows, and radiationless transitions are indicated with dashed arrows.[76]

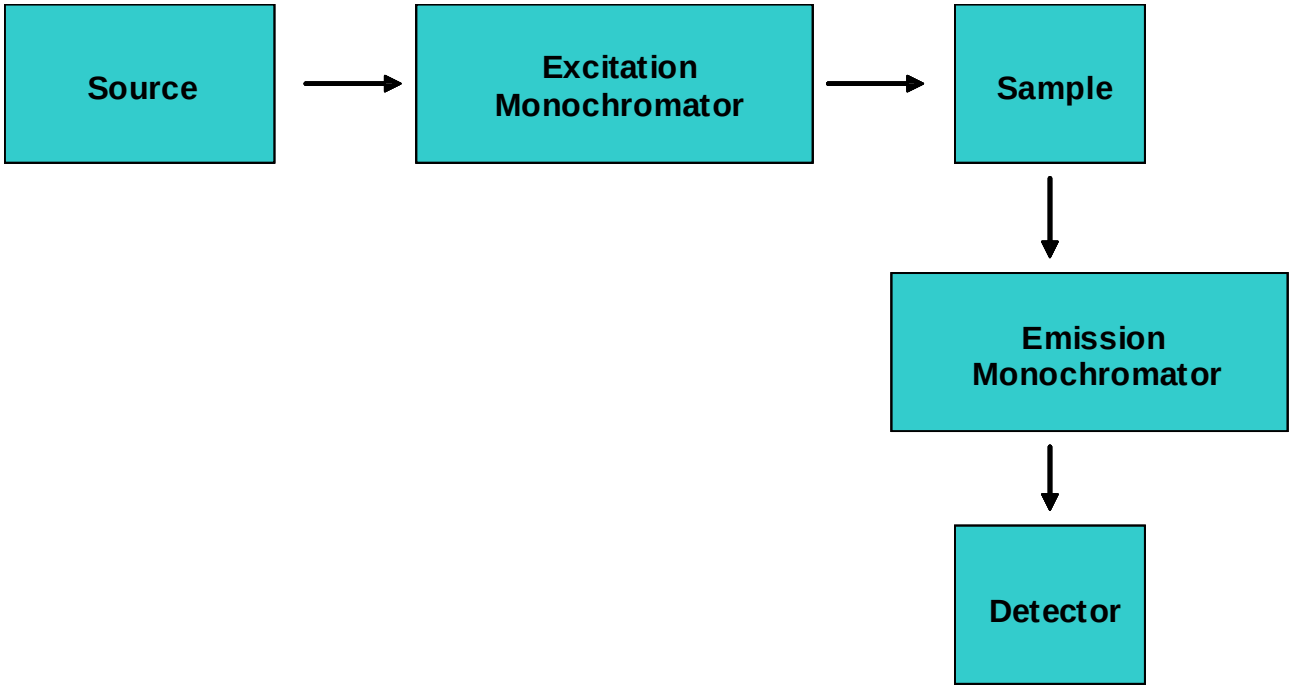

Figure 1.23 Diagram of a Spectrofluorometer.[76]

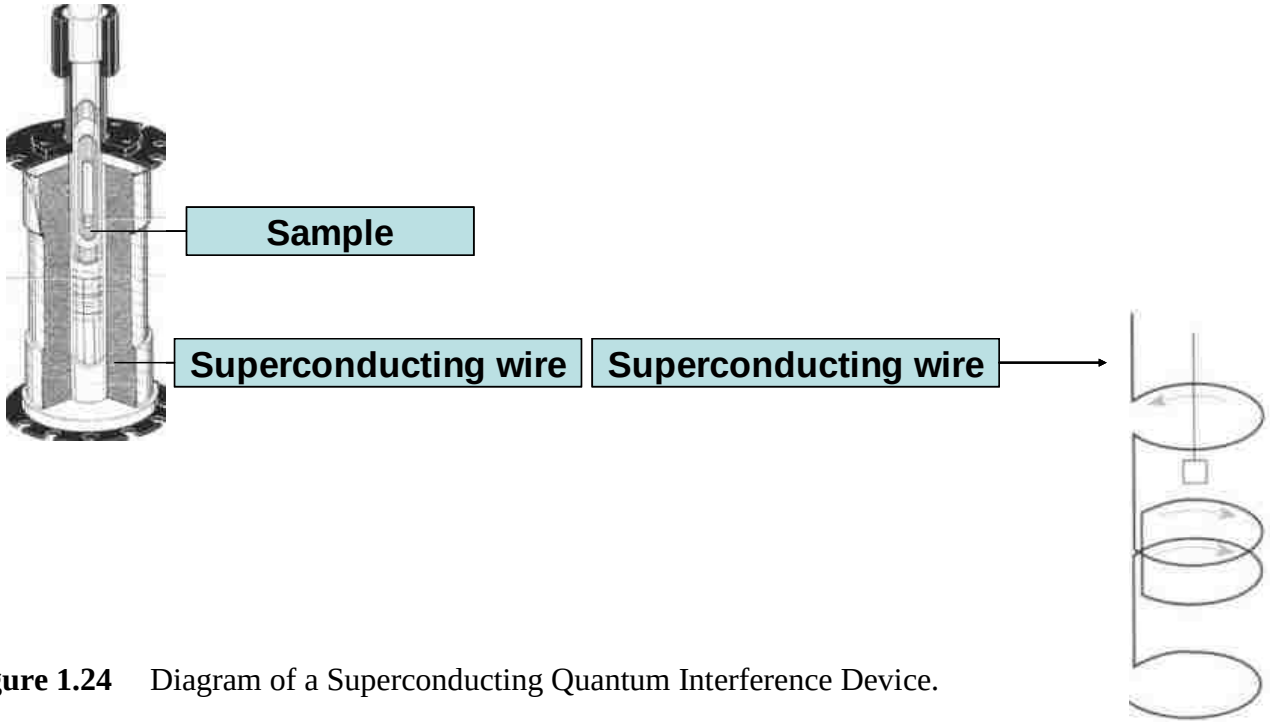

Figure 1.24 Diagram of a Superconducting Quantum Interference Device.

1.7 Scope of Dissertation

The goal of this research was to synthesize and characterize nanoparticles derived from GUMBOS. NanoGUMBOS are expected to exhibit significant advantages over traditional nanoparticles due to their functionality present within the cations and anions of the GUMBOS, thus leading to a myriad of applications in the biomedical, analytical, and materials fields.

In Chapter 2, the first demonstration of nano- and microparticles derived from GUMBOS is reported. Two methods producing particles with average diameters of 45 and 90 nm are discussed. The methods may also be adapted to yield micrometer-sized particles. Preparation of particles from GUMBOS provides for tunable properties based on the chosen cation and anion of the designed GUMBOS. The simplicity of preparation and potential versatility of tailor-made designer nanoGUMBOS makes them ideal for numerous potential applications ranging from biomedical, materials, and analytical fields.

In Chapter 3, the size and uniformity of nanoGUMBOS were controlled by variations in experimental parameters using an *in situ* ion exchange water-in-oil (w/o) emulsion preparation. Parameters such as reagent concentration produced significant and predictable variations in the size and uniformity of the particles. Average size variations for nanoGUMBOS ranging from approximately 14 to 68 nm were achieved by manipulation of these parameters. In addition, average sizes from 98 to 198 nm were achieved for magnetic GUMBOS particles by also varying the aforementioned parameters. Control of the size and uniformity of this new breed of nanoparticles is essential for potential applications in drug delivery and biomedical imaging.

In Chapter 4, novel fluorescent nanoGUMBOS were synthesized and characterized. Nanoparticles from GUMBOS derived from a fluorophore based cation and a bulky hydrophobic anion were prepared using reprecipitation, in-situ ion exchange, and a hydrogel synthetic method. All three methods yielded uniform, spherical, and highly fluorescent nanoGUMBOS. Due to their uniformity, facile and rapid preparation, and high fluorescence, this new class of nanomaterials provides a wealth of potential in the biomedical field.

1.8 References

(1). Earle, M. J.; Seddon, K. R. *Pure Appl. Chem.* **2000,** 72, (7), 1391-1398.

(2). Paul, A.; Mandal, P. K.; Samanta, A. *J. Phys. Chem. B.* **2005,** 109, (18), 9148-9153.

(3). Stalcup, A. M.; Cabovska, B. *J. Liq. Chromatogr. Relat. Technol.* **2004,** 27, (7-9), 1443-1459.

(4). Del Popolo, M. G.; Voth, G. A. *J. Phys. Chem. B* **2004,** 108, (5), 1744-1752.

(5). Pacholec, F.; Poole, C. F. *Chromatographia* **1983,** 17, (7), 370-4.

(6). Waichigo, M. M.; Danielson, N. D. *J. Sep. Sci.* **2006,** 29, (5), 599-606.

(7). Visser, A. E.; Swatloski, R. P.; Reichert, W. M.; Mayton, R.; Sheff, S.; Wierzbicki, A.; Davis, J. H., Jr.; Rogers, R. D. *Environ. Sci. Technol.* **2002,** 36, (11), 2523-2529.

(8). Matsumoto, M.; Mochiduki, K.; Fukunishi, K.; Kondo, K. *Sep. Purif. Technol.* **2004,** 40, (1), 97-101.

(9). Bekou, E.; Dionysiou, D. D.; Qian, R.-Y.; Botsaris, G. D. *ACS Symp. Ser.* **2003,** 856, (Ionic Liquids as Green Solvents), 544-560.

(10). Anderson, J. L.; Ding, R.; Ellern, A.; Armstrong, D. W. *J. Am. Chem. Soc* **2005,** 127, (2), 593-604.

(11). Baker, G. A.; Baker, S. N.; Pandey, S.; Bright, F. V. *Analyst* **2005,** 130, (6), 800-808.

(12). Fei, Z.; Geldbach, T. J.; Zhao, D.; Dyson, P. J. *Chem. Eur. J.* **2006,** 12, (8), 2122-2130.

(13). Deetlefs, M.; Seddon, K. R.; Shara, M. *Phys. Chem. Chem. Phys.* **2006,** 8, (5), 642-649.

(14). Cocalia, V. A.; Visser, A. E.; Rogers, R. D.; Holbrey, J. D. *Ionic Liquids in Synthesis (2nd Edition)* **2008,** 1, 89-102.

(15). Walden, P. *Bull. Acad. Imper. Sci.* **1914,** 1800.

(16). Ding, J.; Welton, T.; Armstrong, D. W. *Anal. Chem.* **2004,** 76, (22), 6819-6822.

(17). Anderson, J. L.; Armstrong, D. W. *Anal. Chem.* **2003,** 75, (18), 4851-4858.

(18). Anderson, J. L.; Armstrong, D. W. *Anal. Chem.* **2005,** 77, (19), 6453-6462.

(19). Xiao, X.; Liang, Z.; Xia, L.; Jiang, S. *Anal. Chim. Acta* **2004,** 519, (2), 207-211.

(20). Pei, Y.; Wang, J.; Wu, K.; Xuan, X.; Lu, X. *Sep. Purif. Technol.* **2009,** 64, (3), 288-295.

(21). Earle, M. J.; Seddon, K. R.; Adams, C. J.; Roberts, G. *Chem. Commun.* **1998**, (19), 2097-2098.

(22). Zhang, C.; Malhotra, S. V. *Talanta* **2005,** 67, (3), 560-563.

(23). Gao, S.; Zhang, H.; Wang, X.; Mai, W.; Peng, C.; Ge, L. *Nanotechnology* **2005,** 16, (8), 1234-1237.

(24). Ryu, H. J.; Sanchez, L.; Keul, H. A.; Raj, A.; Bockstaller, M. R. *Angew. Chem., Int. Ed.* **2008,** 47, (40), 7639-7643.

(25). Shigeyasu, M.; Murayama, H.; Tanaka, H. *Chem. Phys. Lett.* **2008,** 463, (4-6), 373-377.

(26). Wang, Q.; Baker, G. A.; Baker, S. N.; Colon, L. A. *Analyst* **2006,** 131, (9), 1000-1005.

(27). Sun, Y.; Cabovska, B.; Evans, C. E.; Ridgway, T. H.; Stalcup, A. M. *Anal. Bioanal. Chem.* **2005,** 382, (3), 728-734.

(28). Borissova, M.; Vaher, M.; Koel, M.; Kaljurand, M. *J. Chromatogr., A* **2007,** 1160, (1-2), 320-325.

(29). Yanes, E. G.; Gratz, S. R.; Baldwin, M. J.; Robison, S. E.; Stalcup, A. M. *Anal. Chem.* **2001,** 73, (16), 3838-44.

(30). Mwongela Simon, M.; Numan, A.; Gill Nicole, L.; Agbaria Rezik, A.; Warner Isiah, M. *Anal. Chem.* **2003,** 75, (22), 6089-96.

(31). Dietz, M. L.; Horwitz, E. P.; Rogers, R. D. *Solvent Extr. Ion Exch.* **1995,** 13, (1), 1-17.

(32). Huddleston, J. G.; Rogers, R. D. *Chem. Commun.* **1998**, (16), 1765-1766.

(33). Soto, A.; Arce, A.; Khoshkbarchi, M. K. *Sep. Purif. Technol.* **2005,** 44, (3), 242-246.

(34). Du, Z.; Yu, Y.-L.; Wang, J.-H. *Chem.--Eur. J.* **2007,** 13, (7), 2130-2137.

(35). Chauvin, Y.; Mussmann, L.; Olivier, H. *Angew. Chem., Int. Ed.* **1996,** 34, (23/24), 2698-700.

(36). Plechkovaa, N. V.; Seddon, K. R. *Chem. Soc. Rev* **2008,** 37, 123-150.

(37). Rutten, F. J. M.; Tadesse, H.; Licence, P. *Angew. Chem., Int. Ed.* **2007,** 46, (22), 4163-4165.

(38). Tesfai, A.; El-Zahab, B.; Bwambok, D. K.; Baker, G. A.; Fakayode, S. O.; Lowry, M.; Warner, I. M. *Nano Lett.* **2008,** 8, (3), 897-901.

(39). Buzea, C.; Pacheco, I. I.; Robbie, K. *Biointerphases* **2007,** 2, MR17-MR71.

(40). Hornyak, G. L.; Dutta, J.; Tibbals, H. F.; Rao, A. K., *Introduction to Nanoscience*. 2008.

(41). Hans, M. L.; Lowman, A. M. *Curr. Opin. Solid St. M.* **2002,** 6, (4), 319-327.

(42). Erni, R.; Browning, N. D. *Ultramicroscopy* **2007,** 107, (2-3), 267-273.

(43). Pillai, Z. S.; Kamat, P. V. *J. Phys. Chem. B.* **2004,** 108, (3), 945-951.

(44). Creighton, J. A.; Eadon, D. G. *J. Chem. Soc. Farad. T.* **1991,** 87, (24), 3881-91.

(45). Alivisatos, A. P. *Science* **1996,** 271, (5251), 933-7.

(46). Lieber, C. M. *Solid State Commun.* **1998,** 107, (11), 607-616.

(47). Yin, Y.; Xu, X.; Zhang, Z. *Chem. Comm.* **1998**, (16), 1641-1642.

(48). Lakowicz, J. R.; Gryczynski, I.; Gryczynski, Z.; Murphy, C. J. *J. Phys. Chem. B.* **1999,** 103, (36), 7613-7620.

(49). Portney, N. G.; Ozkan, M. *Anal. Bioanal. Chem.* **2006,** 384, (3), 620-630.

(50). Taton, T. A.; Mirkin, C. A.; Letsinger, R. L. *Science* **2000,** 289, (5485), 1757-60.

(51). Kloepfer, J. A.; Mielke, R. E.; Wong, M. S.; Nealson, K. H.; Stucky, G.; Nadeau, J. L. *Appl. Environ. Microbiol.* **2003,** 69, (7), 4205-4213.

(52). Modun, B.; Morrissey, J.; Williams, P. *Trends Microbiol* **2000,** 8, (5), 231-7.

(53). Zhu, L.; Ang, S.; Liu, W.-T. *Appl. Environ. Microbiol.* **2004,** 70, (1), 597-598.

(54). De Windt, W.; Aelterman, P.; Verstraete, W. *Environ. Microbiol.* **2005,** 7, (3), 314-325.

(55). Quan, X.; Yang, S.; Ruan, X.; Zhao, H. *Environ. Sci. Technol.* **2005,** 39, (10), 3770-3775.

(56). Chithrani, B. D.; Ghazani, A. A.; Chan, W. C. W. *Nano Lett.* **2006,** 6, (4), 662-668.

(57). Osaki, F.; Kanamori, T.; Sando, S.; Sera, T.; Aoyama, Y. *J. Am. Chem. Soc* **2004,** 126, (21), 6520-6521.

(58). Mao, Y.; Park, T.-J.; Zhang, F.; Zhou, H.; Wong, S. S. *Small* **2007,** 3, (7), 1122-1139.

(59). Tavakoli, A.; Sohrabi, M.; Kargari, A. *Chem. Pap* **2007,** 61, (3), 151-170.

(60). Wang, L.; Tan, W. *Nano Lett.* **2006,** 6, (1), 84-88.

(61). Ding, L.; Olesik, S. V. *Nano Lett.* **2004,** 4, (11), 2271-2276.

(62). Bruchez, M., Jr.; Moronne, M.; Gin, P.; Weiss, S.; Alivisatos, A. P. *Science* **1998,** 281, (5385), 2013-6.

(63). Tesfai, A.; El-Zahab, B.; Kelley, A. T.; Li, M.; Garno, J. C.; Baker, G. A.; Warner, I. M. *ACS Nano* 3, (10), 3244-3250.

(64). Hong, X.; Li, J.; Wang, M.; Xu, J.; Guo, W.; Li, J.; Bai, Y.; Li, T. *Chem. Mater* **2004,** 16, (21), 4022-4027.

(65). Ren, C.; Sun, J.; Li, J.; Chen, X.; Hu, Z.; Xue, D. *Nanoscale Res. Lett* **2009,** 4, (7), 640-645.

(66). Bwambok, D. K.; El-Zahab, B.; Challa, S. K.; Li, M.; Chandler; Gary A. Baker, L.; Warner, I. M. *ACS Nano* **2009**.

(67). Motte, L.; Billoudet, F.; Pileni, M. P. *J. Phys. Chem.* **1995,** 99, 16425-16429.

(68). Karukstis, K. K.; Frazier, A. A.; Martula, D. S.; Whiles, J. A. *J. Phys. Chem.* **1996,** 100, (26), 11133-11138.

(69). Spirin, M. G.; Brichkin, S. B.; Razumov, V. F. *J. Colloid Interface Sci.* **2008,** 326, (1), 117-120.

(70). Uskokovic, V.; Drofenik, M. *Surf. Rev. Lett.* **2005,** 12, (2), 239-277.

(71). Mukhopadhyay, S.; Maitra, U. *Curr. Sci* **2004,** 87, (12), 1666-1683.

(72). Davidson, M. W.; Abramowitz, M., Optical Microscopy. In.

(73). Lichtman, J. W.; Conchello, J.-A. *Nat Methods* **2005,** 2, 910-919.

(74). Blanchard, C. R. *Chem. Educator* **1996,** 1, 1-8.

(75). Harris, D. C., *Quantitative Chemical Analysis*. 2002; Vol. 6.

(76). Lakowicz, J., *Principles of Fluorescence Spectroscopy*. 1999.

CHAPTER 2

CONTROLLABLE FORMATION OF MICRO- AND NANOGUMBOS *VIA* A MELT–EMULSION–QUENCH APPROACH*

2.1 Introduction

ILs are an interesting group of materials that have gained considerable attention in many analytical areas as evidenced from my review of the literature in chapter one. ILs have been used as solvents, chiral selectors, and in chromatography as stationary phases. The properties of ILs are highly tunable, allowing them to be tailored to meet specific needs by simple variation in either the cation or anion component.[1-6]

The feasibility of incorporating chiral centers within IL building blocks has recently sparked considerable interest in the use of ILs as chiral solvents and selectors.[7, 8] For example, Tran and co-workers have demonstrated that chiral ILs can be used as chiral selectors for diastereomeric interactions in the discrimination of enantiomeric forms of drug molecules.[9] In addition, Ding et al. reported the first use of chiral ILs as novel stationary phases in gas chromatography for the enantiomeric separation of several different compounds.[10]

Apart from their exploration as green solvents and chiral selectors, ILs have also been widely pursued for a range of applications including safer organic reactions (such as the "greening" of Grignard chemistry[11]), analytical chemistry,[3,5] and materials

* The material presented in this chapter is reproduced in part with permission from *Nano Letters*, 2008, volume 8, pages 897 - 901; Tesfai, A.; El-Zahab, B.; Bwambok, D. K.; Baker, G.A.; Fakayode, S.O.; Lowry, M.; Warner, I. M.; Controllable Formation of Ionic Liquid Micro- and Nanoparticles via a Melt-Emulsion-Quench Approach , which was copyrighted in 2008 by the American Chemical Society.

synthesis.[12] For instance, the many benefits attributed to ILs are considered a boon by many researchers in the field of nanotechnology. A number of studies regarding the use of room temperature ILs as polar domains in microemulsions have been published within the last few years.[13-15] A recent review summarizing the use of ILs as media for the synthesis of functional inorganic nanoparticles and other nanostructures has also appeared.[16] In addition, various nanomaterials have been synthesized in IL-based media, including silver, gold and platinum nanoparticles,[18, 19] silver and gold nanowires,[17] and cobalt-platinum nanorods.[18] Furthermore, Kumar et al. recently reported the assembly of conducting organic-metallic composite submicrometer hexagonal rods based on electrostatic complexation between an IL and tetrachloroaurate anions.[19]

Traditionally, the aim of researchers has been to produce ILs with melting points well below room temperature to take full advantage of their beneficial solvent properties in reactions, materials synthesis, and separations at near-ambient conditions. In the current literature, only a few published studies have found general utility for ILs with melting points above room temperature (i.e., frozen ILs). However, to our knowledge, the synthesis of a nanoscale material composed of an IL species in the frozen state has yet to be reported. A **G**roup of **U**niform **M**aterials **B**ased on **O**rganic **S**alts, referred to as GUMBOS, differ from the conventional definition of ILs because GUMBOS are mainly ILs but some have melting points above 100 °C. It is believed that nanoGUMBOS will have distinct properties compared to traditional nanoparticles in that GUMBOS are broadly tunable, which should reduce the need for chemical activation and/or loading of active ingredients. In fact, we believe that the properties of GUMBOS are sufficiently tunable[6] so as to allow them to mimic the fundamental properties of a vast number of

nanoparticle types cited in the current literature.[20-22] We note, for example, a blue-emitting photoluminescent and proton-conductive IL built around a polyamidoamine (PAMAM) dendrimer core,[23] and most recently, phase-tunable fluorophores based upon benzobis(imidazolium) salts.[24] Finally, we believe that GUMBOS, although not intrinsically environmentally-friendly or biocompatible, can be designed to possess such properties, in addition to their hallmark tunability.

One of the simplest methods to manufacture solid nanoparticles containing active pharmaceutical ingredients (APIs) is through evaporation from emulsion systems, and this topic has been reviewed extensively.[25, 26] In this approach, following an emulsification step using high shear mixing with a rotor-stator mixer, high pressure homogenization, or sonication to prepare an o/w or w/o emulsion, particles are formed during solvent evaporation through either increased heat and/or reduced pressure. The melt–emulsion–quench process demonstrated here is well suited to low-melting GUMBOS phases and has vastly improved energy efficiency relative to current methods used in API nanoparticle production. This is especially pertinent with regard to the recent emergence of ILs exhibiting antimicrobial activities and bioactivities, most particularly those containing API anions.[27-29] The first preparation of uniform and ambient-stable micro- and nanoGUMBOS based on an original oil-in-water (o/w) microemulsion approach in which the particle size is correlated to processing conditions is now reported.

2.2 Materials and Methods

Reagents are as follows: 1-Butyl-2,3-dimethylimidazolium hexafluorophosphate (97%), Brij-35 (99%) were purchased from Sigma Aldrich (St. Louis, MO). Ultra pure water

(Elga model PURELAB Ultra water filtration system 18.2 MΩ) was obtained. A homogenizer (PowerGen 125) was obtained from Fisher Scientific. A probe ultrasound processor (CV330 Sonics and Materials Inc., Newton, CT, USA) was obtained. An ultrafiltration cell was obtained from (Millipore).

2.2.1 Electron Microscopy Characterization

A JEOL 100CX-transmission electron microscope was used for characterization of the nanoGUMBOS. Samples were prepared by placing 1 μL of the nanoparticle suspension directly onto a carbon-coated copper grid. The TEM grid containing the nanoparticle crop was allowed to dry in air at room temperature before imaging.

A cambridge stereoscan 260 scanning electron microscope was also used for characterization of nanoGUMBOS. Samples were prepared by placing 1 μL of the nanoparticle suspension directly onto a glass slide which is affixed onto a metal stub. Samples were air dried for 10 min. Next the samples were sputter coated with a layer of platinum and gold for 2 min before imaging.

Particle size and standard deviations were calculated using an image processing technique, Image J 1.38x. Samples were prepared in triplicate to confirm reproducibility. Particle size was measured by selecting 100 particles and measuring their diameter using the Image J software. The average particle diameter and standard deviations were calculated for three samples to prove the reproducibility.

2.2.2 Method 1: (Surfactantless Mode) Preparation of Nano- and MicroGUMBOS

In this study, a proof-of-concept study using as the starting material 1-butyl-2,3-dimethylimidazolium hexafluorophosphate ([bm_2Im][PF_6]), a GUMBOS with a melting point of 42 °C was demonstrated. GUMBOS particles were synthesized using two

different procedures, as summarized in Figure 2.1. The first method involves the melting and subsequent o/w dispersion of liquid-phase $[bm_2Im][PF_6]$ into water poised well above the GUMBOS melting point, followed by rapid cooling to form discrete solid nanoGUMBOS. Using solid, amorphous granules of $[bm_2Im][PF_6]$ as a starting material, the melt–emulsion–quench process in surfactantless mode (Method 1) yielded satisfactorily controlled particle sizes having either nanometer or micron dimensions, depending on the exact conditions. In a typical preparation, 25 mg of $[bm_2Im][PF_6]$ solid was gently rinsed several times in water (Ultrapure water 18.2 MΩ cm) and then added to 8 mL of ultrapure water within a 20 mL scintillation vial. The sealed vial was heated at 70 °C in a water bath until the $[bm_2Im][PF_6]$ formed a clear dense liquid phase. The mixture was then homogenized using a commercial homogenizer operating at 30,000 rpm for 10 min while the sample was maintained at 70 °C in the water bath. The mixture was then sonicated using a probe ultrasound processor at 35% intensity for 10 min. Post-sonication, the mixture was immediately placed into an ice-water bath to quickly reduce the temperature below the melting point of the GUMBOS. The resulting nanoGUMBOS, suspended in the aqueous phase, were washed by use of ultrafiltration three times to remove soluble species. It was found that particle size could be optimized by careful control over experimental conditions: system temperature; homogenization speed and duration; and sonication intensity, duration, and pulse interval sequence.

2.2.3 Method 2: (Surfactant-Assisted Mode) Preparation of NanoGUMBOS

The second method is conceptually identical; however, in this case, nanoparticles are formed with the aid of an emulsifier, the nonionic surfactant Brij 35. Emulsifying agents are expected to preferentially orient between the oil (i.e., $[bm_2Im][PF_6]$) and water

phases at the interface of the droplet to prevent coalescence. Consistent with this assumption, the synthesis of nanoparticles using Brij 35 as an emulsifying agent (Method 2) yielded more monodispersed nanoGUMBOS. A 25 mg quantity of $[bm_2Im][PF_6]$ was added dropwise, previously melted at 70 °C, to a scintillation vial containing 1.0 wt% Brij 35 in 8 mL of hot ultrapure water during the homogenization period (10 min), followed by treatment similar to that outlined above in Method 1. An overview of the melt–emulsion–quench process with photographs illustrating representative stages for Method 1 is provided in Figure 2.2. It is noteworthy that the lipophilic dye Nile Red used as an aid to visualization does not color the aqueous component of solution, but is incorporated into the o/w microemulsion (Figure 2.2C) and into the final nanoGUMBOS (Figure 2.2D). This finding suggests that nanoGUMBOS produced in this manner may be used to entrap various materials including drugs and magnetic or sensory agents.

2.3 Results and Discussion

2.3.1 Method 1: Characterization of NanoGUMBOS

By following the conditions described above in Method 1, SEM images show that $[bm_2Im][PF_6]$ nanoGUMBOS with a diameter of 90 ± 32 nm were produced, as shown in Figure 2.3a, while TEM images of the same sample show that nanoGUMBOS 88 ± 34 nm in diameters were obtained with slightly different morphologies (Figure 2.3-b). It is possible that this difference in morphology results from heat produced from the high-voltage electronic beam which may have distorted the nanoGUMBOS. The heat produced may distort the IL nanoparticles and thus cause the morphologies to change. In fact, it was observed that an electronic beam focused on a spot for an extended time would melt the particles, shown in Figure 2.3c.

The nanoGUMBOS were generally spherical and formed a single layer on the TEM grid surface, with minimal interparticle aggregation. Aggregation of particles was found to be curtailed by chilling the o/w emulsion on ice, which results in swift GUMBOS solidification and so prevents the significant merging of isolated droplets prior to freezing. The average nanoparticle diameter was measured using SEM and TEM imaging, and confirmed by dynamic light scattering (DLS). The DLS polydispersity index (PDI), an estimate of the size distribution width, of the as-prepared $[bm_2Im][PF_6]$ nanoparticles was as low as 0.105. This PDI value indicates that the nanoparticles have a narrow size distribution width.

2.3.2 Modified Method 1: Characterization of MicroGUMBOS

Similar procedures to achieve nanoparticles can also be used to efficiently generate spherical $[bm_2Im][PF_6]$ particles a few micrometers in diameter. For example, 3 μm microspheres were produced by homogenization of the mixture for 30 seconds at 30,000 rpm then chilled on ice without probe sonication.

2.3.3 Fluorescent Labeling of MicroGUMBOS

These microGUMBOS were doped with Nile Red fluorescent dye and imaged using SEM and optical microscopy (Figure 2.4a-d). The measured dimensions of the particles in SEM and optical microscopy images were in agreement confirming minimal deformation due to the high-voltage electronic beam although slightly better sphericity was observed for the latter.

2.3.4 Method 2: Characterization of NanoGUMBOS

The nanoGUMBOS in Method 2 yielded diameters of 45 ± 7 nm. The nanoparticles from Method 2 were generally quite uniform in size and their morphologies

appeared more irregular and less spherical than those prepared in the absence of an emulsifying agent (Method 1), as can be observed from comparing Figure 2.3b to Figure 2.5. The Brij 35 surfactant employed here apparently provides a protective boundary which preserves particle integrity. However, for some applications a surfactant layer is undesirable. In other cases, this approach may provide a convenient route for further functionalizing the nanoparticle surface, further expanding the value of nanoGUMBOS.

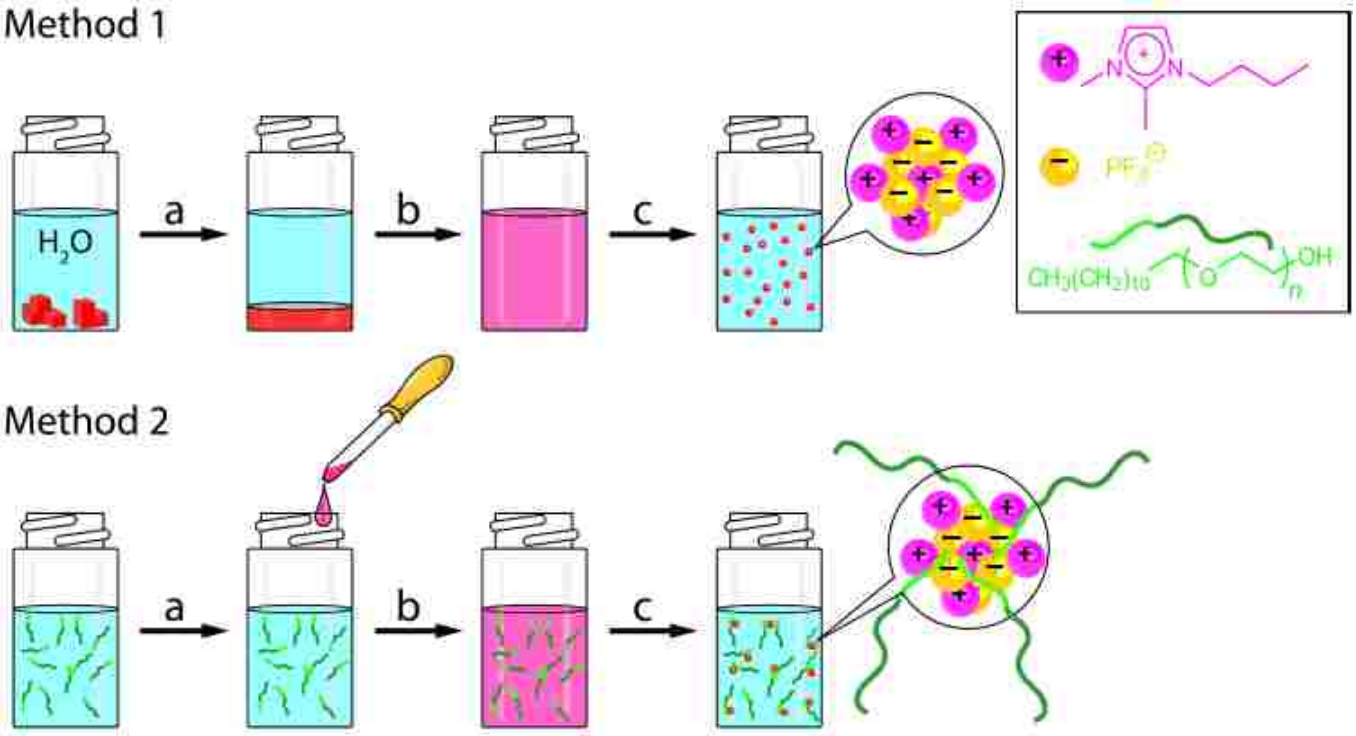

Figure 2.1 Schematic showing the steps involved in the melt–emulsion–quench method for synthesizing nano- and microGUMBOS using surfactantless (Method 1) and surfactant-assisted (Method 2) procedures. In Method 1, the first step (a) entails the melting of $[bm_2Im][PF_6]$ in a hot water bath, whereas dropwise addition of molten $[bm_2Im][PF_6]$ to a surfactant solution is performed at this stage in Method 2. The residual steps are homogenization and probe sonication (b), followed by rapid quenching in an ice bath to achieve particle solidification (c).

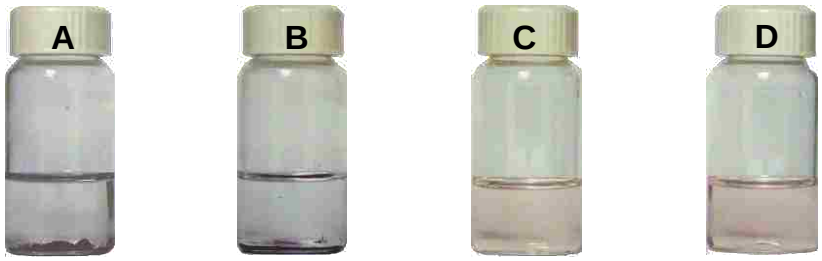

Figure 2.2 Photographs showing the various stages of nanoGUMBOS formation following Method 1, as summarized in 2.1: (A) solid $[bm_2Im][PF_6]$ in water at room temperature; (B) molten-state $[bm_2Im][PF_6]$ phase separated from water at 70 °C; (C) o/w emulsion containing $[bm_2Im][PF_6]$ as the inner phase; (D) $[bm_2Im][PF_6]$ nanoGUMBOS crop suspended in water at room temperature. In these images, $[bm_2Im][PF_6]$ was stained with a water-insoluble dye (Nile Red) for visualization purposes.

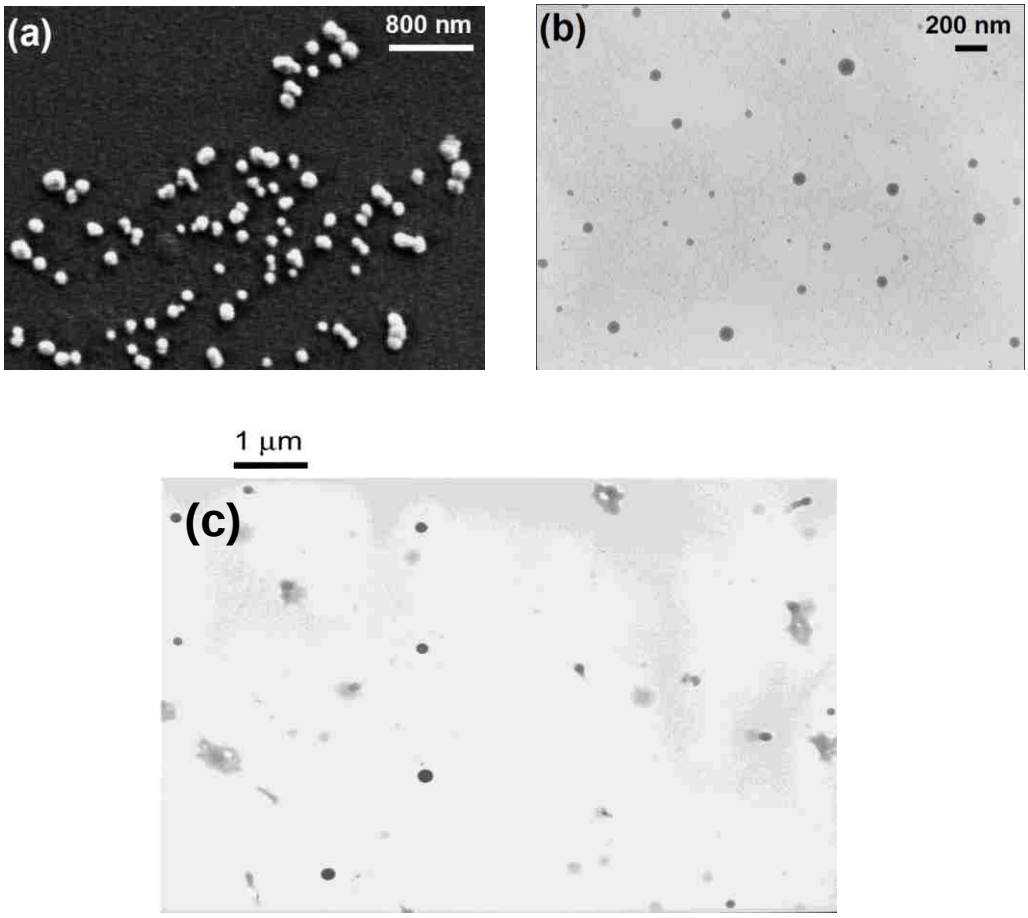

Figure 2.3 Electron micrographs of $[bm_2Im][PF_6]$ nanoGUMBOS synthesized using Method 1: (a) SEM image (15 kV) showing an average nanoparticle diameter of 90 ± 32 nm. (b) TEM image (80 kV) with an average nanoGUMBOS diameter measured as 88 ± 34 nm. It was observed that an electronic beam focused on a spot for an extended time would melt the particles. Therefore, high magnification exposure time was minimized for TEM. (c) Electronic beam focused on a spot showing the particles melting.

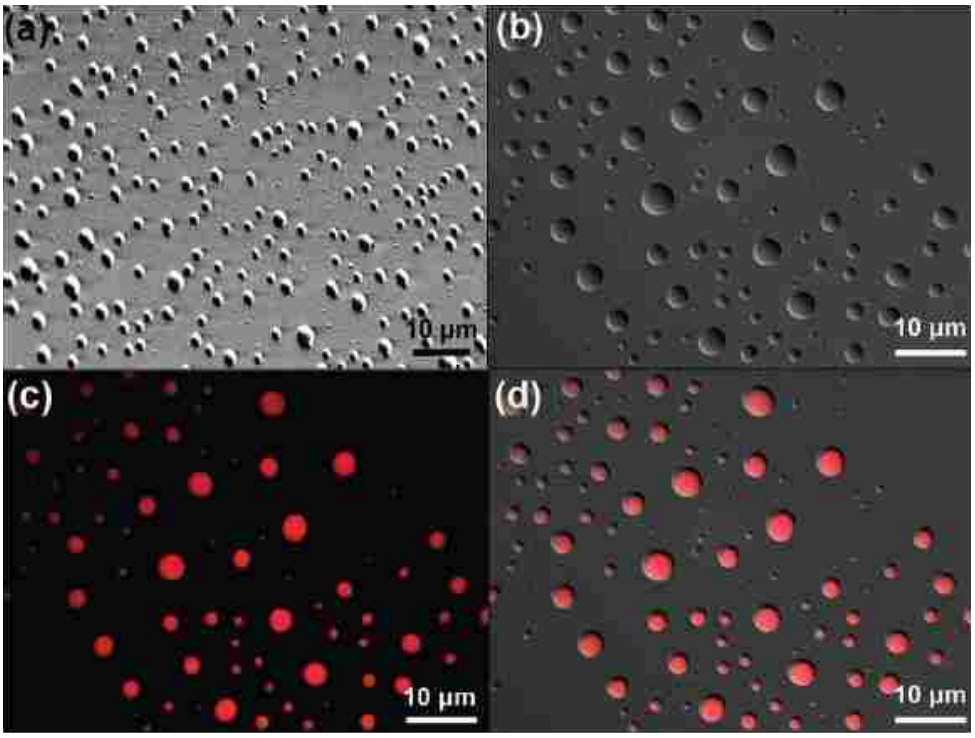

Figure 2.4 Solid [bm_2Im][PF_6] microGUMBOS prepared using Method 1 with average diameter of ~ 3-µm imaged with (a) SEM, (b) Optical microscopy (DIC), (c) Optical microscopy (fluorescence), (d) Overlay of DIC and fluorescence.

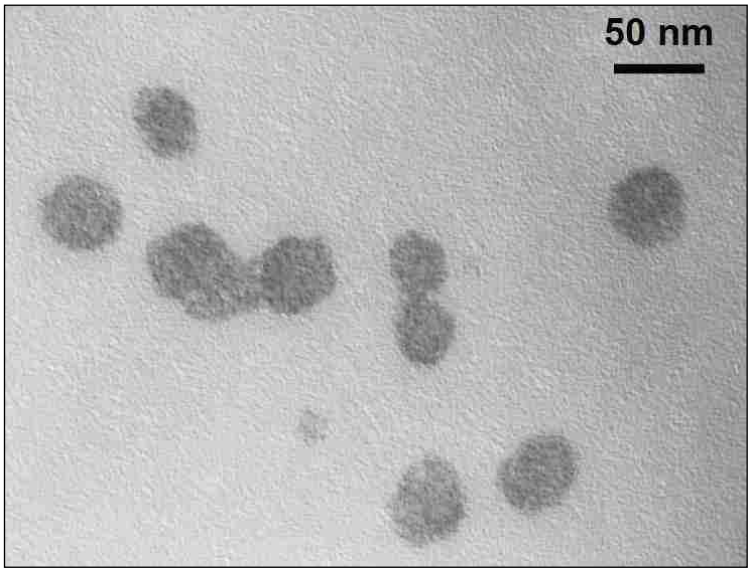

Figure 2.5 Representative TEM image of 45 ± 7 nm [bm_2Im][PF_6] nanoGUMBOS synthesized based upon Method 2, employing Brij® 35 as emulsifying agent.

2.4 Conclusions

In summary, a simple, rapid, and high-purity method for efficiently generating tailored nano- and microGUMBOS under mild conditions based on an original melt–emulsion–quench technique employing the molten GUMBOS itself as the oil phase of an o/w microemulsion has been developed. No costly or specialized equipment is necessary and the route requires the addition of organic solvent at no stage of the process. It is expected that particle geometry, dimensions, and composition can be further controlled by varying a number of parameters such as temperature, pressure, surfactant choice, selection of GUMBOS building blocks, and emulsion type. For example, creating multiple emulsions such as oil-in-water-in-oil (o/w/o) systems may lead to multiple layers allowing further flexibility. While the example we provide in this chapter involves production of a water insoluble nanoparticle, it should be noted that this approach is equally applicable to production of a water soluble nanoparticle. To achieve this, one would simply use a water soluble GUMBOS in an organic solvent to carry out the synthesis process using one of the two methods previously outlined. Furthermore, selectively soluble GUMBOS for specific applications can be developed for use in certain solvents.

Overall, nanoparticles synthesized from GUMBOS should represent an exciting new direction in nanochemistry. Based on a basic knowledge of IL chemistry, it is anticipated that these results will lead to new applications in a variety of areas including biomedical imaging, displays, intelligent inks, actuators, sensory devices, fuel cells, self-healing materials, and separations.

2.5 References

(1). Stalcup, A. M.; Cabovska, B. *J. Liq. Chromatogr. Relat. Technol.* **2004,** 27, (7-9), 1443-1459.

(2). Anderson, J. L.; Ding, R.; Ellern, A.; Armstrong, D. W. *J. Am. Chem. Soc* **2005,** 127, (2), 593-604.

(3). Baker, G. A.; Baker, S. N.; Pandey, S.; Bright, F. V. *Analyst* **2005,** 130, (6), 800-808.

(4). Deetlefs, M.; Seddon, K. R.; Shara, M. *Phys. Chem. Chem. Phys.* **2006,** 8, (5), 642-649.

(5). Earle, M. J.; Seddon, K. R. *Pure Appl. Chem.* **2000,** 72, (7), 1391-1398.

(6). Fei, Z.; Geldbach, T. J.; Zhao, D.; Dyson, P. J. *Chem. Eur. J.* **2006,** 12, (8), 2122-2130.

(7). Baudequin, C.; Baudoux, J.; Levillain, J.; Cahard, D.; Gaumont, A.-C.; Plaquevent, J.-C. *Tetrahedron: Asymmetry* **2003,** 14, (20), 3081-3093.

(8). Bwambok, D. K.; Marwani, H. M.; Fernand, V. E.; Fakayode, S. O.; Lowry, M.; Negulescu, I.; Strongin, R. M.; Warner, I. M. *Chirality* **2008,** 20, (2), 151-158.

(9). Tran, C. D.; Oliveira, D. *Anal. Biochem.* **2006,** 356, (1), 51-58.

(10). Ding, J.; Welton, T.; Armstrong, D. W. *Anal. Chem.* **2004,** 76, (22), 6819-6822.

(11). Ramnial, T.; Ino, D. D.; Clyburne, J. A. C. *Chem. Comm.* **2005**, (3), 325-327.

(12). Li, Z.; Liu, Z.; Zhang, J.; Han, B.; Du, J.; Gao, Y.; Jiang, T. *J. Phys. Chem. B.* **2005,** 109, (30), 14445-14448.

(13). Eastoe, J.; Gold, S.; Rogers, S. E.; Paul, A.; Welton, T.; Heenan, R. K.; Grillo, I. *J. Am. Chem. Soc* **2005,** 127, (20), 7302-7303.

(14). Gao, H.; Li, J.; Han, B.; Chen, W.; Zhang, J.; Zhang, R.; Yan, D. *Phys. Chem. Chem. Phys.* **2004,** 6, (11), 2914-2916.

(15). Gao, Y.; Wang, S.; Zheng, L.; Han, S.; Zhang, X.; Lu, D.; Yu, L.; Ji, Y.; Zhang, G. *J. Colloid Interface Sci.* **2006,** 301, (2), 612-616.

(16). Antonietti, M.; Kuang, D.; Smarsly, B.; Zhou, Y. *Angew. Chem., Int. Ed.* **2004,** 43, (38), 4988-4992.

(17). Bhatt, A. I.; Mechler, A.; Martin, L. L.; Bond, A. M. *J. Mater. Chem.* **2007,** 17, (21), 2241-2250.

(18). Wang, Y.; Yang, H. *J.Am. Chem. Soc.* **2005,** 127, (15), 5316-5317.

(19). Kumar, A.; Murugesan, S.; Pushparaj, V.; Xie, J.; Soldano, C.; John, G.; Nalamasu, O.; Ajayan, P. M.; Linhardt, R. J. *Small* **2007,** 3, (3), 429-433.

(20). Wang, L.; Tan, W. *Nano Lett.* **2006,** 6, (1), 84-88.

(21). Ding, L.; Olesik, S. V. *Nano Lett.* **2004,** 4, (11), 2271-2276.

(22). Bruchez, M., Jr.; Moronne, M.; Gin, P.; Weiss, S.; Alivisatos, A. P. *Science* **1998,** 281, (5385), 2013-6.

(23). Huang, J.-F.; Luo, H.; Liang, C.; Sun, I. W.; Baker, G. A.; Dai, S. *J. Am. Chem. Soc.* **2005,** 127, (37), 12784-12785.

(24). Boydston, A. J.; Pecinovsky, C. S.; Chao, S. T.; Bielawski, C. W. *J. Am. Chem. Soc.* **2007,** 129, (47), 14550-14551.

(25). Solans, C.; Izquierdo, P.; Nolla, J.; Azemar, N.; Garcia-Celma, M. J. *Curr. Opin. Colloid Interface Sci.* **2005,** 10, (3,4), 102-110.

(26). Krauel, K.; Pitaksuteepong, T.; Davies, N. M.; Rades, T. *Am. J. Drug Deliv* **2004,** 2, (4), 251-259.

(27). Hough, W.; Smiglak, M.; Rodriguez, H.; Swatloski, R. P.; Spear, S. K.; Daly, D. T.; Pernak, J.; Grisel, J. E.; Carliss, R. D.; Soutullo, M. D.; Davis, J. J. H.; Rogers, R. D. *New J. Chem* **2007,** 31, 1429-1436.

(28). Laali, K. K., *Ionic Liquids in Synthesis.* . 2003; Vol. 11, p 1752.

(29). Trewyn, B. G.; Whitman, C. M.; Lin, V. S.-Y. *Nano Lett.* **2004**, 2139-2143.

CHAPTER 3

MAGNETIC AND NON-MAGNETIC NANOPARTICLES FROM A GROUP OF UNIFORM MATERIALS BASED ON ORGANIC SALTS*

3.1 Introduction

In recent years, magnetic nanoparticles have garnered considerable interest in various disciplines such as drug delivery,[1] separations,[2] magnetic resonance imaging,[3] and cancer hyperthermia treatment.[4] Iron oxide nanoparticles with diameters typically around 10–20 nm exhibit superparamagnetism and can be magnetized in the presence of an external magnetic field and readily redispersed in the absence of a field with negligible particle aggregation.[5] For many of these applications, modifying the surface of the nano-sized magnetic particles can be a considerably difficult and tedious task. Surface modification is typically achieved by physically adsorbing or chemically attaching molecules to the nanoparticle surface. For example in an article by Hong *et al.,*[6] to synthesize fluorescent magnetic nanoparticles, the process first started by separately preparing iron oxide nanoparticles and quantum dots. Next, a complex linking process to combine the dual functionality of the fluorescent and magnetic particles was employed using polymeric materials. Due to the inherent nature of the linking process and lack of control over crosslinking-caused aggregation, typically the functionalization task is

*The material presented in this chapter is reproduced in part with permission from *ACS Nano*, 2009, volume 3, pages 3244 - 3250; Tesfai, A.; El-Zahab, B.; Kelley, A. T.; Li, M.; Garno, J.C.; Baker, G.A.; Warner, I. M.; Magnetic and Nonmagnetic Nanoparticles from a Group of Uniform Materials Based on Organic Salts, which was copyrighted in 2009 by the American Chemical Society.

neither simple nor does it produce uniformly-functionalized particles. In addition, commonly used metal oxide nanoparticles (e.g., Fe_2O_3, NiO, $CoFe_2O_3$) are relatively toxic and require benign coatings (e.g., polyethylene glycol) for biological applications which further restricts their use *in vivo*.[7] Therefore, routes to biocompatible magnetic nanoparticles with tunable properties that can be easily tailored to a specific application remain of paramount importance. GUMBOS are immediately pertinent in that aspect since they can be designed to be non-toxic and might even play a medicinal or nutritive role by synthesizing GUMBOS from environmentally-responsible "green" materials including various vitamins, amino acids,[8] artificial sweeteners,[9] nutraceuticals, drugs,[10] and phytochemicals.

ILs with anions containing transition metal complexes have sparked considerable recent interest.[11-13] Although these ILs were among the earliest developed, their magnetic behavior was largely overlooked.[11] The first report of a magnetic IL, 1-butyl-3-methyl-imidazolium tetrachloroferrate ([bmim][$FeCl_4$]) and its response to a magnetic field was reported in 2004.[12] To our knowledge, however, the synthesis of a nanoscale material composed solely from magnetic ILs/GUMBOS has yet to be reported. We hypothesize that magnetic nanoGUMBOS will hold significant advantages as compared to other common magnetic nanoparticles because they should also exhibit the tunability and inherent functionality of ILs. In addition, both the anion and the cation may carry unique functional properties, allowing dual- or poly-functional nanoGUMBOS to be prepared. This tunability will ultimately provide superior control over relevant properties of the nanoparticles, such as solubility[14] and melting point.[15] When paired with particle size

control, this provides an ideal platform for targeted drug delivery, as well as for sensory and imaging applications.

Challenges encountered in the synthesis of monodispersed nanoparticles have led to extensive research into size control by use of various organized media.[16, 17] For example, aerosol-OT (AOT, sodium bis(2-ethylhexyl) sulfosuccinate), a well studied surfactant, is known to form stable and spherical reverse micelles in nonpolar solvents such as *n*-heptane.[18] Use of these reverse micellar templates for nanoparticle formation often leads to relatively monodispersed nanoparticles with controlled sizes due to the ability of this reverse micelle system to stabilize relatively large water pools of defined sizes.[19, 20]

In this chapter, the synthesis and behavior of particles composed of GUMBOS containing both the BF_4^- and the $FeCl_4^-$ anion is reported and the tunability of their physicochemical properties evident via changes in the cationic component of the GUMBOS is demonstrated. In this current work, we employ AOT reverse micelles as templates to exert size control over the resultant liquid and solid GUMBOS particles. Parameters such as surfactant concentration, water-to-surfactant molar ratio, temperature, and solvent composition were optimized for size-targeted GUMBOS particles synthesis. The synthesized GUMBOS particles were characterized using transmission electron microscopy (TEM), UV–visible absorption spectroscopy (UV–vis), atomic force microscopy (AFM), and measurements using a superconducting quantum interference device (SQUID).

3.2 Materials and Methods

3.2.1 Materials

1-Butyl-2,3-dimethylimidazolium chloride [Bm_2Im][Cl] (97%), sodium tetrafluoroborate [Na][BF_4] (99%), iron (III) chloride hexahydrate (Fluka, 98%), sodium bis(2-ethylhexyl) sulfosuccinate (AOT), and *n*-heptane (Sigma, 99%) were purchased from Sigma Aldrich (St. Louis, MO) and used as received. Ultra-pure water (18.2 MΩ cm) was obtained using an Elga model PURELAB Ultra water filtration system.

3.2.2 Preparation of NanoGUMBOS and Magnetic NanoGUMBOS

NanoGUMBOS of [Bm_2Im][BF_4] and [Bm_2Im][$FeCl_4$] were prepared via a modified reverse-micellar method.[20] In a typical preparation, two separate 0.3 M solutions of [Bm_2Im][Cl] and [Na][BF_4] were prepared in ultra-pure water. For the magnetic nanoGUMBOS preparation, the [$NaBF_4$] was replaced by [$FeCl_3 \cdot 6H_2O$]. Two additional solutions containing 5 mL of 0.1 M AOT in heptane were prepared separately. First, 120 μL of the aqueous [Bm_2Im][Cl] solution was added into 5 mL of 0.1 M AOT solution in heptane, and then 120 μL of the aqueous [Na][BF_4] solution was added into a separate vial also containing 5 mL of 0.1 M AOT solution in heptane. Each solution was then vortexed for 5 min and allowed to equilibrate for 1 h. The molar ratio between [Bm_2Im][Cl] and [Na][BF_4] was 1:1. The two solutions were then mixed in a tightly sealed 20 mL scintillation vial and stirred for 24 h at room temperature. The nanoGUMBOS size can be controlled by varying the concentrations of [Bm_2Im][Cl] and [Na][BF_4]. For 14.7 nm diameter nanoGUMBOS, 0.3 M [Bm_2Im][Cl] and 0.3 M [Na][BF_4] was used. To produce 20.8 nm diameter nanoGUMBOS, 0.4 M [Bm_2Im][Cl] and 0.4 M [Na][BF_4] were used. To synthesize 34.3 nm diameter nanoGUMBOS, 0.5 M

[Bm_2Im][Cl] and 0.5 M [Na][BF_4] was used. Lastly, use of 0.6 M [Bm_2Im][Cl] and 0.6 M [Na][BF_4] afforded 68.0 nm diameter nanoGUMBOS. The magnetic nanoGUMBOS sizes could also be controlled by varying the concentrations of [Bm_2Im][Cl] and [$FeCl_3 \cdot 6H_2O$]. For approximately 98 nm diameter nanoGUMBOS, 0.3 M [Bm_2Im][Cl] and 0.3 M [$FeCl_3 \cdot 6H_2O$] was used. Likewise, to produce 199 nm diameter particles, 0.4 M [Bm_2Im][Cl] and 0.4 M [$FeCl_3 \cdot 6H_2O$] was employed, other conditions remaining the same.

3.2.3 UV–vis Characterization

To characterize the bulk [Bm_2Im][$FeCl_4$] dissolved in acetonitrile, we first measured its visible absorption spectra using a Shimadzu UV-3101PC UV–Vis–near-IR scanning spectrometer (Shimadzu, Columbia, MD). Absorption was collected using a 1.0 cm^2 quartz cuvette at room temperature and the blank (acetonitrile) was subtracted from each spectrum.

3.2.4 Electron Microscopy Characterization

An LVEM5-TEM (Delong America, Montreal, Canada) was used for characterization of the nanoGUMBOS. Samples were prepared by placing 1 μL of the water-in-oil emulsion (w/o) emulsion containing nanoparticles directly onto a carbon-coated copper grid. After 10 min, the grid was immersed in a solution of heptane for 30 s to remove any excess surfactant. The TEM grids were then air dried at room temperature for 10 min prior to analysis. TEM accelerating voltage was 5 kV. No staining was employed while preparing the TEM samples.

Particle size and standard deviations were calculated using an image processing technique, QCapture Pro 6.0.0.412. Samples were prepared in triplicate to confirm

reproducibility. Particle size was measured by selecting 100 particles and measuring their diameter using the QCapture Pro software. Histogram plots were constructed by measuring the diameter of 100 particles for each desired reagent concentration (plotted on the x-axis), while the number of nanoparticles was plotted on the y-axis.

3.2.5 Atomic Force Microscopy Characterization

A Veeco Bioscope scanning probe microscope (SPM) was used for AFM imaging, operated in tapping mode (Veeco Metrology Inc. Santa Barbara, CA). Topography and phase images were acquired with Nanoscope v5.12 software. Digital images were processed with Gwyddion, using Gwyddion open source software, which is freely available on the internet and supported by the Czech Metrology Institute.[21] Silicon cantilevers with resonance frequency range of 146–236 kHz, and spring constants ranging from 21–98 N/m (Nanosensor, Lady's Island, SC) were used to acquire tapping mode images. Estimates of surface coverage were obtained with *UTHSCA Image Tool for Windows version 3.00 (San Antonio, TX).* Sizes of nanoGUMBOS were measured by manually selecting a representative view of 200 particles and measuring their heights. The percentage of colored pixels was determined subjectively to provide estimates of surface coverage. The topography images were converted to grayscale bitmaps and a threshold value was selected visually for conversion to black and white pixels for quantitative comparisons. Solutions of nanoGUMBOS and magnetic nanoGUMBOS were diluted in heptane and deposited on freshly cleaved pieces (1×1 cm^2) of Ruby muscovite mica (S & J Trading Co., NY). Samples were dried for at least 48 h then imaged in ambient air using tapping mode AFM.

3.2.6 Superconducting Quantum Interference Device Characterization

A MPMS sample magnetometer was used to characterize the magnetic susceptibility of the magnetic nanoGUMBOS. An aliquot of the nanoparticle suspension was placed into an empty capsule. As the capsule is passed through the magnetometer, the magnetization of the sample is recorded as the magnetic field strength is increased. The magnetic susceptibility can be calculated from the slope of the linear line between magnetization of the sample and the magnetic field strength.

3.3 Results and Discussion

3.3.1 Particle Size Control

NanoGUMBOS composed of $[Bm_2Im][BF_4]$ and $[Bm_2Im][FeCl_4]$ GUMBOS particles were prepared following an AOT templating reverse micellar method.[28] The exchanging salts which yielded the GUMBOS were solubilized separately in the water pools of two water-in-oil microemulsions. After combining the two parent solutions, the formation of particles followed the steps outlined in Figure 3.1 in the following order: (1) diffusional approach of reverse micelles; (2) surfactant layer opening and micellar coalescence; (3) diffusion of solubilized molecules within the merged reverse micelles; (4) reaction between solubilized species with concomitant formation of product(s); and (5) decoalescence of reverse micelles carrying a nanoGUMBOS payload (Figure 3.2).[18] It is notable that the pockets of water formed in the core of the reverse micelle act as nanoreactors for the synthesis of these nanoparticles, while the use of self-assembled surfactants limits the particle growth to produce small and stable particles by providing a protective layer to preserve the microdroplets.[18]

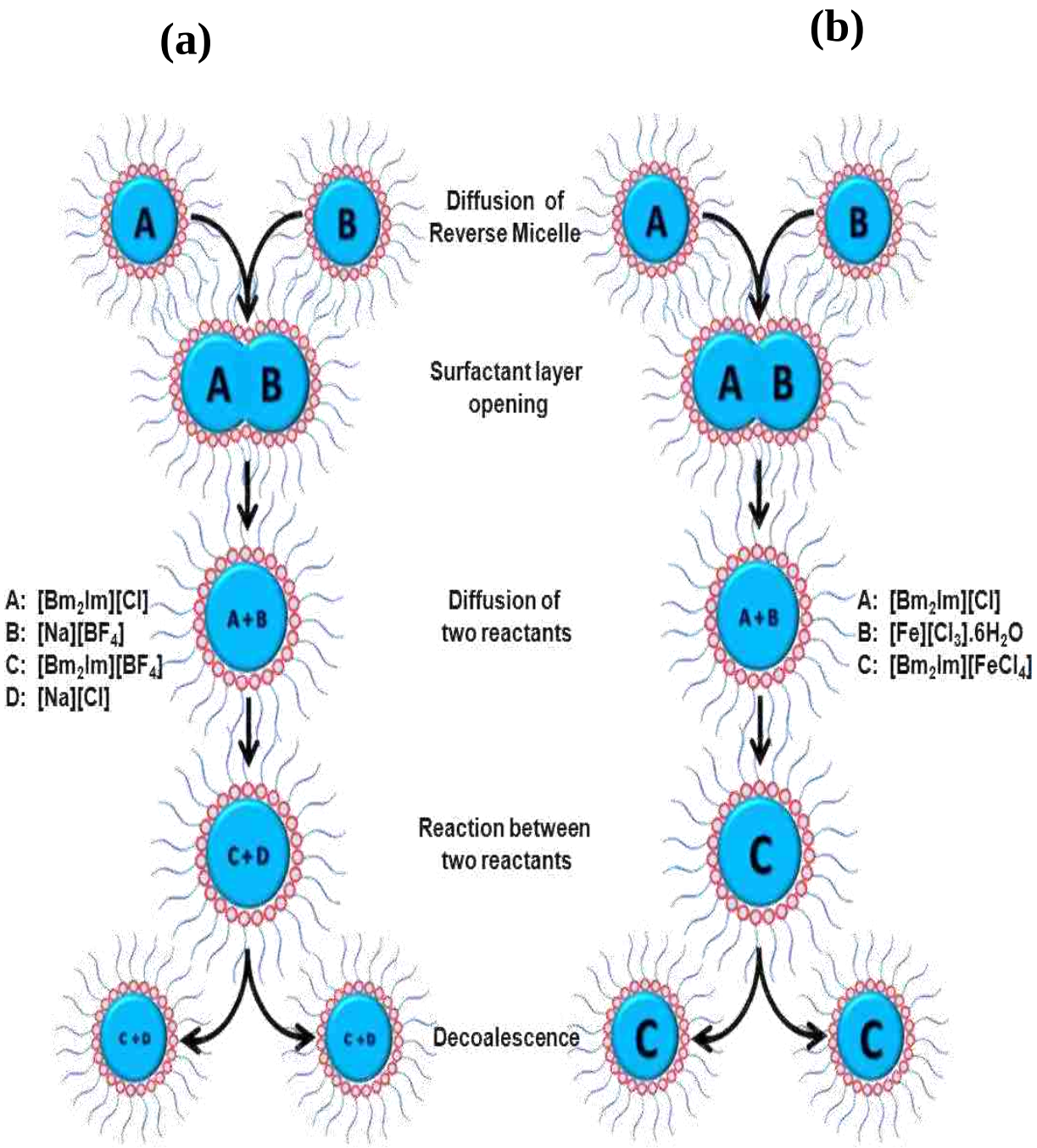

Figure 3.1 Basic processes for nanoparticle formation within AOT reverse micelles. Individual reverse micelles are shown without free surfactants.[18] (a) $[Bm_2Im][BF_4]$ nanoGUMBOS. (b) $[Bm_2Im][FeCl_4]$ magnetic nanoGUMBOS.

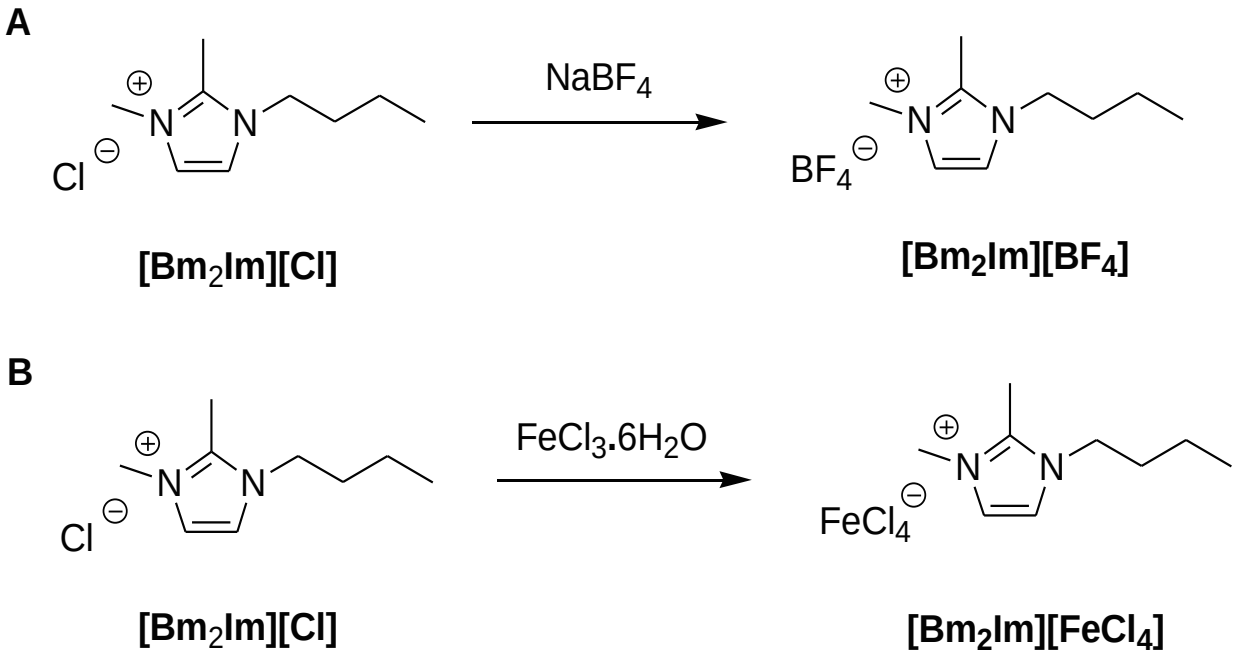

Figure 3.2 Exchange reaction at (A) the micellar core and (B) magnetic GUMBOS synthesis at the micellar core.

3.3.2 Nonmagnetic NanoGUMBOS of [Bm_2Im][BF_4]

Nonmagnetic [Bm_2Im][BF_4] nanoGUMBOS were prepared using the *in situ* ion exchange emulsion preparation outlined above, as summarized in Figure 3.2a. Particle size control was easily achieved by careful variation in the surfactant and reactant concentrations, choice of nonpolar solvent, temperature, mixing regime, and the relative water volume. In terms of the latter, the level of water within the water pool is defined as the molar ratio of water to surfactant, ω_0. It was observed that controlled changes in the concentrations of reactants directly regulated the average size of the harvested nanoGUMBOS. Using reactant concentrations in the 0.3–0.6 M range at a fixed A:B molar ratio of 1:1 Figure 3.2a, average particle diameters of 14.7 ± 2.2 to 68.0 ± 17.0 nm were obtained for 0.1 M AOT in *n*-heptane at a water loading (ω_0 = [H_2O]/[AOT]) of 13.34. Panels a through d of Figure 3.3 present representative TEM images of

[Bm_2Im][BF_4] nanoGUMBOS with average sizes of 14.7, 20.8, 34.3, and 68.0 nm using initial concentrations of 0.3, 0.4, 0.5, and 0.6 M reagent, respectively. NanoGUMBOS shown in Figure 3.3 appear non-aggregated and uniformly dispersed on the carbon film of the TEM grid. The entire surface is covered with relatively uniformly-sized particles with standard deviations of 2.2 nm for Figure 3.3a and 1.8 nm for Figure 3.3b. In contrast, the particles shown in Figures 3.3c and 3.3d are scattered more sparsely on the surface, although the relative standard deviation (RSD) in the particle size remains quite good. In fact, across the entire range of nanoGUMBOS synthesized, the RSD in particle size is near 15%. A higher polydispersity might be expected for the larger nanoGUMBOS. The underlying reason for this observation is that higher concentrations of reactants afford higher ion exchange and reactant diffusional collision rates, shifting the equilibrium-driven coalescence and decoalescence of the reverse micelles during particle formation. Table 1 is a presentation of data on the increase in diameter of [Bm_2Im][BF_4] nanoGUMBOS with increasing reagent concentrations. Histogram plots summarizing the [Bm_2Im][BF_4] nanoGUMBOS particle size distributions resulting from analysis of TEM results are furnished in Figure 3.4. This result clearly illustrates that the nanoGUMBOS particle size can be smoothly modulated simply by control over the reagent concentrations, a boon for simple, uniform nanoparticle production.

Simultaneously acquired topography and phase AFM images of nanoGUMBOS dried on mica are displayed in Figure 3.5 at two different magnifications. These particles are observed to possess highly spherical shapes ranging from 20 to 120 nm in diameter. Aggregation with neighboring particles is minimal, despite the fact that roughly 10% of the imaged surface is covered with particulate. The nanoscale variations in sizes are well

apparent in the wide area frames (60 × 60 μm^2) of Figure 3.5A and B. There is an interesting imaging artifact in the phase image of Figure 3.5B, which shows a bright crescent at the left of each sphere. Zooming in for a close-up view in Figures 3.5C and 3.5D (12 × 12 μm^2), the larger nanoGUMBOS appear to be less spherically symmetric and occasionally show slight ellipticity. These local views are not fully representative of the range of sizes observed for the entire sample. The corresponding phase image indicates a homogeneous surface composition; a uniformly dark color is observed for nanoGUMBOS regardless of size (Figure 3.5D). Further, the crescent artifact is not observed in the phase image at this magnification; this and the fact that it only occurs at the left hand side of the topographical image suggests a tip artifact. Moreover, we note that the size of the AFM tip is quite large compared to the size of the nanoGUMBOS. Likely, the lateral dimensions of the nanoGUMBOS are somewhat broadened by tip-sample convolution.[22, 23] The diameters of the nanoGUMBOS were measured based on the reliable *z*-resolution of the AFM acquired from 200 cursor height profiles to confirm the observations from TEM imaging. The heights were referenced to uncovered bare areas of mica as a baseline. For all of the areas examined throughout the sample, clusters of aggregated nanoGUMBOS were notably absent. However, due to their spherical shapes, nanoGUMBOS were observed to easily roll across the mica surface, along the direction of scanning, as a result of imaging forces induced during tip motion (data not shown). Therefore, strategies involving low forces and tapping mode are required to prevent unwanted perturbation of the nanoGUMBOS samples during AFM scanning. The images in Figure 3.5 were acquired using low imaging force and the nanoparticles were

not displaced. The particle size distributions of $[Bm_2Im][BF_4]$ nanoGUMBOS resulting from analysis of AFM are illustrated in Figure 3.6.

3.3.3 Magnetic $[Bm_2Im][FeCl_4]$ GUMBOS Particles

Magnetic $[Bm_2Im][FeCl_4]$ liquid particles (melting point –2.66 ^oC, Figure 3.7) were similarly produced using the *in situ* ion exchange emulsion method (Figure 3.2b). When prepared in bulk, $[Bm_2Im][FeCl_4]$ liquid GUMBOS show three absorption peaks at (528, 617, and 684 nm) which are known to be characteristic of $[FeCl_4^-]$ (Figure 3.8).[12]

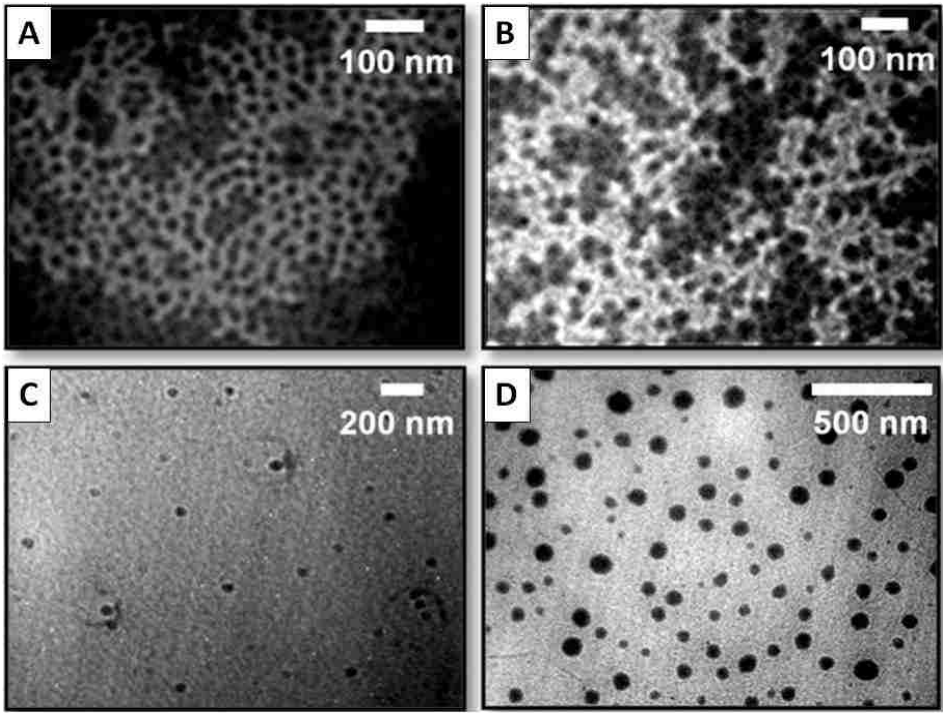

Figure 3.3 TEM micrographs of $[Bm_2Im][BF_4]$ nanoGUMBOS synthesized according to the approach shown in Figure 3.1a and imaged by TEM at the indicated magnifications with average particle diameters of: (A) 14.7 ± 2.2 nm, (B) 20.8 ± 1.8 nm, (C) 34.3 ± 4.8 nm, and (D) 68.0 ± 17.0 nm. Images were taken using an LVEM5 electron microscope with an accelerating voltage of 5 kV without staining.

Table 1. Effect of reagent concentration on particle size.

Reagent Concentration (M)	Particle Size (nm)	Standard Deviation (nm)
0.3	14.7	2.2
0.4	20.8	1.8
0.5	34.3	4.8
0.6	68.0	17

ω_0=13.34, molar ratio: 1:1, AOT concentration: 0.1 M

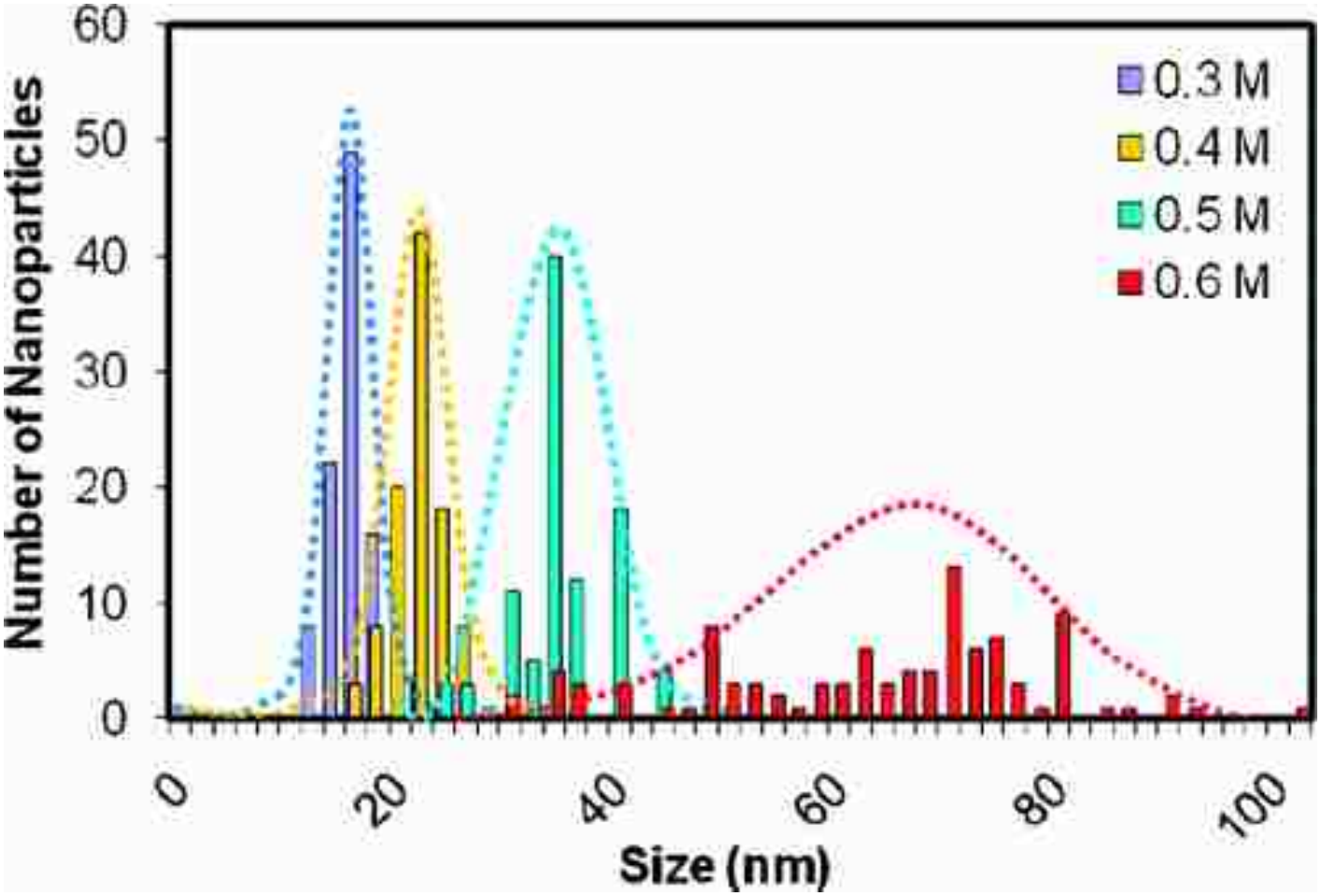

Figure 3.4 Size distributions of nanoGUMBOS synthesized via Figure 3.1a in water-containing AOT reverse micelles at various reagent concentrations: [AOT] = 0.1 M; molar reagent concentrations: 0.3, 0.4, 0.5, and 0.6 M.

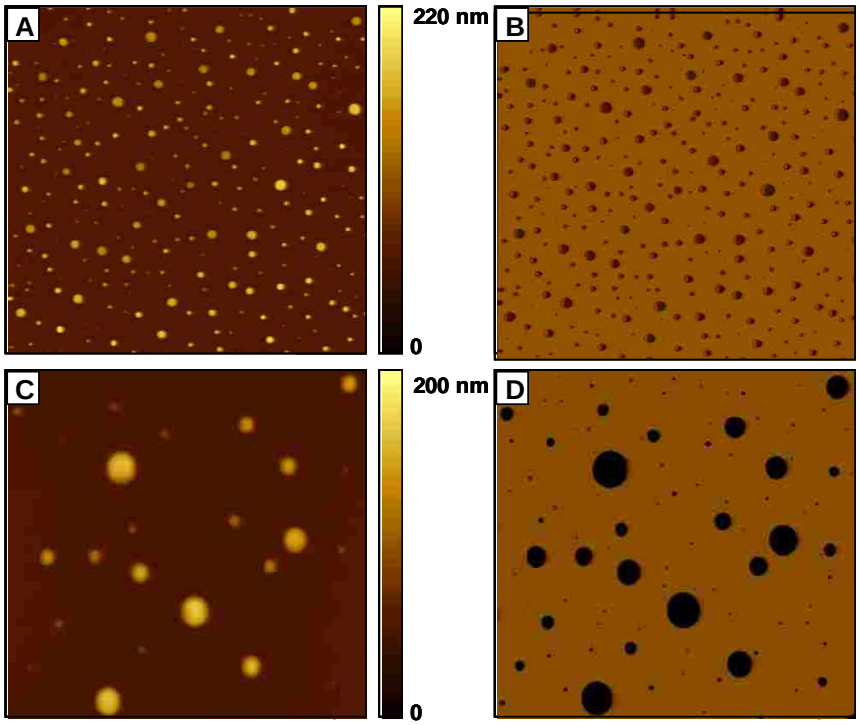

Figure 3.5 Images of $[Bm_2Im][BF_4]$ nanoGUMBOS synthesized in Figure 3.1a acquired with tapping mode AFM at a frequency of 150 kHz. (A) 60 × 60 μm^2 topographical image and (B) simultaneously acquired phase image. (C) Zoom-in view 12 × 12 μm^2 view and (D) corresponding phase channel.

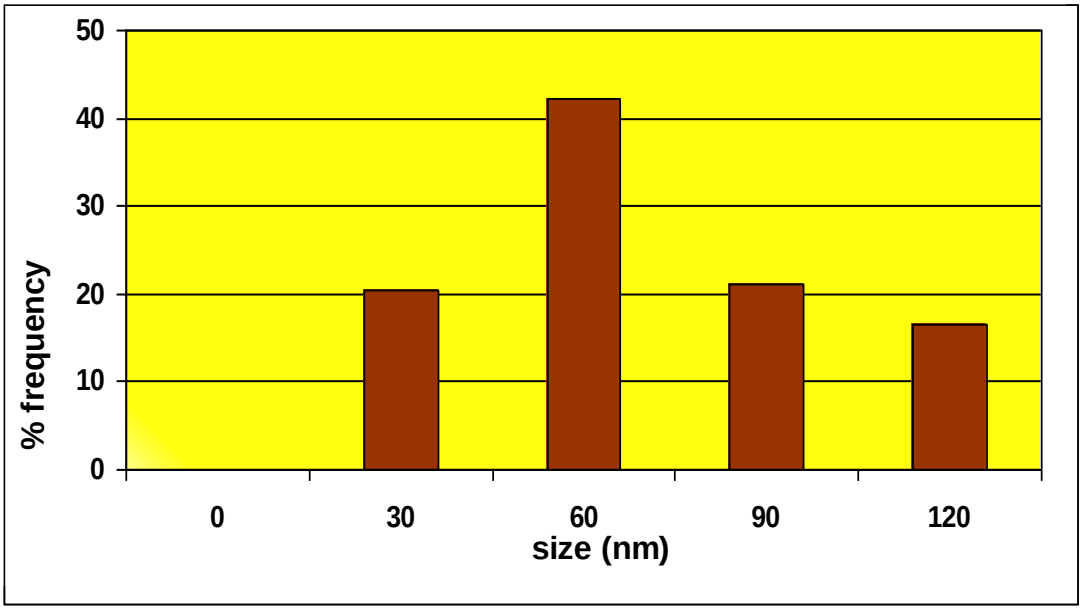

Figure 3.6 Size distributions of nanoGUMBOS synthesized via Figure 3.1a in water-containing AOT reverse micelles at reagent concentration: [AOT] = 0.1 M; molar reagent concentration: 0.4 M.

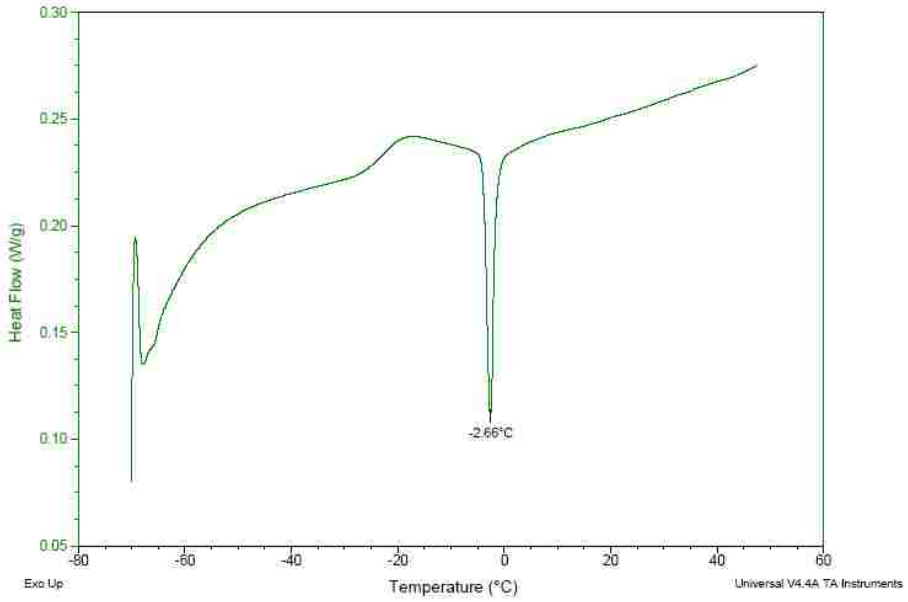

Figure 3.7 Melting point of bulk $[Bm_2Im][FeCl_4]$. The melting point of $[Bm_2Im][FeCl_4]$ is -2.66 °C.

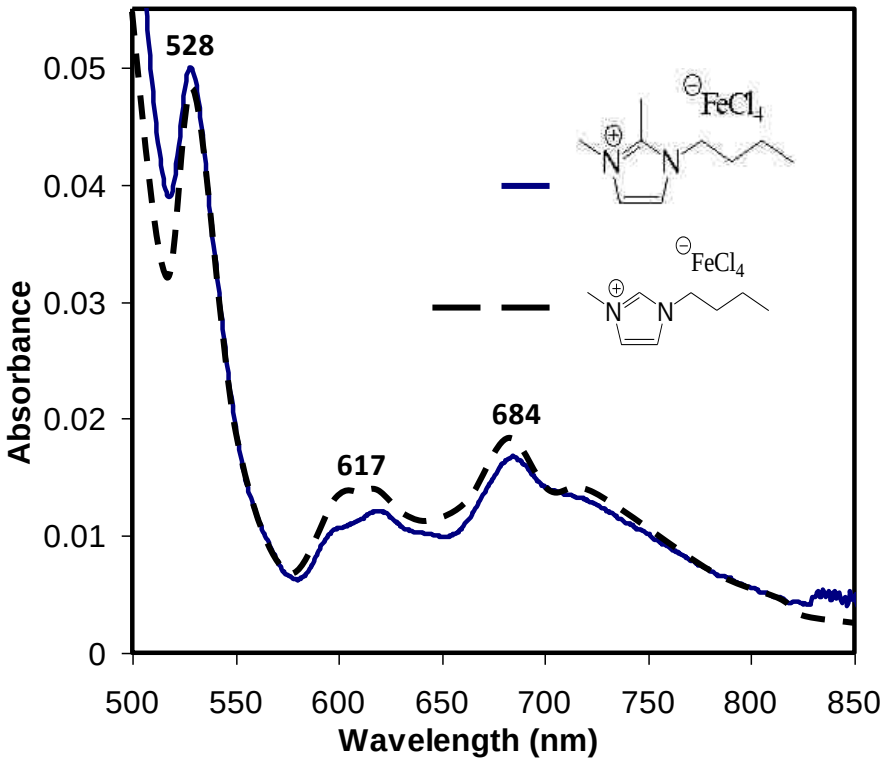

Fig. 3.8 UV-vis of $[Bm_2Im][FeCl_4]$ in acetonitrile GUMBOS show three absorption peaks at (528, 617, and 684 nm) characteristic of $[FeCl_4^-]$.

The liquid particles produced had an average diameter of 98 ± 17 nm when 0.3 M $[Bm_2Im][Cl]$ and 0.3 M $[FeCl_3 \cdot 6H_2O]$ were used for 0.1 M AOT in *n*-heptane (ω_0 = 13.34) based on an optimization study to maximize yield and minimize PDI (data not shown). As the TEM images shown in Figure 3.9 reveal, a higher number density of spherical magnetic GUMBOS particles was observed when compared with non-magnetic nanoGUMBOS of similar dimensions. Interestingly, the $[Bm_2Im][FeCl_4]$ particles were densely packed with frequent particle aggregation and overlapping observed in the TEM images. Similar to our results for non-magnetic nanoGUMBOS discussed above, high reactant concentrations yielded larger particles on average. For the case of increasing the reagent concentration to 0.4 M, all other conditions remaining the same, an effective doubling in particle size to 199 ± 26 nm was obtained (Figure 3.8b). These larger GUMBOS particles were more spherical and well segregated on the surface of the TEM grid. Table 2 clearly shows the increase in diameter of $[Bm_2Im][FeCl_4]$ GUMBOS particles with increasing reagent concentrations. A histogram of the particle size distribution is shown in Figure 3.10. Surprisingly, in both bases, GUMBOS particles deposited onto fresh-cleaved mica were well-dispersed and did not form pronounced aggregates. In fact, despite examination of dozens of areas over multiple samples, no clusters or aggregates of $[Bm_2Im][FeCl_4]$ GUMBOS particles were found. This result reflects the role played by surface hydrophobicity during nanoparticle deposition (indeed, there remains little information on how ILs or ionic solids interact with/solvate solid surfaces and highlights the soft matter nature of the nanoGUMBOS).[24, 25]

Two batches of magnetic GUMBOS particles formed with different target sizes are compared side-by-side in Figure 3.11. A regular spherical morphology is revealed for

100 nm [Bm_2Im][$FeCl_4$] nanoGUMBOS (Figure 3.11A, 3.11B). In contrast, in the lower panels of Figure 3.11, it can be seen that larger magnetic GUMBOS particles sometimes assume slightly egg-shaped morphologies on mica. In both cases, the phase images show uniform dark contrast for the magnetic GUMBOS particles, indicative of a homogeneous surface composition. The phase image of Figure 3.11B also has the sensitivity to reveal numerous tiny magnetic nanoGUMBOS that were not resolved in the topographical view. Fewer magnetic GUMBOS particles were captured within the 20 × 20 μm^2 frames of Figures 3.11C and 3.11D for the nominally 200 nm particles. However, the total surface coverage remains nearly the same as for the 100 nm GUMBOS (approximately 7% and 6% surface coverage is observed in Figure 3.11B and 3.11D, respectively). A few small streak marks were also detected within Figures 3.11C and 3.11D, which is thought to be produced by the action of the AFM tip pushing magnetic nanoGUMBOS across the surface. Overall, it is apparent that variations in the amount of reagent in each reverse micelle play a significant role in the sizes of nanoparticles produced for both nanoGUMBOS and magnetic nanoGUMBOS.

The magnetic properties of bulk magnetic GUMBOS and nanoGUMBOS samples composed of [Bm_2Im][$FeCl_4$] were investigated using SQUID measurements. In these experiments, bulk [Bm_2Im][$FeCl_4$] and nanoGUMBOS samples were contained within two separate capsules and their magnetic moments were measured in the magnetic field range of –10000 to +10000 Oe using an MPMS SQUID measuring system. Capsules containing both bulk and nanoscale [Bm_2Im][$FeCl_4$] GUMBOS show linear responses to the magnetic field as shown in Figure 3.12. The magnetic susceptibility of bulk [Bm_2Im][$FeCl_4$] is 34.3 × 10^{-6} emu/g according to the slope of the response to the

magnetic field. The magnetic susceptibility of the magnetic nanoGUMBOS sample was identical. In comparison, the magnetic susceptibility of bulk [BmIm][$FeCl_4$] is 40.6 × 10^{-6} emu/g, according to the literature.[12] Similar results were obtained for longer alkyl chain imidazolium-based ILs containing the [$FeCl_4^-$] anion. According to the literature, 1-hexyl-3-methylimidizolium and 1-methy-3-octylimidazolium cations coupled with [$FeCl_4^-$] exhibit magnetic susceptibilities of 39.6 × 10^{-6} and 36.6 × 10^{-6} emu/g, respectively.[26]

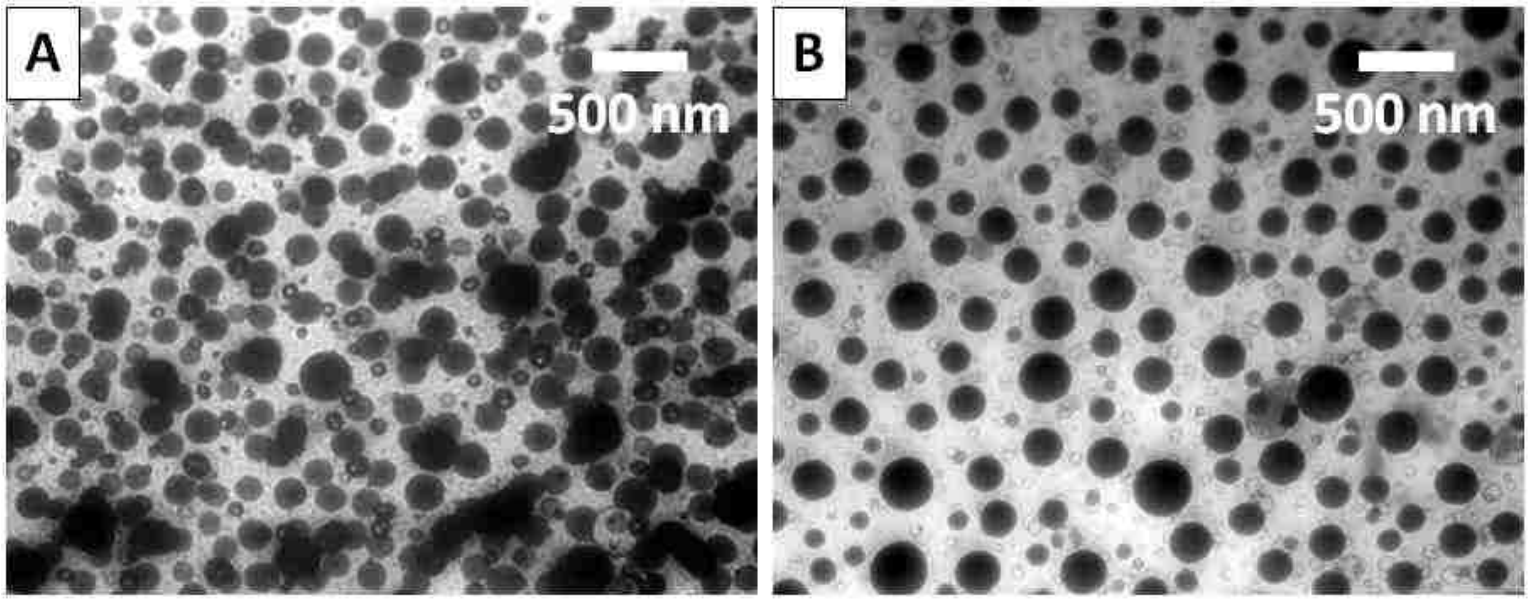

Figure 3.9 Micrographs of magnetic [Bm_2Im][$FeCl_4$] GUMBOS particles synthesized in Figure 3.1b obtained from TEM revealing mean particle sizes of (A) 98.0 ± 17 nm and (B) 199.0 ± 26 nm. Images were taken using an LVEM5 electron microscope with an accelerating voltage of 5 kV without staining.

Table 2 Effect of reagent concentration on particle size.

Reagent Concentration (M)	Particle Size (nm)	Standard Deviation (nm)
0.3	98	17
0.4	199	26

ω_0=13.34, Molar ratio: 1:1, AOT concentration: 0.1M.

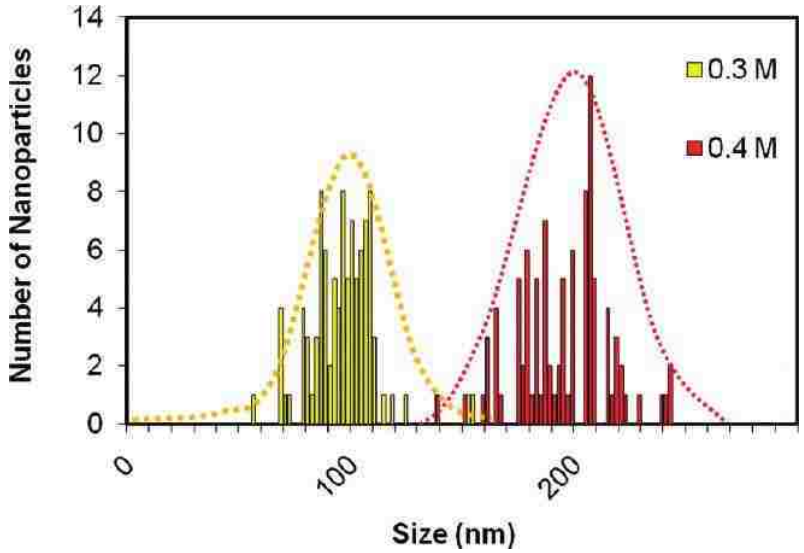

Figure 3.10 Size distributions of magnetic GUMBOS particles (shown in Figure 4) at various reagent concentrations: [AOT] = 0.1 M; molar reagent concentrations: 0.3 and 0.4 M.

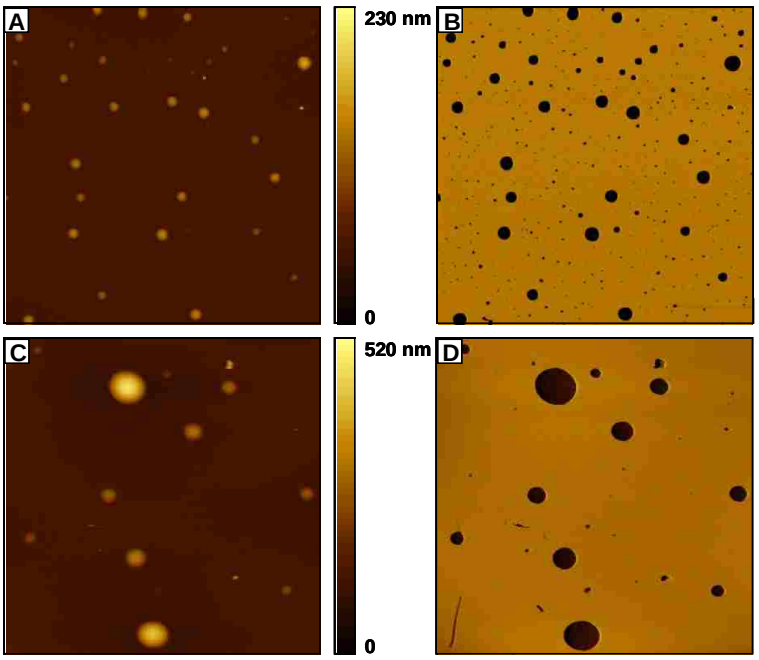

Figure 3.11 Differently sized samples of magnetic $[Bm_2Im][FeCl_4]$ nanoGUMBOS synthesized in Figure 3.1b imaged by tapping mode AFM for 20 × 20 μm2 scan areas at an 180 kHz driving frequency. (A) Topographical image of magnetic nanoGUMBOS with a diameter near 100 nm and (B) the matching phase image. (C) Topography of 200-nm GUMBOS particles and (D) the corresponding phase frame.

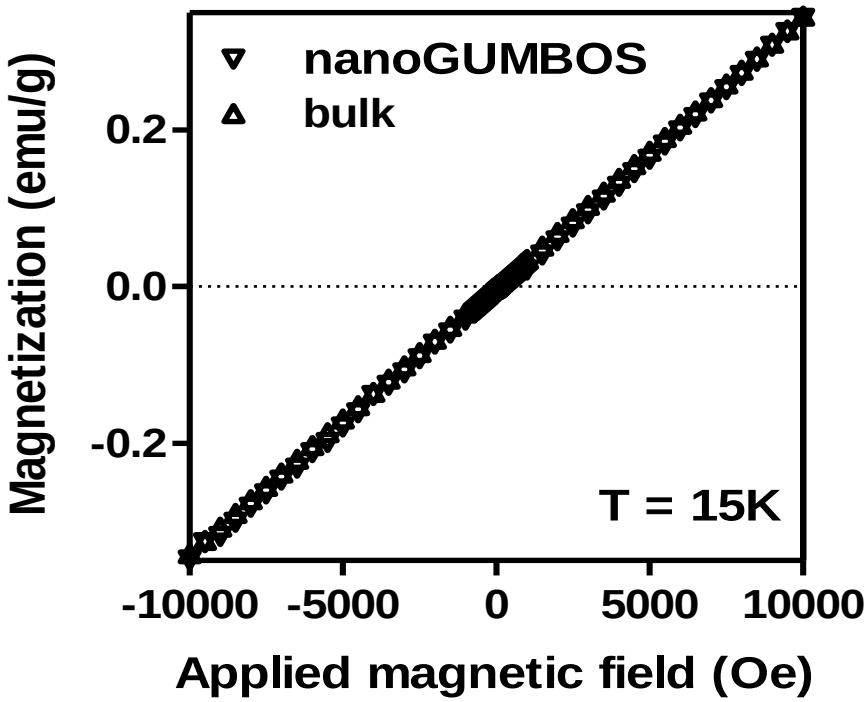

Figure 3.12 Magnetic susceptibility of bulk $[Bm_2Im][FeCl_4]$ alongside $[Bm_2Im][FeCl_4]$ nanoGUMBOS synthesized in Figure 3.1b.

3.4 Conclusions

In summary, a facile and reproducible method for synthesizing controllable sizes of nanoGUMBOS is reported. The ability of nanoGUMBOS to host functional magnetic properties was demonstrated. The overwhelming simplicity and versatility of nanoGUMBOS, particularly illustrated by elaboration of magnetic nanoGUMBOS in the current work, suggests broad application for these emergent nanoscale materials in the biomedical, electronics, analytical, and separations fields.

3.5 References

(1). Giri, S.; Trewyn, B. G.; Stellmaker, M. P.; Lin, V. S. Y. *Angew. Chem., Int. Ed.* **2005,** 44, (32), 5038-5044.

(2). Nunez, L.; Kaminski, M. D. *J. Magn. Magn. Mater.* **1999,** 194, (1-3), 102-107.

(3). Mornet, S.; Vasseur, S.; Grasset, F.; Veverka, P.; Goglio, G.; Demourgues, A.; Portier, J.; Pollert, E.; Duguet, E. *Prog. Solid State Chem.* **2006,** 34, (2-4), 237-247.

(4). Gupta, A. K.; Gupta, M. *Biomaterials* **2005,** 26, (18), 3995-4021.

(5). Lu, A. H.; Salabas, E. L.; Schueth, F. *Angew. Chem., Int. Ed.* **2007,** 46, (8), 1222-1244.

(6). Hong, X.; Li, J.; Wang, M.; Xu, J.; Guo, W.; Li, J.; Bai, Y.; Li, T. *Chem. Mater* **2004,** 16, (21), 4022-4027.

(7). Jeong, J.-R.; Lee, S.-J.; Kim, J.-D.; Shin, S.-C. *IEEE Trans. Magn.* **2004,** 40, (4, Pt. 2), 3015-3017.

(8). Ohno, H.; Fukumoto, K. *Accounts Chem. Res.* **2007,** 40, (11), 1122-1129.

(9). Hough-Troutman, W. L.; Smiglak, M.; Griffin, S.; Reichert, W. M.; Mirska, I.; Jodynis-Liebert, J.; Adamska, T.; Nawrot, J.; Stasiewicz, M.; Rogers, R. D.; Pernak, J. *New J. Chem* **2009,** 33, (1), 26-33.

(10). Hough, W. L.; Smiglak, M.; Rodriguez, H.; Swatloski, R. P.; Spear, S. K.; Daly, D. T.; Pernak, J.; Grisel, J. E.; Carliss, R. D.; Soutullo, M. D.; Davis, J. J. H.; Rogers, R. D. *New J. Chem* **2007,** 31, (8), 1429-1436.

(11). Del Sesto, R. E.; McCleskey, T. M.; Burrell, A. K.; Baker, G. A.; Thompson, J. D.; Scott, B. L.; Wilkes, J. S.; Williams, P. *Chem. Commun.* **2008**, (4), 447-449.

(12). Hayashi, S.; Hamaguchi, H.-o. *Chem. Lett.* **2004,** 33, (12), 1590-1591.

(13). Hayashi, S.; Saha, S.; Hamaguchi, H.-o. *IEEE Trans. Magn.* **2006,** 42, (1), 12-14.

(14). Freire, M. G.; Neves, C. M. S. S.; Carvalho, P. J.; Gardas, R. L.; Fernandes, A. M.; Marrucho, I. M.; Santos, L. M. N. B.; Coutinho, J. A. P. *J. Phys. Chem. B* **2007,** 111, (45), 13082-13089.

(15). Choudhury, A. R.; Winterton, N.; Steiner, A.; Cooper, A. I.; Johnson, K. A. *J. Am. Chem. Soc* **2005,** 127, (48), 16792-16793.

(16). Motte, L.; Billoudet, F.; Pileni, M. P. *J. Phys. Chem.* **1995,** 99, (44), 16425-9.

(17). Wu, M.-L.; Chen, D.-H.; Huang, T.-C. *Langmuir* **2001,** 17, (13), 3877-3883.

(18). Uskokovic, V.; Drofenik, M. *Surf. Rev. Lett.* **2005,** 12, (2), 239-277.

(19). Eastoe, J.; Gold, S.; Rogers, S. E.; Paul, A.; Welton, T.; Heenan, R. K.; Grillo, I. *J. Am. Chem. Soc* **2005,** 127, (20), 7302-7303.

(20). Harruff, B. A.; Bunker, C. E. *Langmuir* **2003,** 19, (3), 893-897.

(21). http://gwyddion.net/

(22). Schwarz, U. D.; Haefke, H.; Reimann, P.; Guentherodt, H. J. *J. Microsc-Oxford* **1994,** 173, (3), 183-97.

(23). Ramirez-Aguilar, K. A.; Rowlen, K. L. *Langmuir* **1998,** 14, (9), 2562-2566.

(24). Gao, L.; McCarthy, T. J. *J. Am. Chem. Soc* **2007,** 129, (13), 3804-3805.

(25). Kilaru, P.; Baker, G. A.; Scovazzo, P. *J. Chem. Eng. Data.* **2007,** 52, (6), 2306-2314.

(26). Yoshida, Y.; Saito, G. *J. Mater. Chem.* **2006,** 16, (13), 1254-1262.

CHAPTER 4

FLUORESCENT NANOPARTICLES FROM A GROUP OF UNIFORM MATERIALS BASED ON ORGANIC SALTS

4.1 Introduction

Fluorescent nanomaterials have garnered much attention for applications in areas such as photodynamic therapy,[1, 2] organic light-emitting diodes (OLEDs),[3] and biomedical imaging.[4] Fluorescent nanomaterials such as quantum dots have advantages when compared to traditional organic dyes such as their high luminescence and lower susceptibility towards photobleaching.[5] However, the toxicity of quantum dots hinders their applications in bioimaging. For example, CdTe quantum dots were shown to be cytotoxic in rat pheochromocytoma cells.[6] Therefore, it is of paramount importance to develop nanoparticles that exhibit biocompatibility, non-toxicity, and ease of tunability.

Traditionally, biocompatible nanoparticles have been prepared using techniques such as doping fluorophores in silica particles.[7] However, encapsulation of fluorophores often leads to dye leakage problems. In addition, traditional methods to control the size and dispersity of the particle involve the use of additives which make the system more complex and require tedious synthetic procedures. Therefore, it is important to develop a method to synthesize uniform fluorescent nanoparticles where the active components are built into the nanoparticle for biomedical applications.

In this chapter, a novel class of material dubbed GUMBOS, defined as a **G**roup of **U**niform **M**aterials **B**ased on **O**rganic **S**alts, were used to prepare fluorescent nanoparticles. GUMBOS by large are ionic liquids; however, some have melting points above 100 °C. GUMBOS are interesting materials because they enjoy the desirable

properties of ionic liquids such as negligible vapor pressure, high thermal stability, and tunability. Altering either the anion or the cation of GUMBOS can lead to changes in their physical properties, allowing them to be used for a myriad of applications.[8, 9]

The fluorescent nanoparticles derived from GUMBOS (nanoGUMBOS) presented in this dissertation were prepared using three different methods namely; reprecipitation, *in situ* ion exchange, and hydrogel preparation. However, the use of any of these methods have not been reported for the preparation of fluorescent nanoGUMBOS except for the reprecipitation method.[10] This study compared the spectral properties of the fluorescent nanoGUMBOS obtained using three different nanofabrication methods. These nanoGUMBOS are advantageous because their fluorescent properties emanate from the parent GUMBOS, thus eliminating the need for complex and laborious dye encapsulation or entrapment procedures to incorporate fluorescent dyes into a silica or polymer network for potential applications in biomedical imaging.

4.2 Materials and Methods

4.2.1 Materials

Rhodamine 6G chloride (≥99%), sodium tetraphenylborate (≥99%), sodium bis(2-ethylhexyl)sulfosuccinate, sodium deoxycholate, tris(hydroxymethyl)aminomethane (TRIS), heptane, acetone, and ethanol (spectroscopic grade) were purchased from Sigma Aldrich and used as received. Triply deionized water (18.2 MΩ cm) from an Elga model PURELAB ultra™ water filtration system was used for all preparations of fluorescent nanoGUMBOS. Carbon coated copper grids (CF400-Cu, Electron Microscopy Sciences, Hatfield, PA) were used for TEM imaging.

4.2.2 Synthesis and Characterization of Fluorescent GUMBOS

The fluorescent GUMBOS were prepared using anion exchange procedures modified from those reported in the literature.[11, 12] The synthesis of rhodamine 6G tetraphenylborate ([Rhod] [TPB]) is described as follows: An amount of 50 mg (0.104 mmol) of Rhodamine 6G chloride [Rhod][Cl] and 35.72 mg (0.104 mmol) of sodium tetraphenylborate [Na][TPB] salt were dissolved in a mixture of chloroform and water (2:1 v/v) and allowed to stir for 24hrs at room temperature (Figure 4.1). The chloroform (bottom layer) was washed several times with water and the product was obtained from the organic lower layer. The chloroform was removed under reduced pressure and the residual water was subsequently freeze dried.

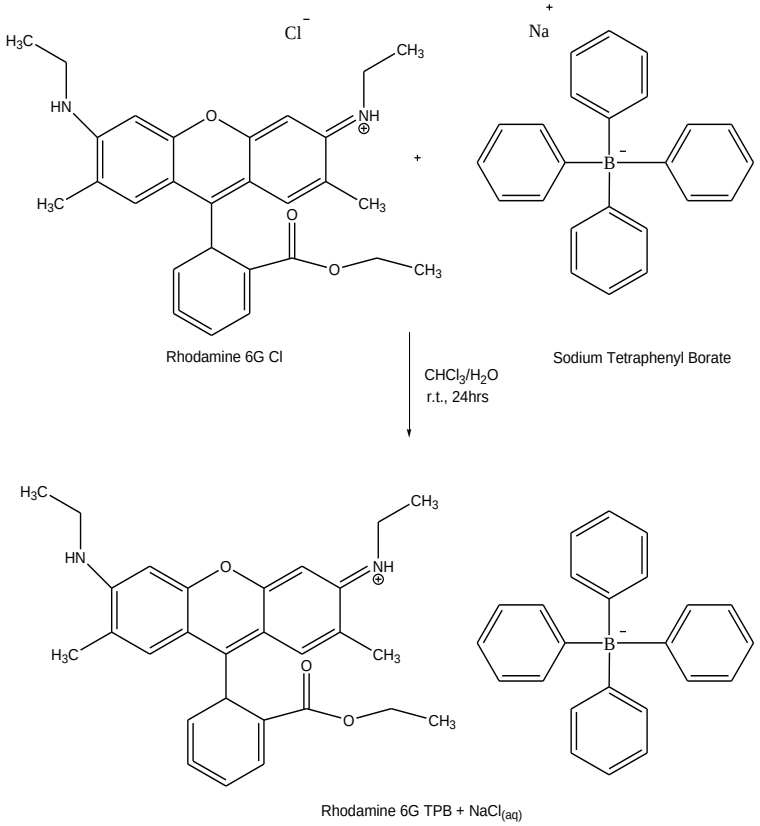

Figure 4.1 Synthesis of [Rhod][TPB] by anion exchange reaction.

4.2.3 Synthesis of Fluorescent NanoGUMBOS

4.2.3.1 Reprecipitation

The nanoGUMBOS were prepared from GUMBOS using a modified reprecipitation method similar to the method reported elsewhere.[13, 14] Typically, 100 µL of a 1 mM solution of GUMBOS dissolved in acetone was rapidly injected into 5 mL of triply-deionized water in an ultrasonic bath, followed by further sonication for 5 min (Figure 4.2)

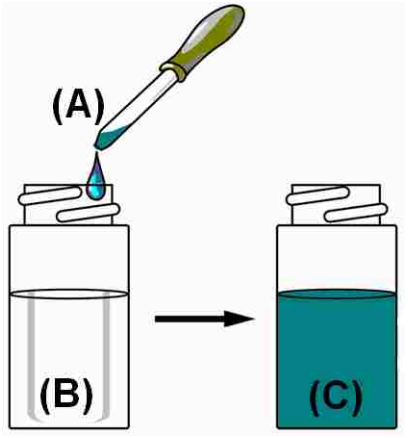

Figure 4.2 Preparation of fluorescent nanoGUMBOS using the reprecipitation method. (A) GUMBOS solution in solvent (1 mM acetone), (B) dispersant (5 mL water), and (C) nanoparticle suspension in dispersant.

4.2.3.2 *In situ* Ion Exchange

NanoGUMBOS of [Rhod][TPB] were prepared via a modified in-situ ion exchange method.[15] In a typical preparation, two separate 0.1 M solutions of [Rhod][Cl] and [Na][TPB] were prepared in ultra-pure water. Two additional solutions containing 5 mL of 0.1 M AOT in heptane were prepared separately. First, 120 µL of the aqueous [Rhod][Cl] solution was added into 5 mL of 0.1 M AOT solution in heptane, and then 120 µL of the aqueous [Na][TPB] solution was added into a separate vial also containing 5 mL of 0.1 M AOT solution in heptane. Each solution was then vortexed for 1 min and

allowed to equilibrate for 1 h. The molar ratio between [Rhod][Cl] and [Na][TPB] was 1:1. The two solutions were then mixed in a tightly sealed 20 mL scintillation vial and stirred for 24 h at room temperature. After combining the two parent solutions, the formation of nanoparticles proceeded in the following steps: (1) diffusion of the reverse micelles containing reagents (A) and (B); (2) surfactant layer opening and micellar coalescence; (3) diffusion of solubilized molecules within the merged reverse micelles; (4) reaction between solubilized species with formation of product(s) (C+D); and (5) decoalescence of reverse micelles (Figure 4.3).[16] It is notable that the pockets of water formed in the core of the reverse micelle act as nanoreactors for the synthesis of these nanoparticles, while the use of self-assembled surfactants limits the particle growth to produce small and stable particles by providing a protective layer to preserve the microdroplets.

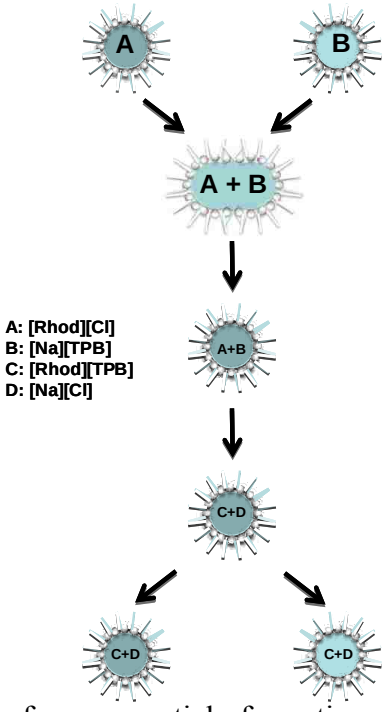

Figure 4.3 Basic processes for nanoparticle formation within AOT reverse micelles. Individual reverse micelles are shown without free surfactants. [Rhod][TPB] nanoGUMBOS.

4.2.3.3 Hydrogel Preparation

NanoGUMBOS of [Rhod][TPB] were prepared with a hydrogel method. A 20 mM solution of sodium deoxycholate was dissolved in pH 6.0 Tris-HCl buffer. A 5.28 μL volume of a 1 mM [Rhod][TPB] solution dissolved in ethanol was rapidly injected into 3 mL of an aqueous sodium deoxycholate solution in an ultrasonic bath, followed by further sonication for 5 min. Sodium deoxycholate (NaDC) possesses an interesting micellization chemistry which is different from conventional surfactants. NaDC has a steroid backbone providing it a hydrophobic face (β) and the OH groups attached to it imparts hydrophilic character to the other face (α). Hence, the micellization of NaDC is first initiated by hydrophobic interactions above its cmc (3-5mM) between the hydrophobic faces forming primary micelles. With further increase in concentration, hydrogen bonding involving the OH groups on the hydrophilic face of the primary micelles leads to the formation of secondary micelles. Lowering the pH below 6.6, which is its pKa, leads to the protonation of the COO^- of NaDC thereby increasing the hydrogen bonding interaction among the individual micellar units forming larger aggregates. These interactions lead to the gelation of water yielding a hydrogel (Figure 4.4). The gels have both a hydrophobic and hydrophilic domain, and this interesting structural feature of the gel was taken advantage of for the preparation of the nanoGUMBOS.

4.3 Characterization of Fluorescent NanoGUMBOS

The average particle size of the nanoGUMBOS was obtained by use of transmission electron microscopy (TEM). TEM micrographs were obtained using a JEOL 100CX transmission electron microscope. The nanoGUMBOS sample (1 μL) was

dropcasted onto a carbon coated copper grid and allowed to dry in air at room temperature before TEM imaging.

4.4 Absorption and Fluorescence Studies of Fluorescent GUMBOS and NanoGUMBOS

Absorbance measurements were performed on a Shimadzu UV- 3101PC UV-Vis-NIR scanning spectrometer (Shimadzu, Columbia, MD). A 1 cm^2 quartz cuvette was used to scan the absorbance and the blank was subtracted from each spectrum. The blank for the reprecipitation method was water and AOT/heptane/H_2O with an R value of 13.3 for the *in situ* ion exchange. Fluorescence emission was collected with a 1 cm pathlength quartz cuvette (Starna Cells) using a Spex Fluorolog-3 spectrofluorimeter (model FL3-22TAU3); Jobin Yvon, Edison, NJ).

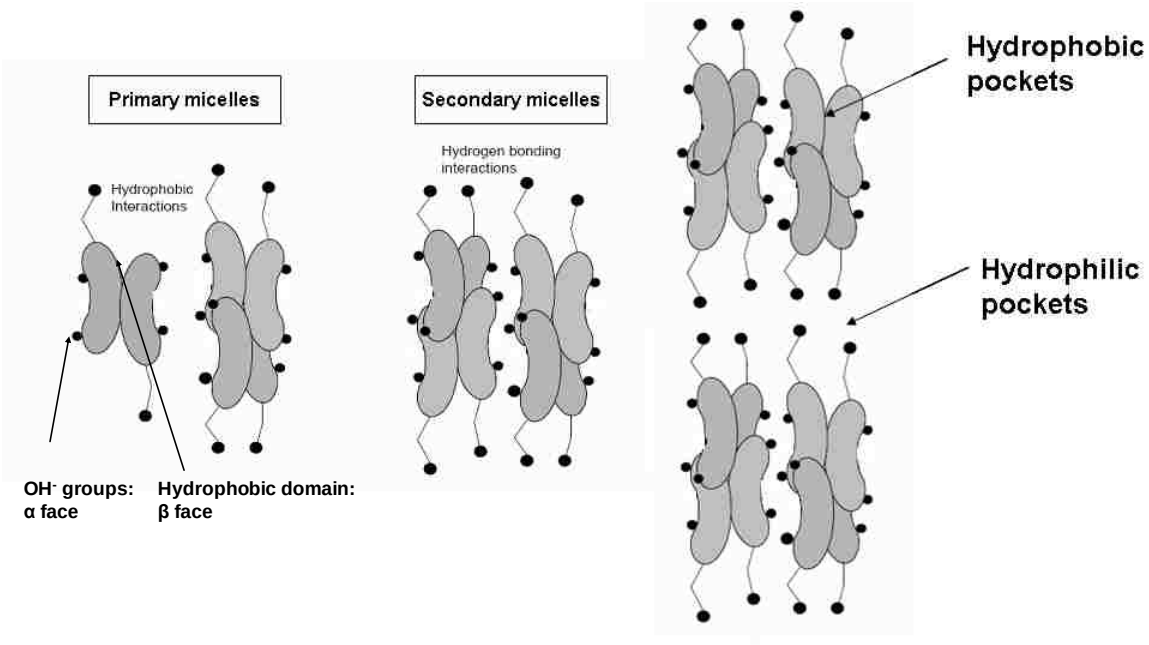

Figure 4.4 Basic processes for nanoparticle formation within hydrogels modified from reference.[17]

4.5 Results and Discussion

4.5.1 Synthesis, Characterization and Optical Properties of Fluorescent GUMBOS

The spectral properties of the produced GUMBOS were studied using absorption and fluorescence spectroscopy. A 1.76 µM acetone solution of [Rhod][TPB] GUMBOS was found to have a strong absorbance with a peak at 525 nm (Figure 4.5). The GUMBOS were found to exhibit an appreciably high fluorescence with maximum emission ~550 nm. The fluorescence excitation and emission spectra followed the mirror-image rule (Figure 4.6) as seen with the Franck-Condon principle.

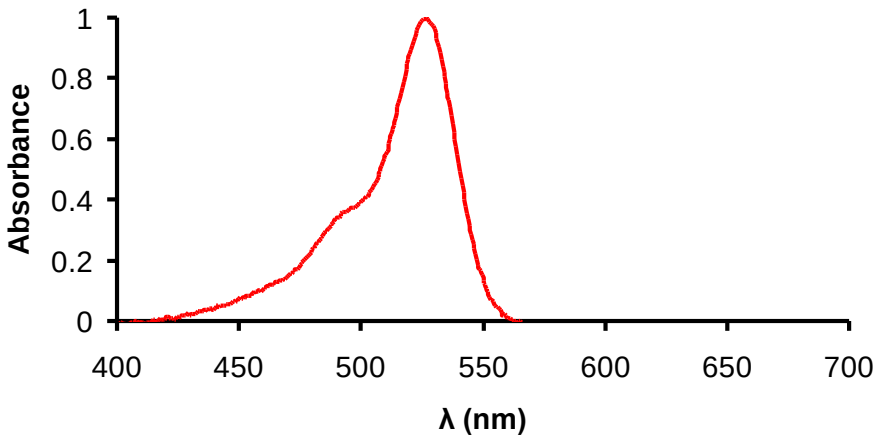

Figure 4.5 Absorbance profile for 1.76 µM [Rhod][TPB] in acetone; λ_{ex} = 525 nm.

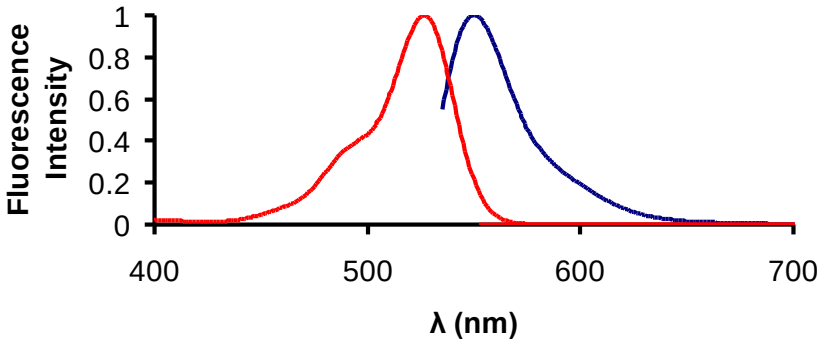

Figure 4.6 Fluorescence excitation and emission spectra for 1.76 µM [Rhod][TPB] in acetone; λ_{ex} = 525 nm, λ_{em} = 550 nm.

4.5.2 Synthesis, Characterization and Optical Properties of Fluorescent NanoGUMBOS

4.5.2.1 Reprecipitation

The reprecipitation synthetic method yields nanoparticles with spherical-oval morphologies measured by TEM. A representative TEM micrograph of nanoGUMBOS with an average particle diameter of 89 ± 17 nm is shown in Figure 4.7.

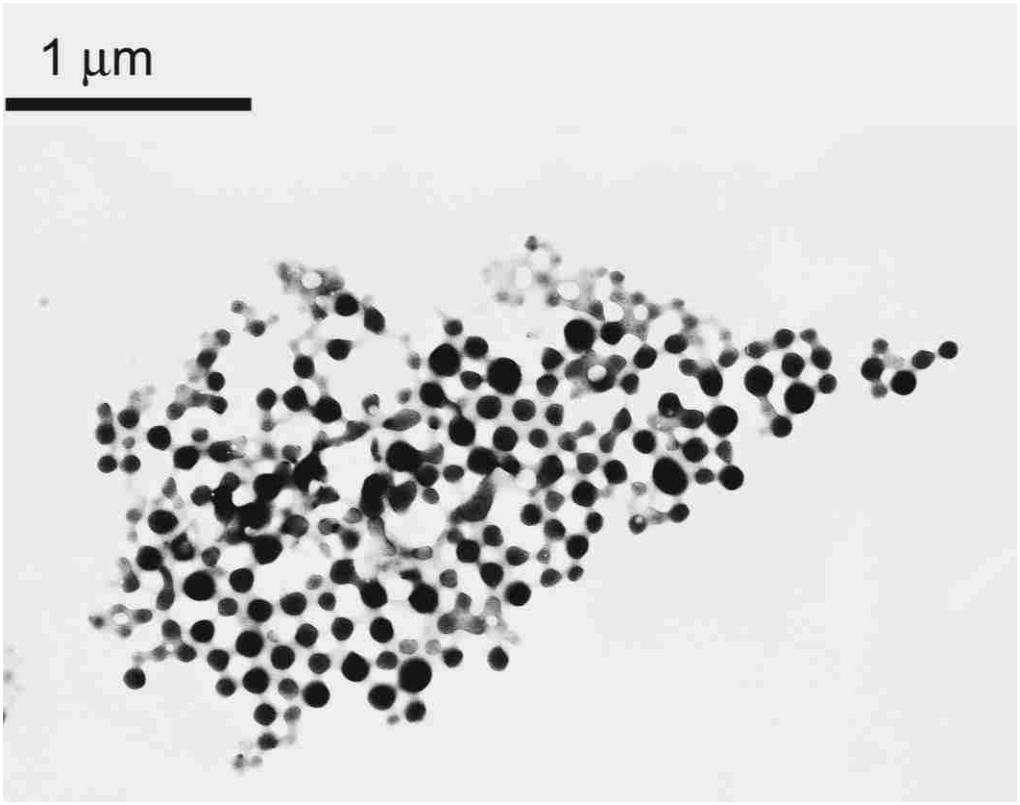

Figure 4.7 Reprecipitation: TEM micrograph of [Rhod][TPB] fluorescent nanoGUMBOS with an average diameter near 89 ± 17 nm.

The fluorescent nanoGUMBOS had optical properties which were different from that of the [Rhod][Cl] aqueous solution. The absorption spectra of the nanoGUMBOS were generally broad, having a FWHM of 66 nm (Figure 4.8 blue) as compared with [Rhod][Cl] dissolved in water at an equivalent concentration having a FWHM of 39 nm

(Figure 4.8 red). When measured at an equivalent concentration, the normalized emission maximum wavelength (λ_{max}) for the nanoparticle suspension remained the same compared with the [Rhod][TPB] water solution (Figure 4.9). The fluorescence intensity of the nanoGUMBOS suspension was also observed to be lower than the bulk [Rhod][Cl] aqueous solution (Figure 4.10). Lower fluorescence of [Rhod][TPB] nanoGUMBOS compared to [Rhod][Cl] in water may be attributed to the enhanced non-radiative decay processes in the solid state due to increased intermolecular interactions.

4.5.2.2 In-situ Ion Exchange

The in-situ ion exchange yields spherical nanoparticles as confirmed by TEM. A representative TEM micrograph of nanoGUMBOS with an average particle diameter of 89 ± 11 nm is shown in Figure 4.11.

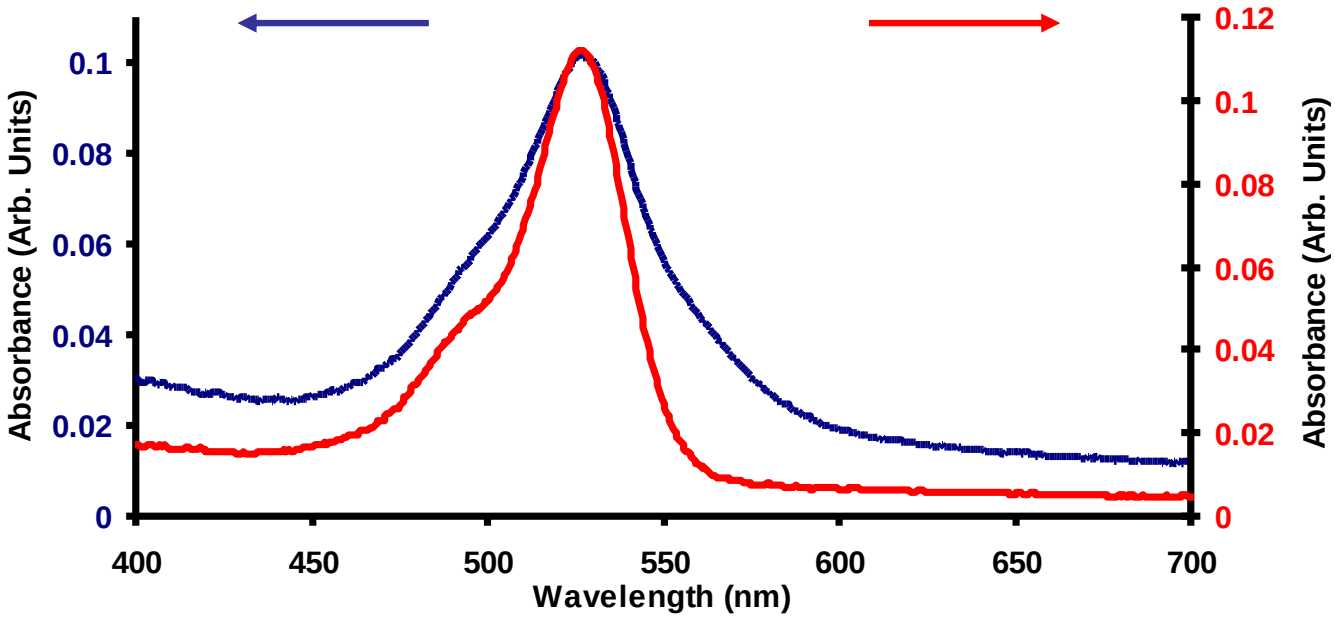

Figure 4.8 Reprecipitation: Absorbance spectrum of the [Rhod][TPB] nanoGUMBOS (blue) 1.76 μM. Absorbance spectrum of [Rhod][Cl] dissolved in water (red) 1.76 μM.

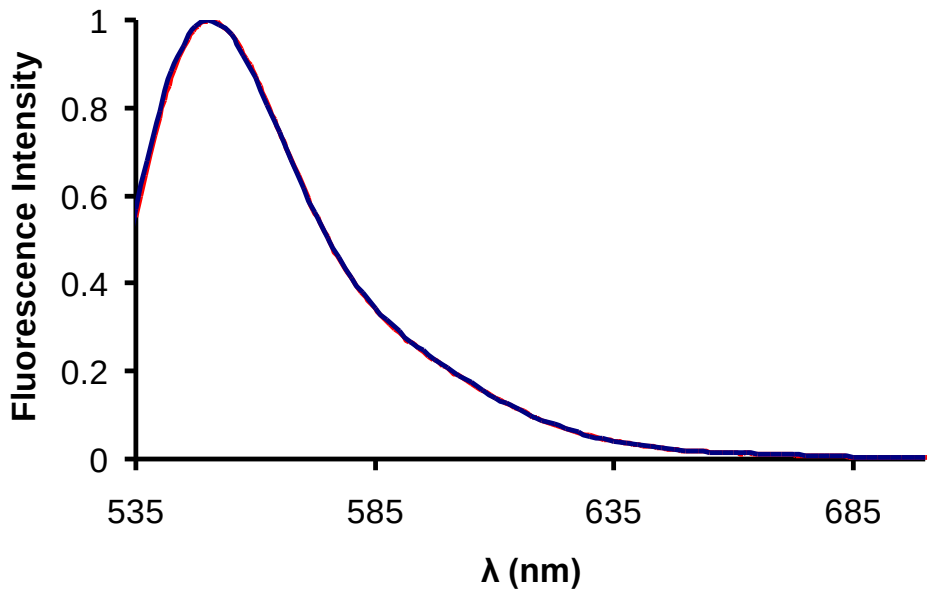

Figure 4.9 Reprecipitation: Normalized fluorescence spectrum of the [Rhod][TPB] nanoGUMBOS (blue) 1.76 µM. Fluorescence spectrum of [Rhod][Cl] dissolved in water (red) 1.76 µM at the excitation wavelength (λ_{ex} = 525 nm).

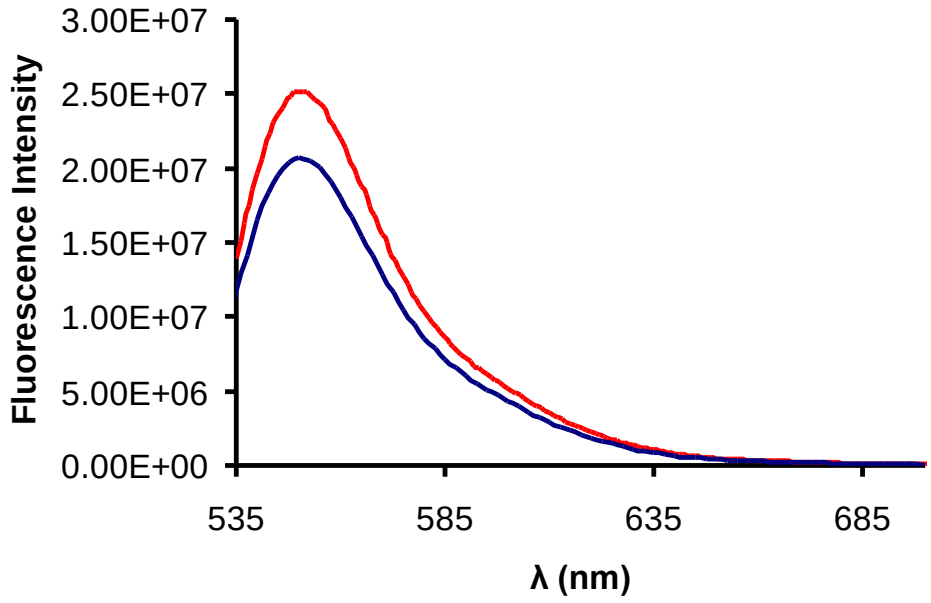

Figure 4.10 Reprecipitation: Comparison between the fluorescence emission spectrum of the freely dissolved [Rhod][Cl] GUMBOS (1.76 µM in water; red profile) and [Rhod][TPB] nanoGUMBOS (blue profile) for matched concentration at the excitation wavelength (λ_{ex} = 525 nm).

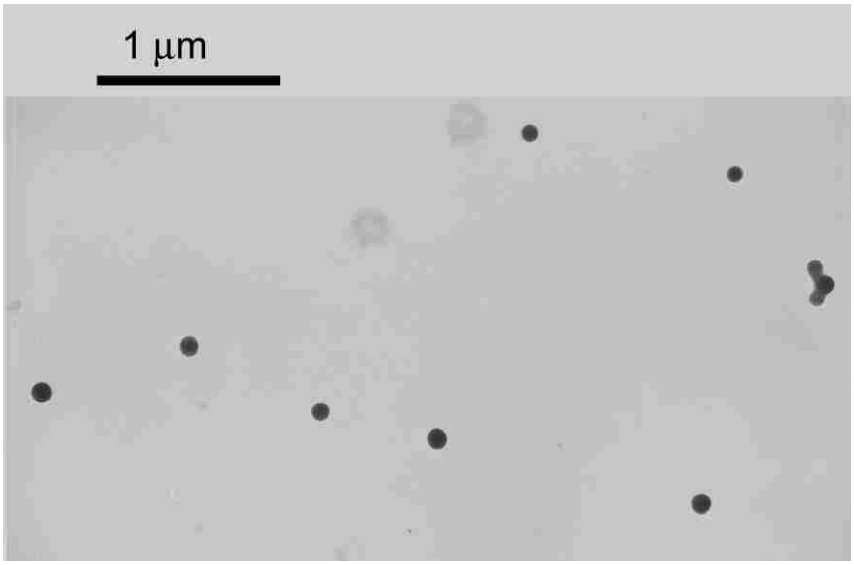

Figure 4.11 In-situ ion exchange: TEM micrograph of [Rhod][TPB] fluorescent nanoGUMBOS with an average diameter near 89 ± 11 nm.

The absorbance spectra for the nanoGUMBOS were bathochromically shifted by ~ 5 nm compared with [Rhod][Cl] dissolved in water at a matched concentration. (Figure 4.12).

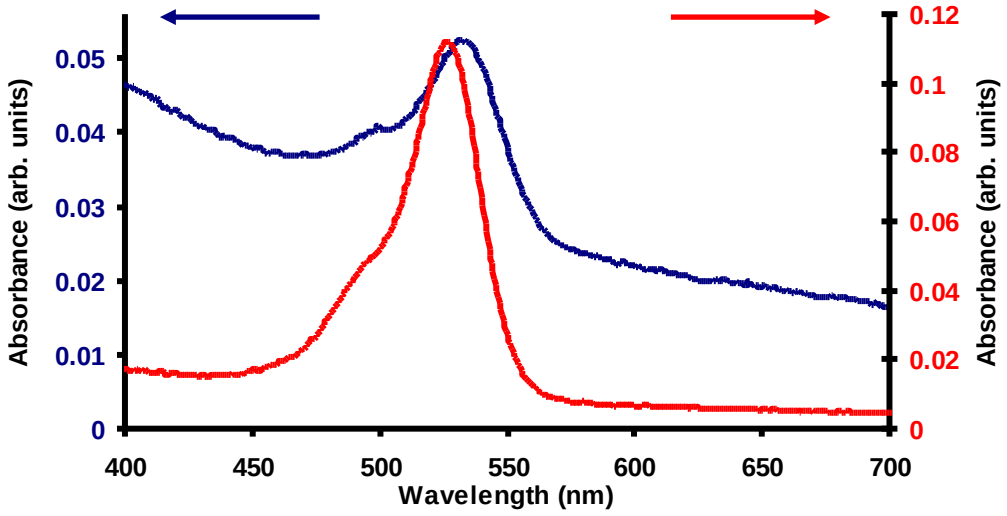

Figure 4.12 In-situ ion exchange: Absorbance spectrum of the [Rhod][TPB] nanoparticles (blue) 1.76 µM. Absorbance spectrum of [Rhod][Cl] dissolved in water (red) 1.76 µM.

The emission λ_{max} for both [Rhod][TPB] nanoGUMBOS and [Rhod][Cl] was red shifted by 10 nm in the reverse micelle as compared to the [Rhod][Cl] dissolved in water (Figure 4.13). The reverse micellar water pool has a different environment compared to bulk water[18] A layer of water molecules are bound to the negatively charged sulfonate head groups of AOT and the microenvironment is termed as "bound water layer." Water that is loosely bound to the polar head groups is termed "bulk water." The water pools can vary with the molar ratio of water to the concentration of the surfactant, or R = $[H_2O]$/[surfactant]. With an increase in the molar ratio of water to surfactant, bound water behaves similar to that of bulk water. However, at lower molar ratios of water to surfactant, where the water is more tightly bound to the negatively charged sulfonate head groups or the sodium counter ions, the properties of the bound water differ from that of bulk water.[18-20] The water pool in this study is considered "bound water." The nanoGUMBOS are synthesized within the water pool and reside in the "bound water" micronenvironment. Thus, the bound water is tightly associated to the negatively charged sulfosuccinate head groups of the reverse micelle which will experience a different environment than that of bulk water. The observed 5 nm bathochromic shift in absorption and 10 nm red shift in fluorescence emission of the [Rhod][TPB] nanoGUMBOS and [Rhod][Cl] in the reverse micellar pool compared to the [Rhod][Cl] dissolved in water may be attributed to the change in microenvironment.

The fluorescence intensity of the nanoparticle suspension in the reverse micellar pool was observed to be higher than the free [Rhod][Cl] in the reverse micellar pool (Figure 4.14). The fluorescence intensity of the nanoGUMBOS is greater than that of free [Rhod][Cl] in the reverse micelle which may be due to an effect of the

microenvironment on two different states of the dye; one in particle and the other in the dissolved state.

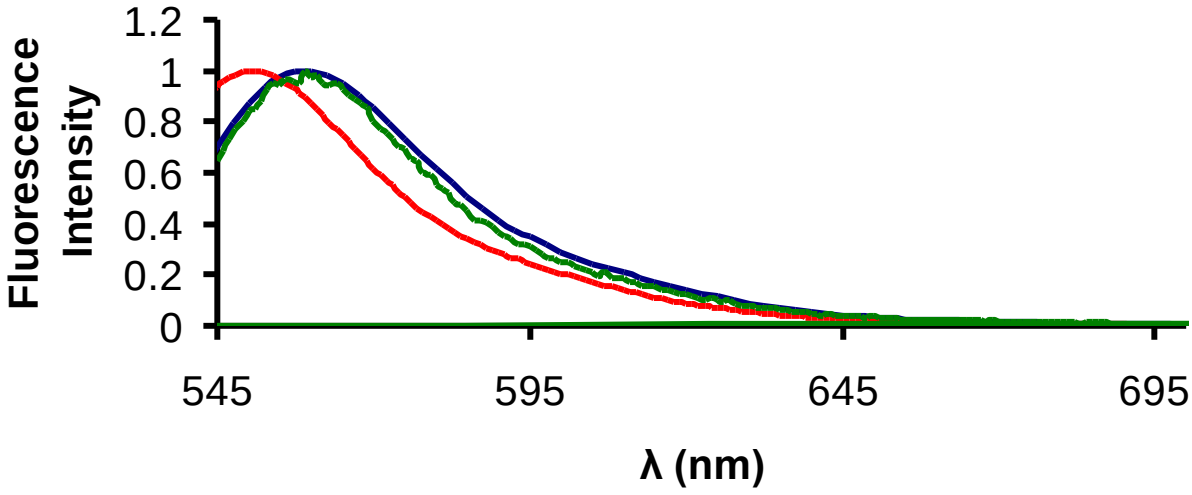

Figure 4.13 In-situ ion exchange: Comparison between the normalized fluorescence emission spectrum of the freely dissolved [Rhod][Cl] (in water; red profile), freely dissolved [Rhod][Cl] (in reverse micelle; green profile) and [Rhod][TPB] nanoGUMBOS (blue profile) for matched concentration.

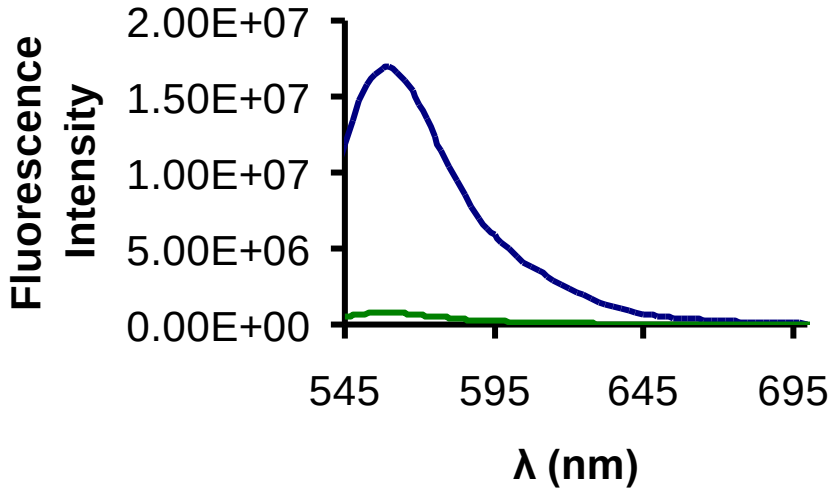

Figure 4.14 In-situ ion exchange: Comparison between the fluorescence emission spectrum of freely dissolved [Rhod][Cl] (in reverse micelle; green profile) and [Rhod][TPB] nanoGUMBOS (blue profile) for matched concentration.

4.5.2.3 Hydrogel Preparation

The hydrogel synthetic method yielded spherical particles as confirmed by TEM. A representative TEM micrograph of GUMBOS particles with an average particle diameter of 124 ± 35 nm is shown in Figure 4.15.

The fluorescent GUMBOS particles displayed optical properties which were different from that of the [Rhod][Cl] dissolved in water. The FWHM was 39 nm for the [Rhod][Cl] solution dissolved in water (Figure 4.16 red). The absorbance spectra for the nanoGUMBOS were generally broad having a FWHM of 97 nm (Figure 4.16 blue).

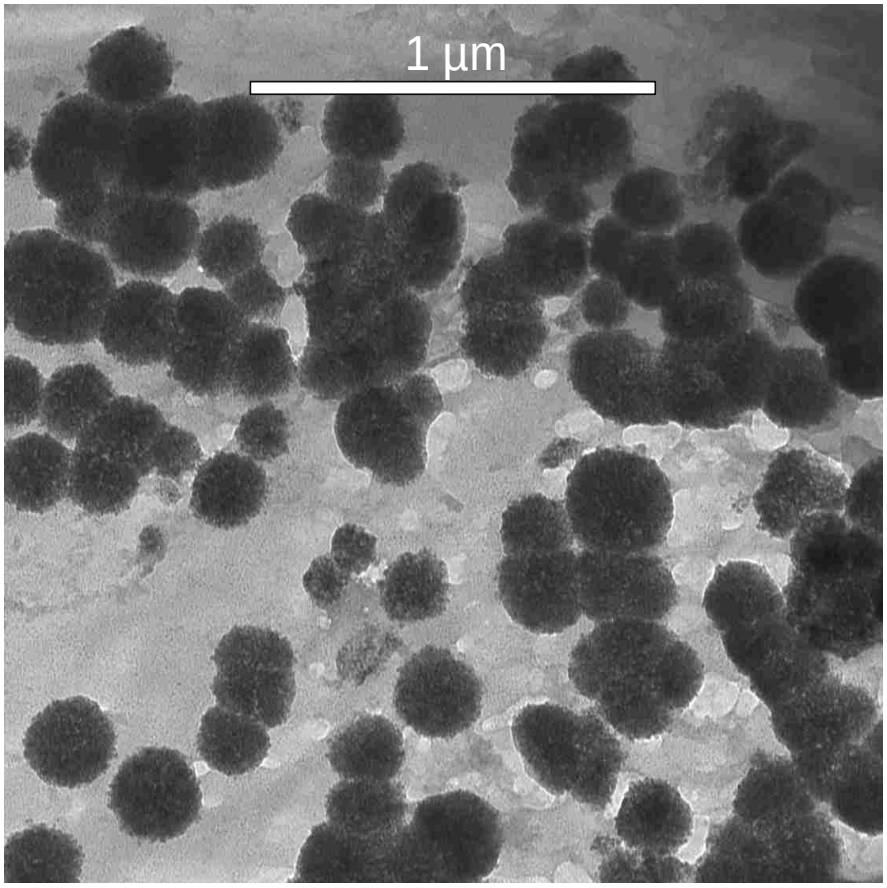

Figure 4.15 Hydrogel Synthesis: TEM micrograph of [Rhod][TPB] fluorescent nanoGUMBOS with an average diameter near 124 ± 35 nm.

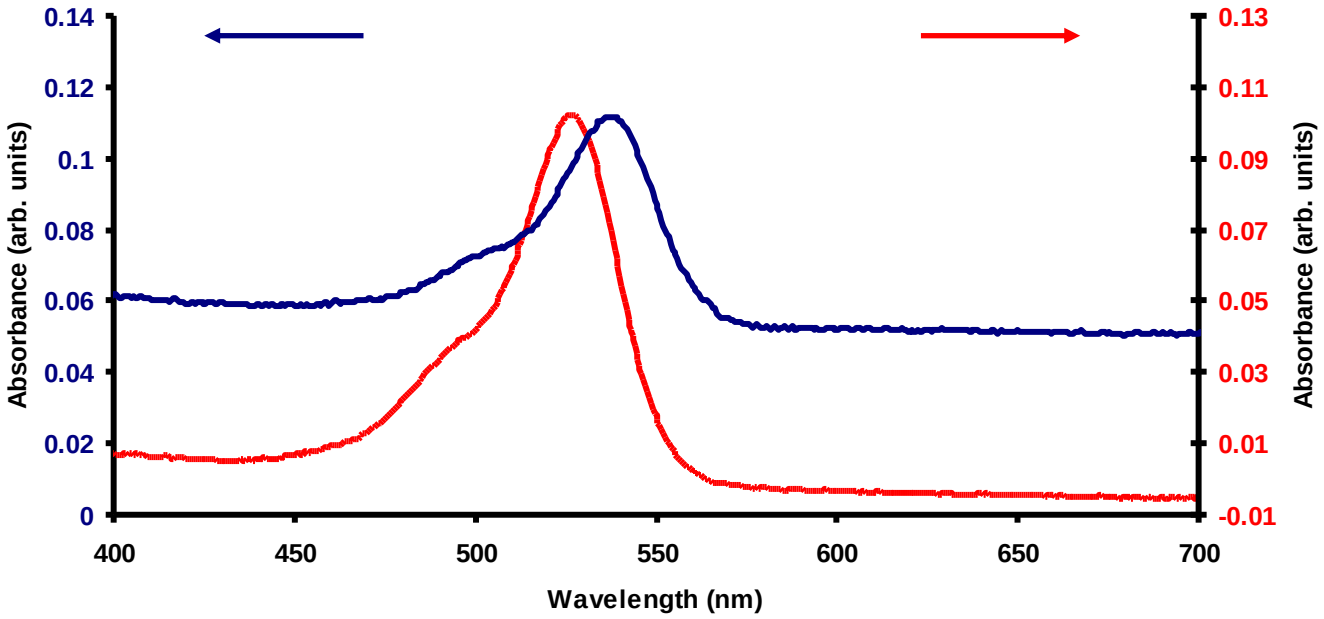

Figure 4.16 Hydrogel synthesis: Absorbance spectrum of the [Rhod][TPB] particles (blue) 1.76 μM. Absorbance spectrum of [Rhod][Cl] dissolved in water (red) 1.76 μM.

Figure 4.17 illustrates the fluorescence spectra of the [Rhod][Cl] dissolved in water compared with that of the [Rhod][TPB] GUMBOS particles synthesized within the hydrogel. [Rhod][Cl] has a significantly lower fluorescence (red) as compared with the highly fluorescent nanoGUMBOS within the hydrogel (blue). The GUMBOS particles reside in a very rigid microenvironment within the hydrogel, thus minimizing the non radiative loss of energy due to collisions and thereby increasing the fluorescence yield. [Rhod][Cl] dissolved in the hydrogel (Figure 4.18 green) has a lower fluorescence compared to [Rhod][Cl] dissolved in water (Figure 4.18 red). Thus, the increased intensity in GUMBOS particles of [Rhod][TPB] in the gel may be due to the

planarization of the individual molecules in the solid state within the gel environment, thereby favoring a specific kind of dye assembly within the GUMBOS particles.

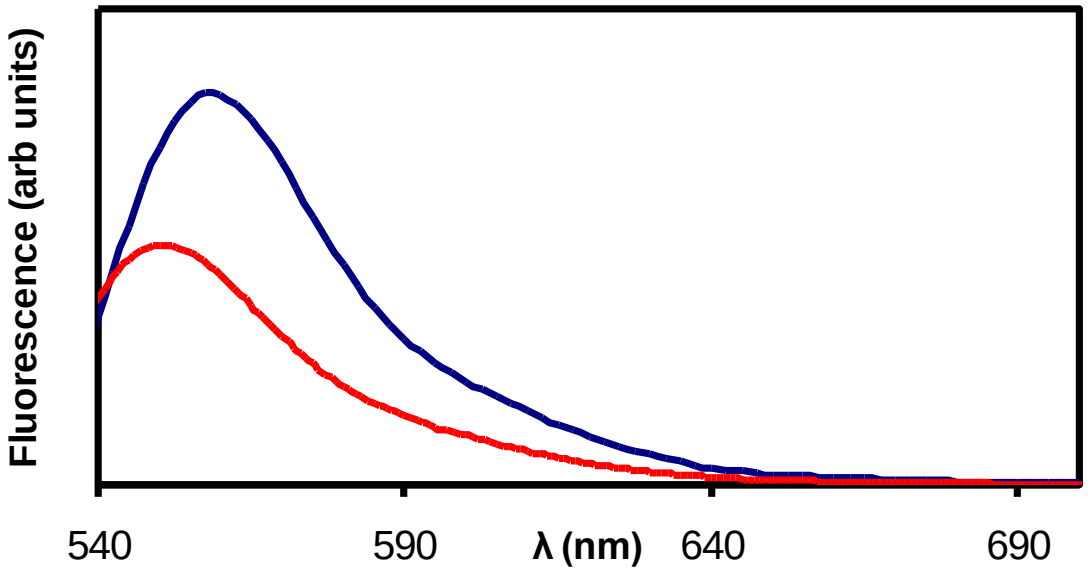

Figure 4.17 Hydrogel preparation: Comparison between the fluorescence emission spectrum of the freely dissolved [Rhod][Cl] (in water; red profile) and [Rhod][TPB] GUMBOS particles (blue profile) for matched concentration.

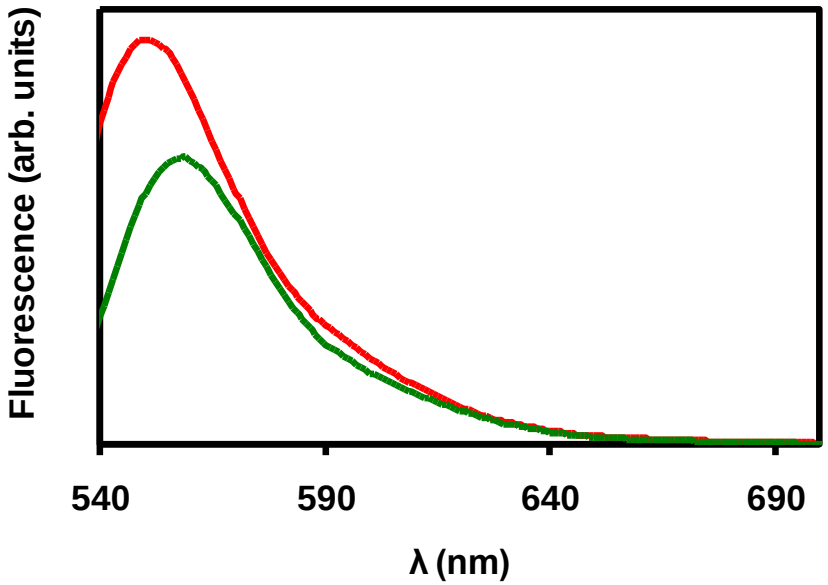

Fig. 4.18 Fluorecence emission of [Rhod][Cl] in water(red) and [Rhod][Cl] in gel(green) excited at their respective absorption maxima.

4.5.3 Comparison of Three Synthetic Methods

The particles were highly fluorescent with all three methods, especially when synthesized in hydrogels (Figure 4.19). During the gelation process, the particles precipitated within the rigid environment of the hydrogel when the pH was lowered and the GUMBOS particles ceased to diffuse. The GUMBOS particles were tightly encapsulated within the hydrogel thus minimizing non-radiative decay, which in turn significantly increased the fluorescence. The fluorescent intensity was lower when the nanoGUMBOS were synthesized with the reprecipitation method. The in-situ ion exchange method proved to have the lowest fluorescence intensity of all the three methods. The lower fluorescence for the latter two methods can be possibly due to non-radiative decay processes.

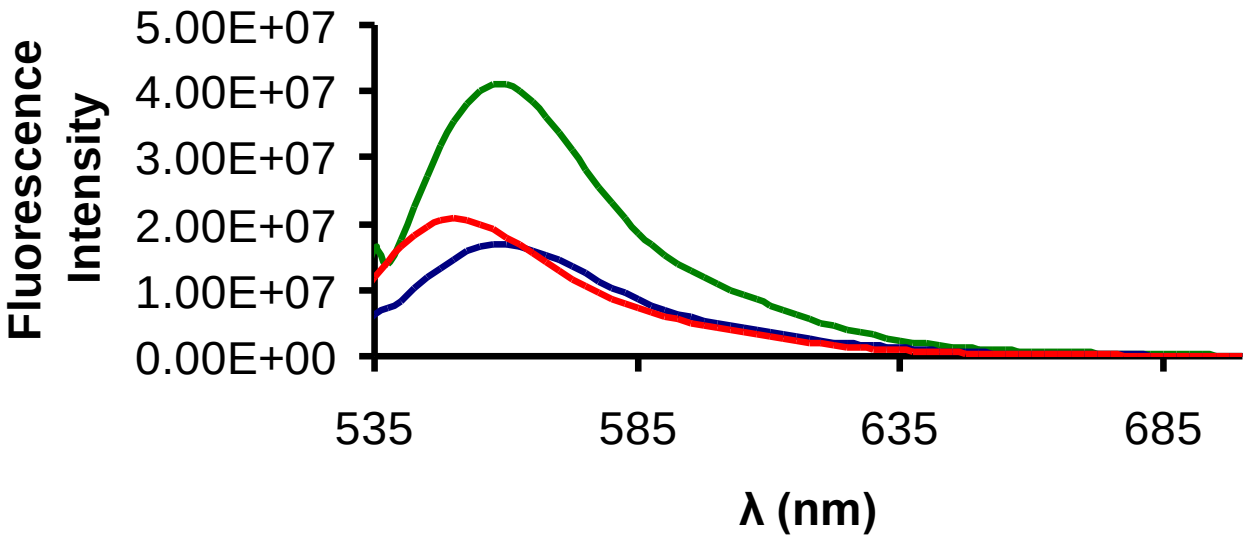

Figure 4.19 Comparison between the fluorescence emission spectrum of the [Rhod][TPB] particles using reprecipitation, in-situ ion exchange, and hydrogel methods. [Rhod][TPB] nanoGUMBOS synthesized using (In-situ ion exchange; blue profile), [Rhod][TPB] GUMBOS particles (Hydrogel; green profile), and [Rhod][TPB] nanoGUMBOS (Reprecipitation; red profile). [Rhod][TPB] nanoGUMBOS were synthesized at the same concentration.

4.6 Conclusions

In summary, the synthesis, characterization, and investigation of the spectral properties of fluorescent GUMBOS particles were performed. A comparison of spectral properties of GUMBOS particles from three preparation methods suggested that the fabrication method had a significant role on the resultant spectral properties. With all three methods, the particles were highly fluorescent, especially when synthesized in hydrogels. The microenvironment of the gel is rigid thus minimizing different types of non-radiative decay and in turn causing an enhancement in fluorescence. In this study, particles of 89 ± 17 nm, 89 ± 11 nm, and 124 ± 35 nm were synthesized using the reprecipitation, in-situ ion exchange, and hydrogel methods, respectively. The reprecipitation method proved to be rapid and additive free, however it led to aggregation of particles. The in-situ ion exchange synthesis yielded the most spherical particles with a very low polydispersity. However, the fluorescent intensity was lower when the nanoGUMBOS were synthesized with the in-situ ion exchange method as compared to the reprecipitation method. Employing hydrogels yielded superior fluorescence intensity compared with both the reprecipitation and in-situ ion exchange. It should also be noted that the spectral properties of the GUMBOS were significantly different from the dissolved bulk materials.

4.7 References

(1). Qian, H. S.; Guo, H. C.; Ho, P. C.-L.; Mahendran, R.; Zhang, Y. *Small* **2009,** 5, (20), 2285-2290.

(2). Zhang, P.; Steelant, W.; Kumar, M.; Scholfield, M. *J. Am. Chem. Soc* **2007,** 129, (15), 4526-4527.

(3). Qian, G.; Zhong, Z.; Luo, M.; Yu, D.; Zhang, Z.; Ma, D.; Wang, Z. Y. *J. Phys. Chem. C.* **2009,** 113, (4), 1589-1595.

(4). Iyer, S.; Woodworth, C. D.; Gaikwad, R. M.; Kievsky, Y. Y.; Sokolov, I. *Small* **2009,** 5, (20), 2277-2284.

(5). Resch-Genger, U.; Grabolle, M.; Cavaliere-Jaricot, S.; Nitschke, R.; Nann, T. *Nat. Methods* **2008,** 5, (9), 763-775.

(6). Rzigalinski, B. A.; Strobl, J. S. *Toxicol. Appl. Pharmacol* **2009,** 238, (3), 280-288.

(7). Santra, S.; Wang, K.; Tapec, R.; Tan, W. *J. Biomed. Opt* **2001,** 6, (2), 160-166.

(8). Tran, C. D.; Oliveira, D. *Anal. Biochem.* **2006,** 356, (1), 51-58.

(9). Huddleston, J. G.; Rogers, R. D. *Chem. Commun.* **1998**, (16), 1765-1766.

(10). Bwambok, D. K.; El-Zahab, B.; Challa, S. K.; Li, M.; Chandler; Gary A. Baker, L.; Warner, I. M. *ACS Nano* **2009**.

(11). Bwambok, D. K.; Marwani, H. M.; Fernand, V. E.; Fakayode, S. O.; Lowry, M.; Negulescu, I.; Strongin, R. M.; Warner, I. M. *Chirality* **2007,** In press.

(12). Del Sesto, R. E.; McCleskey, T. M.; Burrell, A. K.; Baker, G. A.; Thompson, J. D.; Scott, B. L.; Wilkes, J. S.; Williams, P. *Chem. Commun.* **2008**, (4), 447-449.

(13). An, B.-K.; Kwon, S.-K.; Jung, S.-D.; Park, S. Y. *J. Am. Chem. Soc* **2002,** 124, 14410-14415.

(14). Peng, A.-D.; Xiao, D.-B.; Ma, Y.; Yang, W.-S.; Yao, J.-N. *Adv. Mater.* **2005,** 17, 2070-2073.

(15). Harruff, B. A.; Bunker, C. E. *Langmuir* **2003,** 19, (3), 893-897.

(16). Uskokovic, V.; Drofenik, M. *Surf. Rev. Lett.* **2005,** 12, (2), 239-277.

(17). Mukhopadhyay, S.; Maitra, U. *Curr. Sci* **2004,** 87, (12), 1666-1683.

(18). Karukstis, K. K.; Frazier, A. A.; Martula, D. S.; Whiles, J. A. *J. Phys. Chem.* **1996,** 100, (26), 11133-11138.

(19). Altamirano, M. S.; Borsarelli, C. D.; Cosa, J. J.; Previtali, C. M. *J. Colloid Interface Sci.* **1998,** 205, 390-396.

(20). Motte, L.; Billoudet, F.; Pileni, M. P. *J. Phys. Chem.* **1995,** 99, (44), 16425-9.

CHAPTER 5

CONCLUSIONS AND FUTURE STUDIES

5.1 Concluding Remarks

In this dissertation, the synthesis and characterization of nanoparticles derived from GUMBOS is discussed. NanoGUMBOS have distinct properties over traditional nanoparticles due to the inherent functionality present within the cation and anionic component of the GUMBOS, thus rendering nanoGUMBOS suitable for a myriad of applications in the biomedical, electronics, analytical, and separations field.

In Chapter 1, ILs, GUMBOS, nanoparticles, types of synthesis/methods of size control for traditional nanoparticles, nanoGUMBOS, and analytical techniques used in this study were discussed.

In Chapter 2, novel methods leading to the formation of stable, micro- and nanoGUMBOS are reported. Two o/w melt–emulsion–quench approaches yielded spherical or quasi-spherical particles with mean nanometer diameters dependent on the droplet size of the internal phase. Microparticles were achieved by procedure modification. This simple and rapid preparation, requires neither specialized equipment or harsh conditions. The designer properties of nanoGUMBOS renders them ideal for numerous potential applications in the biomedical, materials, and analytical communities.

In Chapter 3, the size and uniformity of non-magnetic and magnetic GUMBOS particles were controlled by variations in experimental parameters using an *in situ,* ion exchange, water-in-oil (w/o) emulsion preparation. These nanoGUMBOS are task specific in that they are magnetic as compared to the nonfunctional nanoGUMBOS

synthesized in chapter two. Parameters such as reagent concentration produced significant and predictable variations in the size and uniformity of the particles. Average size variations for non-magnetic nanoGUMBOS ranging from approximately 14 to 68 nm were achieved by manipulation of these parameters. In addition, average sizes from 98 to 198 nm were achieved for magnetic GUMBOS particles by also varying the aforementioned parameter. The morphology of the nanoGUMBOS and GUMBOS particles were also assessed with AFM in this chapter, thus yielding more information about the sphericity of the particles. In addition, the magnetic susceptibility or the degree of magnetization of the nanoGUMBOS was investigated with SQUID. Control of the size and uniformity of this new breed of nanoparticles is essential for potential applications in drug delivery, biomedical imaging, and in environmental remediation.

In Chapter 4, novel fluorescent GUMBOS particles were synthesized and characterized. These GUMBOS particles are also task specific as in chapter three because the active component is present within the GUMBOS. Particles from GUMBOS derived from a fluorophore based cation and a bulky hydrophobic anion were prepared using three different methods: reprecipitation, *in-situ* ion exchange, and hydrogel synthesis. Particles synthesized using all three methods were uniform and highly fluorescent. Due to their uniformity and facile and rapid preparation, particles derived from GUMBOS will be important for many applications in the biomedical fields.

5.2 Future Studies

Until now, various approaches have been employed to prepare multifunctional nanoparticles composed of, but not limited to, iron oxide nanoparticle and CdTe quantum dots (QDs), iron oxide nanoparticles and fluorescent silica, gadolinium (Gd^{3+}) and

quantum dots. In general, to synthesize multifunctional nanoparticles, magnetic nanoparticles have to be synthesized first. Next, a protective silica matrix has to be coated around the particle before attaching the fluorescent tag to protect the dyes from quenching, thereby improving the fluorescence. Due to the ability to combine the dual property nanoparticle, fluorescent magnetic nanoparticles can potentially be used in magnetic hyperthermia and drug delivery applications. Although these approaches are successful in preparing fluorescent magnetic nanoparticles, they are rather laborious, time consuming, toxic, and require intricate procedures for combining the dual functional nature of the particle.

It is of paramount importance to improve medical diagnoses in the early detection of cancer and treatment of tumors. Researchers have explored and identified methods for localizing cancer within the body by immobilizing quantum dots on the surfaces of nanoparticles. Multifunctional nanomaterials which are composed solely of GUMBOS could potentially enjoy both the advantages of being magnetic while simultaneously being fluorescent because the dual properties are built into the cation and anion of the GUMBOS. Fluorescent magnetic nanoGUMBOS can possibly exhibit great potential in biological applications. These multifunctional nanoGUMBOS can potentially serve as fluorescent markers and can be capable of being driven by an external magnetic field to a specific location. For example, in a targeting drug-delivery system, magnetic nanoparticles labeled drugs could be easily administered and guided to the target of interest under an applied external magnetic field, resulting in a localized delivery of drugs. Fluorescent magnetic nanoparticles could be used in hyperthermia treatment. For example, the fluorescent portion of the GUMBOS could be used to localize tumors. Next,

one can subject the dual functional nanoGUMBOS under a high frequency magnetic field. When the dual functional nanoGUMBOS are under an alternating magnetic field, the nanoGUMBOS can become powerful sources of heat and ultimately destroy tumors which are sensitive to temperatures above 41 °C. The synthesis of magnetic fluorescent nanoGUMBOS can be achieved in less than 30 min and the functional components comprise the nanoGUMBOS allowing for a uniformly functionalized nanoparticle as compared with traditional magnetic fluorescent nanoparticles.

APPENDIX

LETTERS OF PERMISSION

From: Aaron Tesfai <atesfa1@tigers.lsu.edu>
Date: Thu, Dec 3, 2009 at 11:49 AM
Subject: Permission to Reproduce Published Work in Dissertation
To: copyright@acs.org

To whom it may concern:

I hereby request permission to reproduce text and/or figures from the journal articles listed below in my doctoral dissertation. Note that I am the first author for both articles. Per university protocol, the dissertation will be archived in the Louisiana State University electronic thesis database.

1) Controllable Formation of Ionic Liquid Micro- and Nanoparticles via a Melt-Emulsion-Quench Approach. Nano Letters.2008, 8, 897-901.
2) Magnetic and Nonmagnetic Nanoparticles from a Group of Uniform Materials Based on Organic Salts. ACS Nano.2009, 3, 3244-3250.

Please fax your decision to my attention at 225-578-3971.

Thank you very much for your consideration.

Regards,
Aaron Tesfai
Ph.D. Candidate,
Louisiana State University
Department of Chemistry
432 Choppin Hall
Baton Rouge, LA. 70802
Phone: 225-578-3919

From: <donotreply@copyright.com>
Date: Thu, Dec 3, 2009 at 12:33 PM
Subject: Thank you for your Rightslink / American Chemical Society order
To: atesfa1@lsu.edu

Thank you for placing your order through Copyright Clearance Center's Rightslink service. American Chemical Society has partnered with Rightslink to license its content online. Note: Payee for this order is Copyright Clearance Center.
Copyright Clearance Center

Rightslink
Tel (toll free): +1-877-622-5543
Tel: +1-978-646-2777
E-mail: mailto:customercare@copyright.com
Web: http://www.copyright.com

This is a License Agreement between Aaron Tesfai ("You") and American Chemical Society ("American Chemical Society") provided by Copyright Clearance Center ("CCC"). The license consists of your order details, the terms and conditions provided by American Chemical Society, and the payment terms and conditions.

All payments must be made in full to CCC. For payment instructions, please see information listed at the bottom of this form.

License Number	2321460833626
License Date	Dec 03, 2009
Licensed content publisher	American Chemical Society
Licensed content publication	Nano Letters
Licensed content title	Controllable Formation of Ionic Liquid Micro- and Nanoparticles via a Melt–Emulsion–Quench Approach
Licensed content author	Aaron Tesfai et al.
Licensed content date	Mar 1, 2008
Volume number	8
Issue number	3
Type of Use	Thesis/Dissertation
Requestor type	Not specified
Format	Electronic
Portion	Table/Figure/Chart
Number of Table/Figure/Charts	5
Author of this ACS article	Yes
Order reference number	
Title of the thesis / dissertation	STUDIES OF NANOPARTICLES FROM A GROUP OF UNIFORM MATERIALS BASED ON ORGANIC SALTS (GUMBOS)
Expected completion date	Dec 2009
Estimated size(pages)	120
Billing Type	Invoice
Billing Address	8939 Jefferson Hwy Apt##14 Baton Rouge, LA 70809 United States

Customer reference info	
Total	0.00 USD

This is a License Agreement between Aaron Tesfai ("You") and American Chemical Society ("American Chemical Society") provided by Copyright Clearance Center ("CCC"). The license consists of your order details, the terms and conditions provided by American Chemical Society, and the payment terms and conditions.

All payments must be made in full to CCC. For payment instructions, please see information listed at the bottom of this form.

License Number	2321461201201
License Date	Dec 03, 2009
Licensed content publisher	American Chemical Society
Licensed content publication	ACS Nano
Licensed content title	Magnetic and Nonmagnetic Nanoparticles from a Group of Uniform Materials Based on Organic Salts
Licensed content author	Aaron Tesfai et al.
Licensed content date	Oct 1, 2009
Volume number	3
Issue number	10
Type of Use	Thesis/Dissertation
Requestor type	Not specified
Format	Electronic
Portion	Table/Figure/Chart
Number of Table/Figure/Charts	11
Author of this ACS article	Yes
Order reference number	
Title of the thesis / dissertation	STUDIES OF NANOPARTICLES FROM A GROUP OF UNIFORM MATERIALS BASED ON ORGANIC SALTS (GUMBOS)
Expected completion date	Dec 2009
Estimated size(pages)	120
Billing Type	Invoice
Billing Address	8939 Jefferson Hwy Apt##14 Baton Rouge, LA 70809

	United States
Customer reference info	
Total	0.00 USD
Terms and Conditions	

VITA

Aaron Tesfai was born in Jefferson City, Missouri, to Tesfai Tsehaie and Turu Negash. He attended Thorpe Gordon elementary school. He attended high school at Jefferson City High School and graduated in 1999. Thereafter, he received his Bachelor of Science (Honors Scholar) in biochemistry (May 2003) and his Bachelor of Arts in classics (August 2003) from the University of Missouri, Columbia (MU). As an undergraduate student, Aaron began his career as a research assistant under Dr. Sheryl Tucker in the Department of Chemistry. He began working with the group through MU's EXPRESS program, which encourages underrepresented minorities to participate in scientific research. He also participated in the Life Sciences Undergraduate Research Opportunity Program at MU. He also received the Goldwater Scholarship, a highly selective award for students in mathematics, engineering, and natural sciences. In August 2003, Aaron began his graduate studies as an analytical chemist and received several honors during his graduate career including the *Board of Regents Fellowship (BOR)*, Graduate *Alliance for Education in Louisiana Dissertation Writing Fellowship (GAELA)*, *Huel Perkins Fellowship*. Aaron will graduate with the degree of Doctor of Philosophy in chemistry from Louisiana State University in May 2010. His publications, patents, and conference presentations during his graduate career include:

"Magnetic and Non-Magnetic Nanoparticles from a Group of Uniform Materials Based on Organic Salts", **A. Tesfai**, B. El-Zahab, A.T. Kelley, M. Li, J.C. Garno G. A. Baker, and I. M. Warner. ACS Nano., 3, 3244 (2009).

"Controllable Formation of Ionic Liquid Micro- and Nanoparticles *via* a Melt–Emulsion–Quench Approach", **A. Tesfai**, B. El-Zahab, D. Bwambok, G. A. Baker, S. O. Fakayode, M. Lowry, and I. M. Warner. Nano Lett., 8, 897 (2008).

"Synthesis and Analysis of a Solvatochromic Dye, 1-(p-Dimethylaminophenyl)-2-nitroethylene: An Advanced Undergraduate Laboratory Experiment", D.L. Richter-Egger, **A. Tesfai**, S.J. Flamm and S.A. Tucker, J. Chem. Educ., 78, 1375 (2001).

"Spectrofluorometric Investigations of Polyamido Amine Starburst Dendrimers Using the Solvatochromic Probe Phenol Blue", D.L. Richter-Egger, J.C. Landry, **A. Tesfai**, S.J. Flamm and S.A. Tucker, J. Phys. Chem. A, 105, 6826 (2001)

"Spectroscopic Investigations of Poly(propyleneimine) Dendrimers Using the Solvatochromic Probe Phenol Blue and Comparisons to Poly(amidoamine) Dendrimers", D.L Richter-Egger, **A. Tesfai** and S.A. Tucker, Anal Chem., 73, 5743 (2001).

His patents include:
WO/2009/082618) FROZEN LONIC LIQUID MICROPARTICLES AND NANOPARTICLES, AND METHODS FOR THEIR SYNTHESIS AND USE. Inventors: WARNER, Isiah, M.; (US).**TESFAI, Aaron**; (US).EL-ZAHAB, Bilal, M.; (US).
BWAMBOK, David; (US).BAKER, Gary, A.; (US).FAKAYODE, Sayo, O.; (US). LOWRY, Mark; (US).TOLOCKA, Michael, P.; (US).DE ROOY, Sergio; (US).

PROFESSIONAL PRESENTATIONS

Oral

"Synthesis and Characterization of Novel Nano- and Micro- Particles" **A. Tesfai**, B. El-Zahab, D. Bwambok, H. M. Marwani, G. Ganea, G A. Baker, S. O. Fakayode, M. A. Lowry, and I. M. Warner, presented at The 35th Annual Conference of The National Organization for the Professional Advancement of Black Chemists and Chemical Engineers, Philadelphia Marriott Downtown, March 16-21st, 2008

Poster

"Synthesis and Characterization of Aerosol-OT (AOT) Derivatives" **A. Tesfai**, K A. Fletcher, H. M. Marwani, M. A. Lowry, S. Jiang, O. Alptürk, R. M. Strongin, and I. M. Warner, presented at PITTCON '08", New Orleans, Louisiana, March 2nd-7th, 2008, poster.

"Spectrofluorometric Investigations of Amine-Terminated Poly(amidoamine) Dendrimers Using the Solvatochromic Probe Phenol Blue" **A. Tesfai**, R.D. Otte and S.A. Tucker, presented at the 12th Annual Undergraduate Research Science Spring Symposium", Columbia, Missouri, April 30, 2002 poster.

"Spectrofluorometric Investigations of Amine-Terminated Poly(amidoamine) Dendrimers Using the Solvatochromic Probe Phenol Blue" **A. Tesfai**, R.D. Otte and S.A. Tucker, presented at PITTCON '02", New Orleans, Louisiana, March 17-22, 2002, poster 1783P. Invited presentation for Celebrating Diversity in Analytical Chemistry Symposium poster session via competitive abstract submission.

"Spectroscopic Investigations of Poly(amidoamine) and Poly(propyleneimine) Dendrimers Using the Solvatochromic Probes", S.A. Tucker, D.L. Richter-Egger, **A.**

Tesfai, E.L Jacobs and C.L. Larson, presented at "PITTCON '02", New Orleans, Louisiana, March 17-22, 2002, abstract.

"Spectroscopic Comparison of Amine-Terminated PAMAM and PPI Dendrimers", **A. Tesfai**, D.L. Richter-Egger, and S.A. Tucker, presented at the "12th Annual Undergraduate Research Science Summer Symposium", Columbia, Missouri, August 2, 2001 poster.